

Republic of Iraq  
Ministry of Higher Education  
& Scientific Research  
Al-Muthanna University  
College of Science  
Department of Chemistry



# **Synthesis, characterization and study the Biological activity of New azo dye Ligand with Some Metal Complexes**

A thesis Submitted to the Council of College of Science /  
Al-Muthanna University as Partial Fulfillment of the  
Requirements for the Degree of Master of Science in Chemistry

By:

**Suha Hassan Majhool**

B. Sc. In Chemistry 2018

Supervised by:

**Assistant Professor**

**Dr. Azal Shakir Waheeb**

**Lecturer**

**Dr. Masar Ali Awad**

2024 A.D

1445 A.H

بِسْمِ اللَّهِ الرَّحْمَنِ الرَّحِيمِ

﴿يَأْتِبِ هَذَا تَأْوِيلُ رُؤْيِي مِنْ قَبْلُ قَدْ  
جَعَلَهَا رَبِّي حَقًّا﴾

صدق الله العليّ العظيم

سورة يوسف

(الآية ١٠٠)

## *Certification of the Supervisor*

I certify that this thesis, which is entitled “**Synthesis, Characterization and Study the Biological activity of new azo dye ligand with Some Metal Complexes**” is done under my supervision in the Department of Chemistry /College of Science /Al-Muthanna University, in partial fulfillment of the requirements for the Master’s degree in chemistry.

Signature:

**Assistant Professor**  
**Dr. Azal Shakir Waheeb**

Al-Muthanna University/  
College of Science  
Data: / / 2024

Signature:

**Lecturer**  
**Dr. Masar Ali Awad**

Al-Muthanna University/  
College of Science  
Data: / / 2024

Based on the available recommendations, I am forwarding this thesis for discussion.

Signature:

**Assist. Prof.**

**Dr. Azal Shakir Waheeb**

Head of Department of Chemistry

Data: / / 2024

## ***Dedication***

*To my first school in life ...*

*To the one who honored me to bear his name ...*

*To the one who was my support in this world...to the one who strove for my comfort and success...to the greatest and dearest man in the universe....*

*To the one who believed in me and encouraged me to achieve my dreams, and left before seeing the fruit of his planting, my beloved father... may God have mercy on him.*

*To the light of my eyes, to the one who gave my happiness and comfort over her happiness.....*

*To whom were her prayers and words a companion of brilliance and excellence... my beloved mother... may God prolong her life.*

*The enormous gratitude goes out to my beloved **family**, especially my parents, brothers, and sisters, who never ceased loving, caring for, and motivating me during the study period.*

***Suha***

## ***Acknowledgment***

*First, I want to thank Allah for all the blessings, especially for giving me the strength and endurance to finish this thesis.*

*I sincerely and deeply thank my supervisor, **Asst.Prof. Dr. Azal Shakir Waheeb**, and lecturer, **Dr. Masar Ali Awad**, for their help with this project and for offering feedback.*

*I want to express my gratitude to the staff of the Department of Chemistry /Collage of Sciences / University of AL-Muthanna, especially to **Dr. Khawla Kani Jassim, Dr. Kassim Mohammed. Hello, Dr.Tamar Hussain, Dr. Hussain Kyhoiesh, MSc. Hassanein salah, Ms. Hala kadhim and MSc. Marwa Adnan.***

*Special thanks are also due to my **colleagues** and close friends who supported me during all the hard times in my work.*

***Suha***

***13 / 11 / 2023***

## List of contents

<b>Contents</b>		i
List of tables		v
List of figures		vii
List of abbreviations		xiii
Abstract		xi
<b>Section</b>	<b>Subjects</b>	<b>Pages No.</b>
	Chapter One (Introduction)	1-25
<b>1.0</b>	Introduction	1
<b>1.1</b>	General Introduction	1
<b>1.2</b>	Azo Compounds	1
<b>1.2.1</b>	Synthesis of azo compound	3
<b>1.2.2</b>	Classification of azo compound	3
<b>1.3</b>	Classification of Azo Compounds according to azo grouping number	4
<b>1.3.1</b>	The monoazo dyes	4
<b>1.3.2</b>	Diazo dyes	5
<b>1.3.3</b>	Poly azo dyes	5
<b>1.4</b>	The Chelating Behavior for Azo compound.	6
<b>1.4.1</b>	Monodentate Ligand	6
<b>1.4.2</b>	Bidentate reagent	7
<b>1.4.3</b>	Tridentate reagent	8
<b>1.5</b>	Applications of azo dyes	8
<b>1.5.1</b>	Biological activity of azo dyes	9
<b>1.5.2</b>	Antibacterial activity	9

<b>1.5.3</b>	Antifungal activity	10
<b>1.5.4</b>	Anticancer activity	10
<b>1.6</b>	Imidazole compound	11
<b>1.7</b>	Thiazole chemistry	13
<b>1.7.1</b>	Synthesis of thiazole	13
<b>1.7.2</b>	Application of thiazolyl azo compounds	14
<b>1.8</b>	Biological Activity	18
<b>1.9</b>	Cancerous tumor	20
<b>1.9.1</b>	Lung cancer	21
<b>1.9.2</b>	Pancreas cancer	21
<b>1.10</b>	MTT Assay	22
<b>1.11</b>	The aim of the study	25
	Chapter Two (Materials and methods)	26-39
<b>2.0</b>	Materials and methods	26
<b>2.1</b>	Materials	26
<b>2.2</b>	Apparatuses	27
<b>2.2.1</b>	UV-Visible spectrophotometer	27
<b>2.2.2</b>	FT-IR spectra	27
<b>2.2.3</b>	<sup>1</sup> H and <sup>13</sup> C-NMR Spectroscopy	27
<b>2.2.4</b>	Mass Spectra	28
<b>2.2.5</b>	Micro Elemental analysis CHNS	28
<b>2.2.6</b>	Melting Points	28
<b>2.2.7</b>	Atomic Absorption Apparatus	28
<b>2.2.8</b>	Molar Conductivity Apparatus	28
<b>2.2.9</b>	Magnetic Susceptibility	29
<b>2.2.10</b>	XRD Study	29

<b>2.2.11</b>	Thermogravimetric Analysis	29
<b>2.2.12</b>	(FE-SEM) Analysis	29
<b>2.3</b>	Preparation of Azo dye Ligand (5-MTADMBI)	30
<b>2.4</b>	Preparation of Buffer Solutions	31
<b>2.5</b>	General procedure for synthesis metallic complexes	31
<b>2.6</b>	Preparation of Ligand Solutions	33
<b>2.7</b>	Determine the best Conditions	33
<b>2.7.1</b>	Identify the best Concentrations	34
<b>2.8</b>	Mole Ratio	34
<b>2.9</b>	Spectroscopy Measurements of Metallic Complexes	34
<b>2.10</b>	Measurements of Conductivity	35
<b>2.11</b>	Magnetic Susceptibility Measurements	35
<b>2.12</b>	Find the Percentage of Chloride in the Metal Complexes	36
<b>2.13</b>	Biological Activity	36
<b>2.13.1</b>	Preparation of the Plant's Bacterial Media and Calculation of the Inhibition zone	37
<b>2.13.2</b>	Preparation of the Artificial Center of Fungi and Calculation of the Inhibition zone	38
<b>2.13.3</b>	Gram Stain Solution	38
<b>2.14</b>	Cytotoxicity Assays Cell Lines	38
<b>2.14.1</b>	Cell Lines	38
<b>2.14.2</b>	Measurements of Cell Proliferation	38
	Chapter Three (Results and Discussion)	40-84
<b>3.0</b>	Results and Discussion	40
<b>3.1</b>	Spectacular spectroscopy of ligand (5-MTADMBI) and their metallic complexes	40

<b>3.2</b>	Determine Optimum Conditions	41
<b>3.2.1</b>	Metal Salts Selection	41
<b>3.2.2</b>	Determination Optimum Concentrations	42
<b>3.2.3</b>	Determining Calibration Curves of Metal Complexes	42
<b>3.3</b>	Determination of Possible Compositions of the Chelating Complexes	45
<b>3.4</b>	Stability Studies of Metal Complexes Solutions	48
<b>3.4.1</b>	Studying effect of solvent	48
<b>3.5</b>	Molar electrical conductivity measurements	50
<b>3.6</b>	Magnetic Susceptibility Measurements	52
<b>3.6.1</b>	Co (III)-complex	56
<b>3.6.2</b>	Cu(II)-Complex	57
<b>3.6.3</b>	Ni (II), Ag (I), and Au (III)-Complexes	57
<b>3.7</b>	Electronic Spectra	58
<b>3.7.1</b>	Electronic Spectra of Free Ligand	58
<b>3.7.2</b>	Electronic spectra of Co(III)-Complex	58
<b>3.7.3</b>	Electronic spectra of Ni-(II)-Complex	58
<b>3.7.4</b>	Electronic spectra of Cu-(II)-Complex	59
<b>3.7.5.</b>	Electronic spectra of Ag (I)-Complex	60
<b>3.7.6</b>	Electronic spectra of Au (III)-Complex	60
<b>3.8</b>	C.H.N.S Elemental Analysis	63
<b>3.9</b>	<sup>1</sup> HNMR Spectra	64
<b>3.9.1</b>	<sup>1</sup> HNMR spectrum of the ligand (L <sub>1</sub> H)	64
<b>3.9.2</b>	<sup>1</sup> HNMR spectra of Co(III)-Complex [Co(L <sub>2</sub> )Cl <sub>2</sub> ]Cl.H <sub>2</sub> O	65
<b>3.10</b>	<sup>13</sup> CNMR Spectra	66

<b>3.10.1</b>	<sup>13</sup> CNMR Spectrum of the Ligand (L <sub>1</sub> H)	66
<b>3.10.2</b>	<sup>13</sup> CNMR spectrum of [Co(L) <sub>2</sub> Cl <sub>2</sub> ]Cl.H <sub>2</sub> O Complex	67
<b>3.11</b>	The Mass Spectra Analysis	68
<b>3.11.1</b>	The Mass Spectra Analysis of Ligand and Ni (II)-Complex	68
<b>3.12</b>	Infrared Spectra	70
<b>3.13</b>	Study of Thermal stability	73
<b>3.14</b>	X-ray crystallography description of the synthesis compounds	76
<b>3.15</b>	Field-Emission Scanning Electron Microscope Apparatus (FESEM)	79
<b>3.16</b>	Suggested Structural Formula of Chelate Complexes	82
<b>3.17</b>	Biological Activity	82
<b>3.17.1</b>	Antibacterial action in vitro	82
<b>3.18</b>	Assays for cytotoxicity using (MTT)	85
<b>3.18.1</b>	Cytotoxic activity of the (5-MTADMBI) ligand and Co (III)-complex on A549 cell viability.	85
<b>3.18.2</b>	Cytotoxic activity of the (5-MTADMBI) ligand and Ag (I)-complex on TP-53 cell viability	88
	Chapter four (Conclusion & Recommendation)	92-94
<b>4.0</b>	Conclusion & Recommendation	92
<b>4.1</b>	Conclusion	92
<b>4.2</b>	Recommendation	94
	References	95-110

## List of Tables

Table	Title	Pages No.
<b>2.1</b>	Chemicals material used in this work and manufacturing companies	26
<b>2.2</b>	Some physical properties of metal chelates with azo ligand	33
<b>3.1</b>	Maximum wavelength, best concentration and molar absorbance of the ligand and their metallic complexes	41
<b>3.2</b>	The maximum absorbance at ( $\lambda_{\max}$ ) for the selected concentrations of mixing solutions of the metal ions under study with the azo dye ligand (5-MTADMBI)	43
<b>3.3</b>	Ultraviolet -visible spectrum values for the mole ratio methodology at ( $\lambda_{\max}$ ), at the optimum concentration of mix metallic ion solutions with azo-dye ligand	46
<b>3.4</b>	Stability Constants for complexes of metal ions under study with azo dye ligand at the best concentration and laboratory temperature	49
<b>3.5</b>	Molar electrical conductivity values at a concentration for electrolytes in multiple solvents	51
<b>3.6</b>	Molar electrical conductivity values at a concentration of $1 \times 10^{-3}$ M in ethanol solvent at ambient temperature	51
<b>3.7</b>	Electronic spectra, magnetic measurements, geometric shapes and hybridization of metallic complexes with ligand at laboratory temperature	61
<b>3.8</b>	(CHNS) analysis, and some of physical properties of (5-MTADMBI) ligand and the synthesized complexes	63
<b>3.9</b>	Assignment of the $^{13}\text{C}$ NMR spectrum of the ligand (5-MTADMBI) and its Co(III)-Complex	68
<b>3.10</b>	FTIR spectrum of the (5-MTADMBI) ligand's and its metallic complexes	
<b>3.11</b>	Thermoanalytical finding (TG-DTG) of ligand (5-MTADMBI) and metal complexes	74

<b>3.12</b>	Crystallographic data for (5-MTADMBI) and chelate complexes	78
<b>3.14</b>	Biological activity data for ligand and their metallic complexes with respect to inhibitory zone	86
<b>3.15</b>	The cytotoxicity of (5-MTADMBI) was assessed on the A549 carcinoma cell line and the HdFn cell line following a 24-hour incubation period at 37 <sup>0</sup> C	89
<b>3.16</b>	The cytotoxicity of Co(III)-Complex was evaluated versus the HdFn cell line and the A549 cancer cell line following a 24-hour incubation period at 37 <sup>0</sup> C	89
<b>3.17</b>	The cytotoxicity of (5-MTADMBI) was assessed on the TP-53 carcinoma cell line and the HdFn cell line following a 24-hour incubation period at 37 <sup>0</sup> C	91
<b>3.18</b>	The cytotoxicity of Ag(I) -Complex was assessed versus the HdFn cell line and the TP-53 cancer cell line following a 24-hour incubation period at 37 <sup>0</sup> C	92

### List of Figures

<b>Section</b>	<b>Subject</b>	<b>Pages No.</b>
<b>1.1</b>	(Bismarck Brown) Structure	2
<b>1.2</b>	Resonance phenomenon of azo dyes	2
<b>1.3</b>	Homocyclic azo compound	3
<b>1.4</b>	Heterocyclic azo compound	4
<b>1.5</b>	Mono azo dyes structure	5
<b>1.6</b>	Diazo dye structure	5
<b>1.7</b>	Polyazo dye structure	6
<b>1.8</b>	Mono dentate reagent structure	7
<b>1.9</b>	Bidentate reagent structure	7
<b>1.10</b>	Tridentate reagent structure	8

<b>1.11</b>	Structures of heterocyclic-modified azo dye derivatives with antibacterial activity	9
<b>1.12</b>	Derivatives of azo dyes that are active against fungi	10
<b>1.13</b>	Anticancer azo dye derivatives with heterocyclic scaffolds and their chemical structures	11
<b>1.14</b>	1H- imidazole	11
<b>1.15</b>	Substituted imidazole azo ligand	12
<b>1.16</b>	Preparation of imidazole derivatives	12
<b>1.17</b>	1, 3-thiazole structure	13
<b>1.18</b>	Hantzsch thiazole synthesis reaction mechanism	14
<b>1.19</b>	Chemical structure of azo amino thiazole disperse dye	14
<b>1.20</b>	Au(III) complex with (6- MBTADB) Structure	16
<b>1.21</b>	The chemical structure of metal chelate complexes DMeTAEP where M =Co(III), Ni (II) , Hg(II) , Cu(II) , Zn (II) and Cd (II)	17
<b>1.22</b>	The chemical structure of metal chelate complexes DMeTAMP where M = Cu(II) ,Mn(II) , and Zn (II)	18
<b>1.23</b>	2-(4-amino phenyl benzo thiazole) structure	19
<b>1.24</b>	Lung cells and tissues infected with a cancerous tumor	21
<b>1.25</b>	Pancreatic cells and tissues infected with a cancerous tumor	22
<b>1.26</b>	Mechanism of action of (MTT) dye	23
<b>2.1</b>	Synthesis of (5-MeTADMBI) ligand	31
<b>3.1</b>	The linear relationship between the absorbance and the range of concentrations selected at ( $\lambda_{max}$ ) for each of the metal complexes prepared with ligand	44
<b>3.2</b>	The linear relationship between the absorbance and the range of concentrations selected at ( $\lambda_{max}$ ) for each of the metal complexes prepared with ligand	44

<b>3.3</b>	Molar ratio curves at ( $\lambda_{\max}$ ) for cobalt (III), nickel (II), copper (II), silver (I), and gold (III) with ligand	47
<b>3.4</b>	Electronic transitions of distorted ( $d^9$ ) octahedral complexes	59
<b>3.5</b>	UV-Vis spectrum of ligand (5-MTADMBI) and chelate complexes	62
<b>3.6</b>	$^1\text{H}$ NMR Spectrum of azo dye ligand (5-MTADMBI) in ( $d_6$ -DMSO) solvent	64
<b>3.7</b>	$^1\text{H}$ NMR spectrum of Cobalt complex in (DMSO- $d_6$ ) solvent	65
<b>3.8</b>	$^{13}\text{C}$ NMR spectrum of ( $L_1H$ ) ligand	66
<b>3.9</b>	$^{13}\text{C}$ NMR spectrum of Cobalt Complex	67
<b>3.10</b>	The mass fragmentation of (5-MTADMBI) ligand	69
<b>3.11</b>	The mass fragmentation of Nickel Complex	69
<b>3.12</b>	FTIR spectra of the (5-MeTADMBI) and its metallic complexes	72
<b>3.13</b>	Thermal gravimetric analysis of (a) (5-MTADMBI) ,(b) Co (III)- Complex,(c) Ni (II)- Complex, (d) Cu (II)- Complex ,(e) Ag(I)- Complex,and (f) Au(III)- Complex	75
<b>3.14</b>	XRD spectra for ligand (5-MTADMBI) and chelate complexes	77
<b>3.15</b>	FESEM images of the (5-MTADMBI) and its metallic complexes	81
<b>3.16</b>	Possible geometric for (5-MTADMBI) and their metallic complexes	84
<b>3.17</b>	Organic ligand (5-MTADMBI) and their complexes' in vitro antibacterial activity	86
<b>3.18</b>	The inhibition zone for (5-MTADMBI) and their complexes with gram positive Bacteria (Streptococcus)	87
<b>3.19</b>	The inhibition zone for (3) (5-MTADMBI), (a) (Co), (b) (Ni), (c) (Cu), (d) (Ag), (e) (Au) with gram negative Bacteria (Escherichia coli)	87

<b>3.20</b>	The inhibition zone for (1) (5-MTADMBI), (2) (Co), (3) (Ni), (4) (Cu), (5) (Ag), (6) (Au) with fungi ( <i>Penicillium</i> sp)	87
<b>3.21</b>	IC50 for ligand (5-MTADMBI) in normal (HdFn) and (A549) cell lines	90
<b>3.22</b>	IC50 for Co(III)-Complex in normal (HdFn) and (A549) cell lines	90
<b>3.23</b>	IC50 for ligand (5-MTADMBI) in normal (HdFn) and (TP-53) cell lines	92
<b>3.24</b>	IC50 for Ag(I)-Complex in normal (HdFn) and (TP-53) cell lines	92

### List of Scheme

<b>Section</b>	<b>Subject</b>	<b>Pages No.</b>
<b>2.1</b>	Synthesis of metal chelates	32

### List of Abbreviations

<b>Symbols</b>	<b>Meaning</b>
$\Lambda_{\infty}$	The molar conductivity at infinite dilution
$\Lambda_M$	The molar conductivity solutions
<sup>13</sup> C-NMR	13 Carbon nuclear magnetic resonance
<b>5-MeTADMBI</b>	2-[2-(5-Methyle thiazolyl) azo]-5,6-dimethyl benzimidazole
<b>A</b>	Absorbance
<b>A549</b>	hypotriploid alveolar basal epithelial cells (lung cancer)
<b>Am</b>	Molar absorptivity at increase of ligand in solution
<b>As</b>	Molar absorptivity at molar ratio selected for the complex
<b>B.M</b>	Bohr magnetons

<b>Bismarck Brown</b>	4,4'-((1Z, 1'Z)-1,3-phenylenebis(diazene-2,1-diyl))bis (benzene-1,3-diamine)
<b>C</b>	The salt concentration of the ion user metal
<b>C.H.N.S</b>	Carbon (C), Hydrogen (H), and Nitrogen (N) elemental analysis
<b>D</b>	Correction factor
<b>DDW</b>	Deionized distilled water
<b>DMF</b>	Dimethylformamide
<b>DMSO</b>	Dimethyl sulfoxide
<b>DTA</b>	Differential thermal analysis
<b>DTG</b>	Derivative thermogravimetric analysis
<b>EDTA</b>	Ethylene diamine tetra acetic acid
<b>EtOH</b>	Ethanol
$\epsilon$	Microstrain
<b>FESEM</b>	Field emission scanning electron microscopy
<b>FT-IR</b>	Infrared spectroscopy
<b>FWHM</b>	Full width at half maximum
<b>HdFn</b>	Human dermal fibroblasts normal
<b><sup>1</sup>H-NMR</b>	Proton nuclear magnetic resonance spectroscopy
<b>IC<sub>50</sub></b>	The half-maximal inhibitory concentration
<b>M:L</b>	Ratio Metal:Ligand
<b>m</b>	Medium absorption peaks
<b>M.P °C</b>	Melting point
<b>MeOH</b>	Methanol
<b>M-N</b>	Association metal - nitrogen
<b>MTT</b>	3-(4,5 Dimethyl thiazol- 2-yl)-2,5-Diphenyl Tetrazolium Bromide

<b>n</b>	Mole ratio ligand number associated with the ion metal
<b>NO2BTAHBA</b>	2-(6-nitro-2-benzothiazolyl azo)-4-hydroxybenzoic acid
<b>NSCALC</b>	Non-small cell
<b>pH</b>	The concentration of hydrogen ions
<b>ppm</b>	Part per million
<b>S</b>	Strong absorption peaks
<b>SCLC</b>	Small cell lung cancer
<b>SEM</b>	Scanning electron microscopy
<b>Sh</b>	Shoulder absorption peaks
<b>t</b>	Time
<b>T</b>	Absolute temperature
<b>TGA</b>	Thermogravimetric analysis
<b>TMS</b>	Tetramethylsilane
<b>TP-53</b>	Tumor protein 53 (pancreas cancer)
<b>UV-Visb</b>	Ultraviolet-visible spectroscopy
<b>V</b>	Volume
<b>W</b>	Weak absorption peaks
<b>X<sub>A</sub></b>	Atomic sensitivity
<b>X<sub>g</sub></b>	Gravimetric sensitivity
<b>X<sub>M</sub></b>	Molar sensitivity
<b>XRD</b>	X-ray Diffraction
<b><math>\alpha</math></b>	Dissociation constant of complexes
<b><math>\beta</math></b>	Stability constants of complexes
<b><math>\delta</math></b>	Dislocation density
<b><math>\lambda_{\max}</math></b>	Wavelength greatest
<b><math>\mu_{\text{eff}}</math></b>	Magnetic moment

## **Abstract**

The study involved the preparation and characterisation of a new hetero cyclic azo ligand 2-[2'-(5- methylthiazolyl) azo]-5-,6-dimethyl benzoimidazol derived from 2-amino-5-methyl thiazole. A series of metal complexes were prepared with the metal ions Co(III), Ni(II), Cu(II), Ag(I), and Au(III).The prepared compounds were identified by FTIR spectra, <sup>1</sup>HNMR , <sup>13</sup>CNMR spectra, mass spectrometry, UV-Vis spectrometry, TGA technique, FESEM ,and XRD spectroscopy as well as elemental microanalysis (C.H.N.S).

The results showed the azo ligand 2-[2'-(5- methylthiazolyl) azo]-5-,6-dimethyl benzoimidazol behaves as a bidentate ligand. The molar ratio of the studied metal ions Co(III) and Cu(II) in their coordination complexes were determined (1:2) [ M:L], and the expected shape of these complexes is octahedral. On the other hand, the Ni(II), Ag (I), and Au (III) were (1:1) [M: L] and the expected shape of these complexes were tetrahedral with ion Ag(I), and square planar with Ni(II), Au(III) ions.

Finally, the new azo ligand and its metal complexes were tested in vitro for antimicrobial activity against two types of bacteria (*Streptococcus*, *Escherichia coli*) and one type of fungus (*Penicillium sp*).

Toxicity examinations of some compounds prepared on human cells for cancer (lung, and pancreas) were studied to find out the possibility of using this type of compound as a drug by treating it with human cancer cells.

# *Chapter One*

*(Introduction)*

## 1.0 Introduction

### 1.1. General Introduction

Coordination chemistry is the study of compounds in which metal ions are coordinated to ligands with neutrality or negatively charged atoms that contribute electrons to the metallic. Nobel Prize winner Alfred Werner (1866-1919) made the first significant contribution to the discovery of this field of chemistry in 1913 with his coordination theory of metal-ammine complexes like  $[\text{Co}(\text{NH}_3)_6\text{Cl}_3]$  [1].

Coordination compounds are significant to researchers and scholars because of the important roles in analytical chemistry, medicine, agriculture, and industry [2],[3]. Coordination theory among the metallic and the ligand can be interpreted as a Lewis (acid-base) interaction, where by a ligand that has a non-bonding electron pair (Lewis base) is shareable with the metal ion has empty orbitals to accommodate the electron pair of the ligand (Lewis acid) [4],[5].

Compounds containing sulfur and nitrogen have occupied great importance among several organic compounds, so these compounds are vital. It was found that some of them have essential significance and great effectiveness against tumors, fungi, bacteria, HIV, and as inhibitors of the beta-lactamase enzyme in life interactions [6].

### 1.2. Azo Compounds

Peter Geriss discovered this type of organic compound in 1858 [7]. The association of two nitrogen atoms in the molecule is double bound. They get hold of the basic configuration of  $(\text{X}-\text{N}=\text{N}-\text{X}')$ , while X and X' can be aliphatic or aromatic moieties. If substituents are aliphatic; in this case, compounds are named aliphatic azo compounds [8]. These are least preferable as compounds because of their rapid disintegration into nitrogen and hydrocarbons and are not stable. When substituents

are aromatic; in this case, compounds are named aromatic azo compounds. When the R groups are aryl rings, the aromatic azo compound structure is more stable than when the R groups are alkyl, because the aryl groups include the (-N=N-) group in an extended delocalized system [9].

The first type of azo dye was prepared in 1862 when (Martins) prepared a dye (Bismarck Brown) [10] illustrated in Figure (1.1).

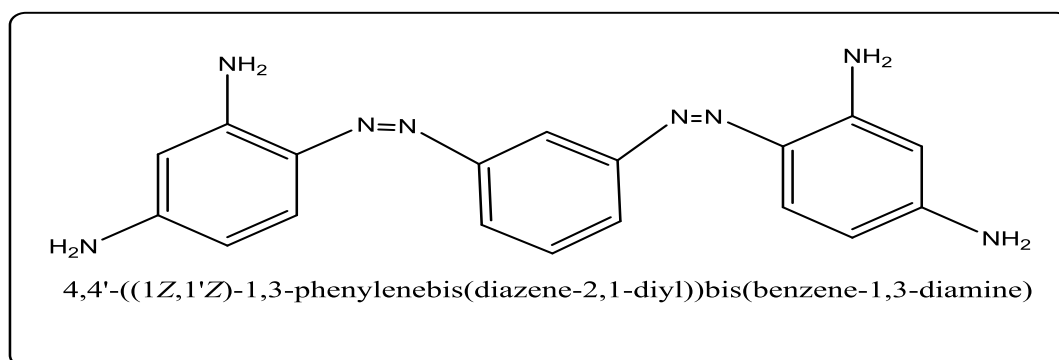


**Figure 1.1:** (Bismarck Brown) structure [10].

The aromatic azo compounds are highly colored and stable. These are the most critical and widespread azo compounds because they contain the powerful double bond azo moiety, the difference of the associated groups on both sides of the azo moiety, and the number of these groups [11],[12]. Figure (1.2) illustrated the resonance phenomenon of azo dyes.

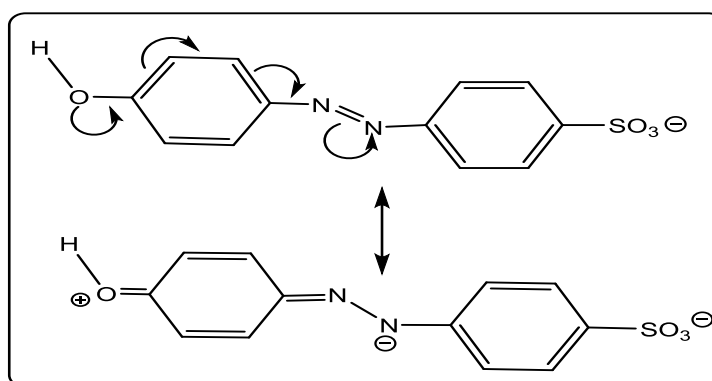


**Figure 1.2:** Resonance phenomenon of azo dyes [12].

### 1.2.1. Synthesis of azo compound

Diazotization and azo coupling are the two steps of a consistent chemical sequence utilized for creating azo compounds on an industrial scale [13]. In the process of diazotization, primary aromatic amines are converted into aryl diazonium salts, which, are stable at 0°C, a primary amine is altered into a diazonium ion. The azo compounds are synthesized by reacting the diazonium salt with a coupling component such as phenol, this process is known as "azo coupling" [14].

### 1.2.2. Classification of azo compounds

The azo-aromatic compounds are also classified into two classes, depending on the rings attached to the two ends of the azo group. They are homocyclic azo compounds whose aromatic rings do not contain hetero atoms such as (N, O, S) as azobenzene and its derivatives [15]. The (*E*)-8-(*p*-tolyl diazenyl)naphthalen-2-ol is one of the examples, as shown in Figure (1.3) and it is one of the most widely used classes of azo compounds due to its diverse applications in various fields such as medical and industrial fields [16].

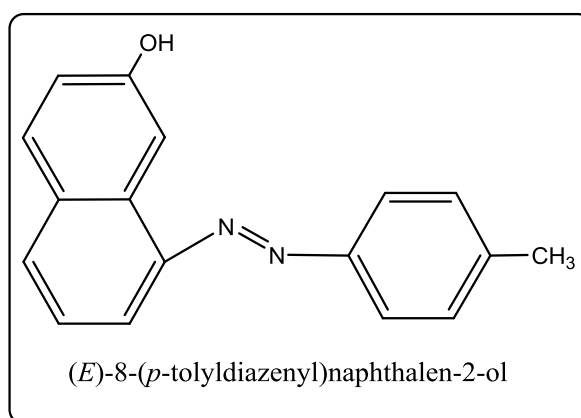


**Figure 1.3:** Homocyclic azo compound [16].

Heterocyclic azo compounds, which contain one or both ends of the azo group on heterocyclic aromatic rings containing one or more heteroatoms (N,O,S), which are

widely used as reagents in the field of analytical chemistry for spectroscopic determination of many chemical elements, where they have received a great deal of attention due to their high selectivity and sensitivity [17] Figure (1.4) shows one example of a heterocyclic azo compound [18].

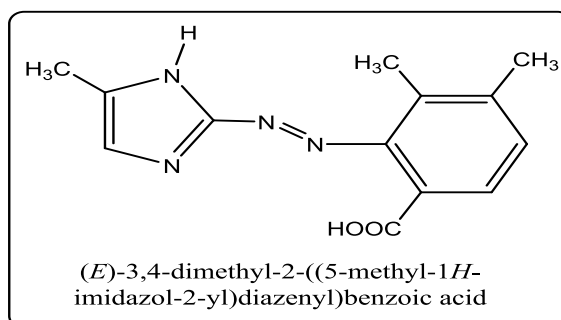


Figure 1.4: Heterocyclic azo compound [18].

### 1.3. Classification of Azo Compounds according to azo grouping number

The azo compounds can be classified according to the number of the azo group it includes into (mono-azo) compounds, (di-azo) compounds, and (tri-azo) compounds [15].

#### 1.3.1. The monoazo dyes

The monoazo dyes can be schematically represented by the following formula:  $Z-N=N-W$ . Z and W the benzene or heterocyclic derivatives. S. Prakash, et al were synthesized novel azo incorporated heterocyclic bioactive compounds via diazo-coupling reaction between the 2-amino benzothiazole and phenolic antioxidant molecules like 2,4-di-*tert*-butylphenol as shown in Figure (1.5) [19],[20].

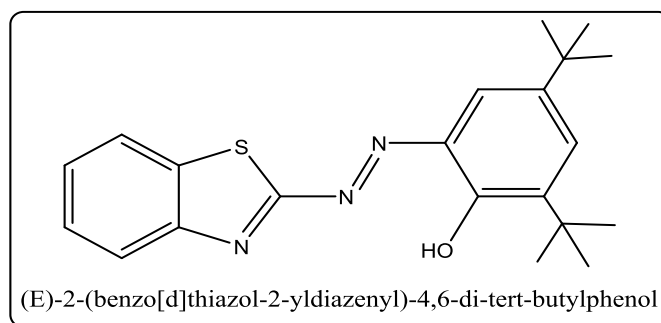


Figure 1.5: Mono azo dyes structure [20]

### 1.3.2. Diazo dyes

In general, diazo dyes are composed of two groups  $-N=N-$ , its colors range from yellow, orange and blue. The blue direct dye, for example, has a benzidine function in its molecule [21], [22]. Figure (1.6) shows the diazo dyes compound.

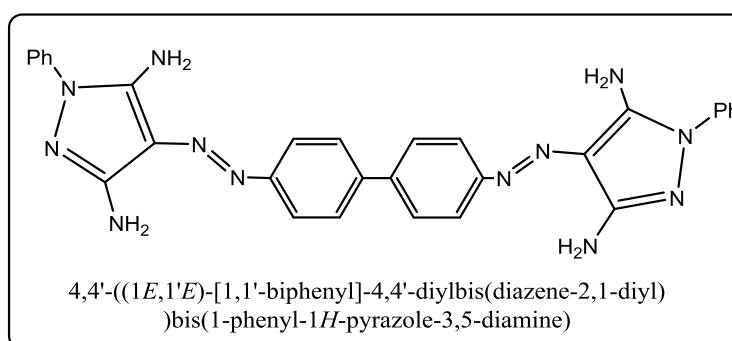


Figure 1.6: Diazo dyes structure [22]

### 1.3.3. Poly azo dyes

Polyazo dyes are complex dyes that contain the azo group three or more times in the same molecule [23], [24]. Figure (1.7) shows the poly azo dyes structure.

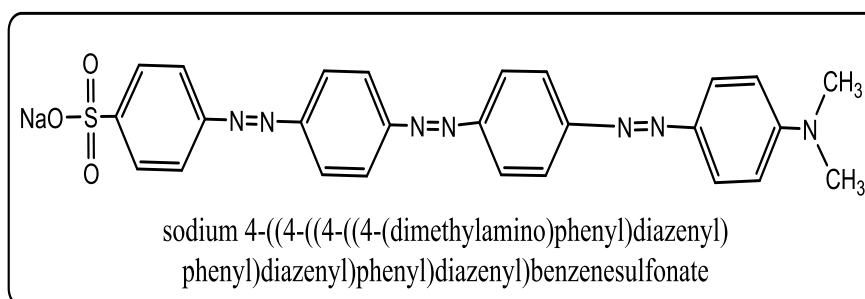


Figure 1.7: Polyazo dye structure [24]

## 1.4. The Chelating Behavior for Azo compound

Azo compounds are divided into three types in terms of how they bind to metal ions.

### 1.4. 1. Monodentate Ligand

These reagents are mono coordinate, meaning they can only make covalent bonds with metal atoms on one side, so this type of reagent is weak, and the complexes resulting from its association with the metal ions are unstable [25], [26]. Figure (1.8) shows the connection method of the monodentate reagent.

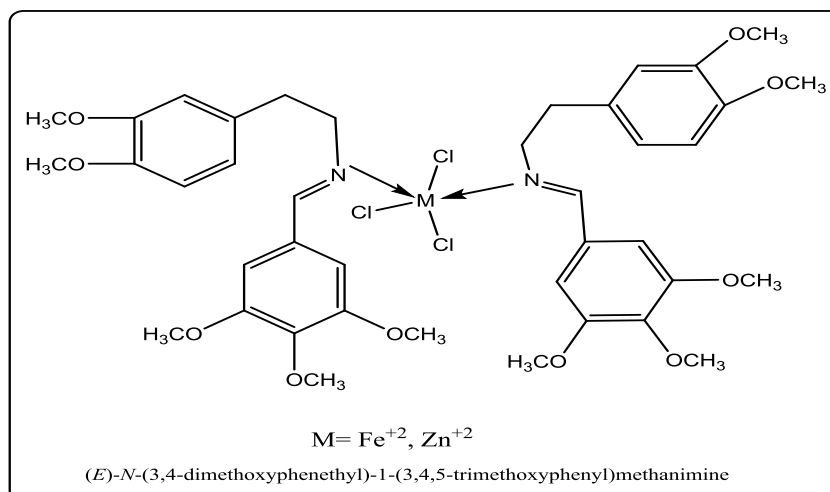
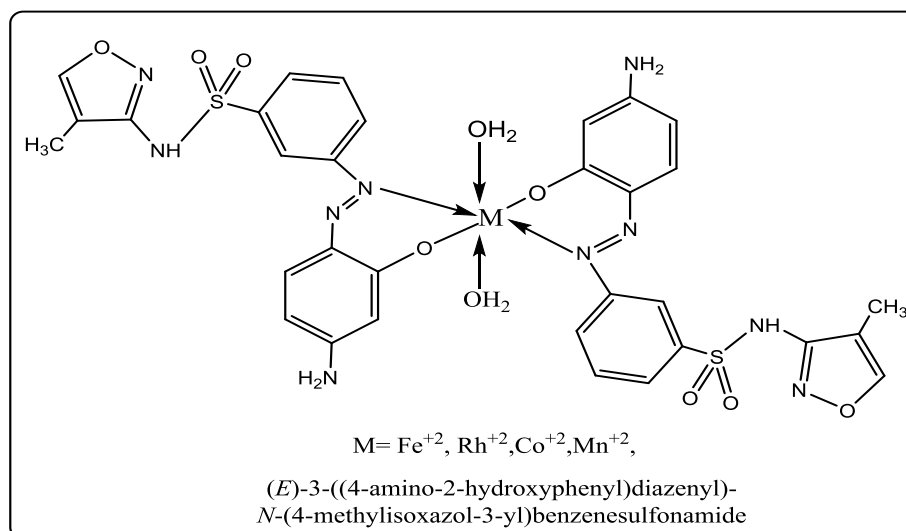


Figure 1.8: Mono dentate reagent structure [26].

### 1.4.2. Bidentate reagent

They are the reagents coordinate with the metal ions by means of the nitrogen atom, the heterocyclic ring or any substituted group on the ring is linked by one hand, and the nitrogen atom of the group so far from the ring, so that the azo group is within a total ring. The complex of this type is more stable than the complexes of monodentate ligand [27], [28]. Figure (1.9) shows the coordinates of this reagent with different metal ions as following form.



**Figure 1.9:** Bidentate reagent structure [28].

### 1.4.3. Tridentate reagent

The metal ion is linked with the reagent through three sites: the first is the nitrogen atom of the heterocyclic ring. The second is the nitrogen atom of the azo group far from the heterogeneous ring, as for the third symmetry site it is replaced by a basic or acid group at the ortho site relative to the bridge azo group which has the ability to lose its proton. This link leads to the formation of a pentagonal ring, and in this case, the complexes formed have high stability compared to their counterparts in the first and second types [29], [30] and the most prominent reagents of this type are shown in the Figure (1.10).

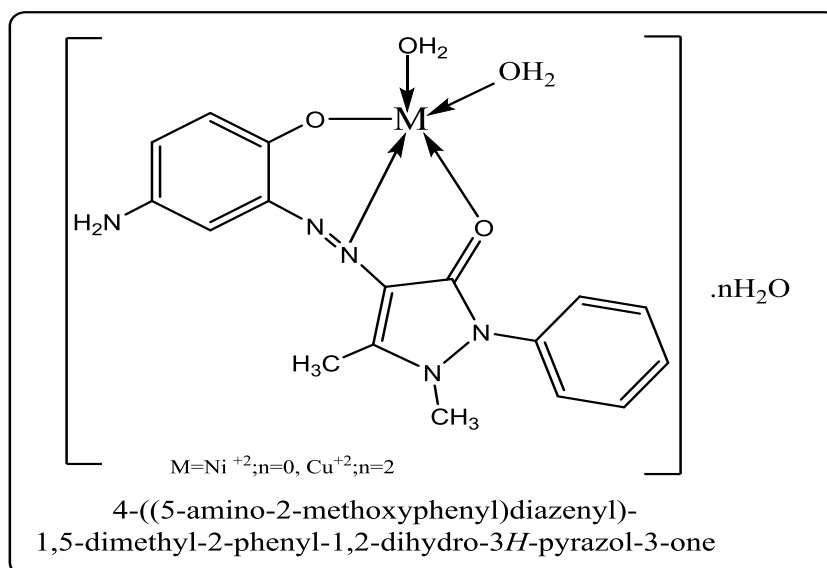


**Figure 1.10:** Tridentate reagent structure [30].

## 1.5. Applications of azo dyes

Dyeing textiles, leather, paper, food, cosmetics, and medicines are some of the many uses for this highly diverse synthetic dye (-N=N-). Other typical applications include pharmacology, pharmaceuticals, cancer in living cells, hypnotic medicines, plastics, biology, and advanced technology applications like nonlinear optical systems and lasers [31]. In addition, azo dyes are useful in liquid crystals and nanotubes due to their physicochemical stability and unique optical characteristics. Recently, azo-functionalized dyes containing aromatic heterocyclic compounds have gained popularity due to their abundance of color options, brightness, ease of production, and effective dyeing properties [32].

### 1.5.1. Biological activity of azo dyes

Various pharmaceutical and biological uses for heterocycle azo dyes have been explored, including their antibacterial, antioxidant, anticancer, antitumor, and anti-inflammatory activities, heterocyclic are essential components of the azo dyes [33].

### 1.5.2. Antibacterial activity

Antibacterial efficiency of azo modified phenolic compounds was (4a-4d) studied against human pathogenic bacterial strains such as two gram-positive bacteria *Bacillus subtilis* (*B. subtilis*), *Staphylococcus aureus* (*S. aureus*) and two gram-negative bacteria *Pseudomonas aeruginosa* (*P. aeruginosa*), *Escherichia coli* (*E. coli*) [34].

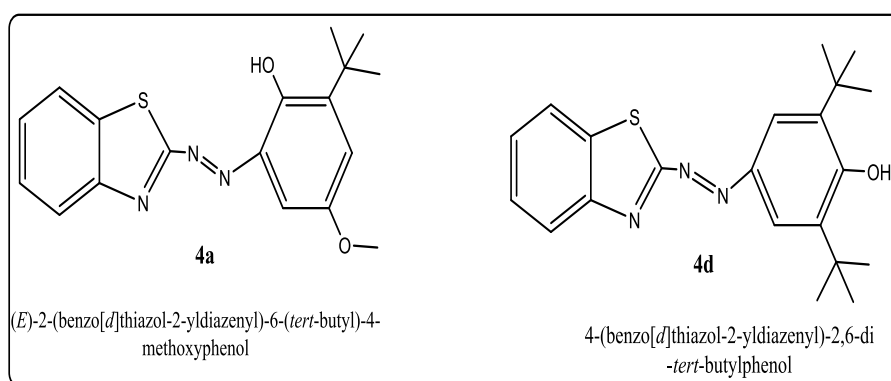


**Figure 1.11:** Structures of heterocyclic-modified azo dye derivatives with antibacterial activity [34].

### 1.5.3. Antifungal activity

Novel S-heterocyclic azo dyes made from 1, 3-benzothiazole-2-thiol with different amines using the diazo-coupling process were recently described by M. N. Matada, K. Jathi, M. M. Rangappa, K. Geoffry, S. Ravi Kumar, R. B. Nagarajappa, and F. Noor Zahara [35]. The azo compounds generated from benzothiazole against *Candida albicans* and *Aspergillus flavus*, the results showed a correlation with fluconazole regarding microbial inhibition. Promising outcomes were observed in Figure (1.12).

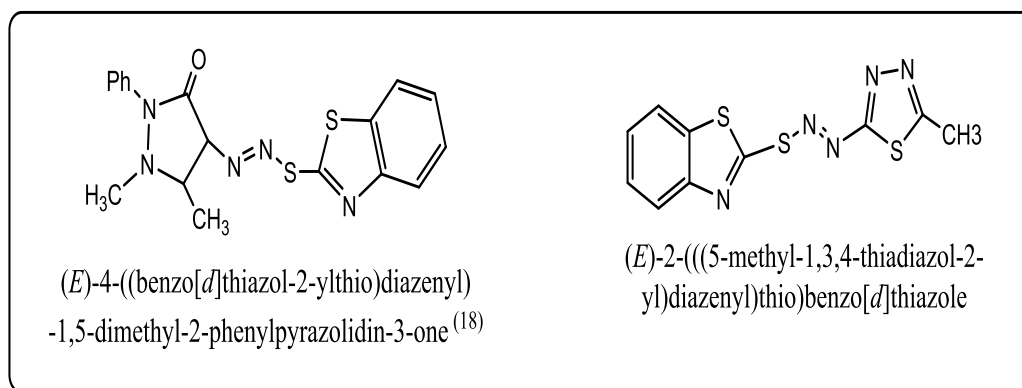


**Figure 1.12:** Derivatives of azo dyes that are active against fungi [35].

### 1.5.4. Anticancer activity

M.R. Maliyappa, J. Keshavayya, N.M. Mallikarjuna, and I. Pushpavathi created and reported novel heterocyclic azo dyes with anticancer activity using a standard diazo-coupling method. Human cancer cell lines such as the colon (HCT116), lung carcinoma (A549), T-lymphocyte (Jurkat), and chronic myeloid leukemia (K562) were used to test the compounds' anticancer potential. The 5-methyl-2-(5-methyl-benzothiazol-2-yl)-4-p-tolylazo-1,2-dihydro-pyrazol-3-one and 4-(4-bromophenylazo)-5-methyl-2-(5-methyl-benzothiazol-2-yl)-1,2-dihydropyrazol-3-one displayed good effectiveness in inhibiting the formation of cancerous cells [36], Figure (1.13).

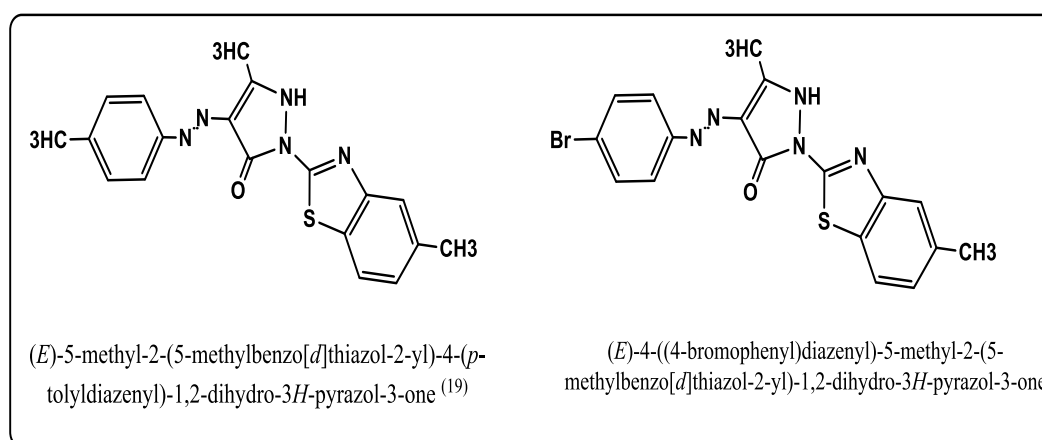


**Figure 1.13:** Anticancer azo dye derivatives with heterocyclic scaffolds and their chemical structures [36].

## 1.6. Imidazole compound

Imidazole contains five-heterocyclic rings containing amino groups and an additional nitrogen atom [37]. Imidazole is a crystalline solid that dissolves in water and has a melting point of 90° C. It was prepared for the first time in 1855 by scientist Debus [38], and its molecular formula is C<sub>3</sub>H<sub>4</sub>N<sub>2</sub>, as shown in Figure (1.14).

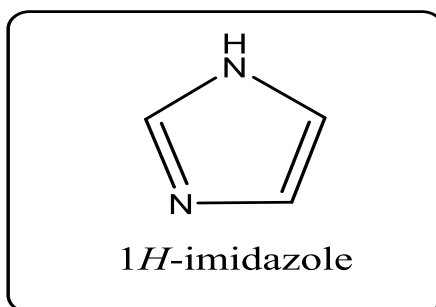


**Figure 1.14:** 1H- imidazole [38]

Natural products and various bioactive compounds in human metabolism often contain imidazole rings. The imidazole ring is present in numerous biological molecules like histamine, vitaminB12, deoxyribonucleic acid (DNA), and hemoglobin, suggesting that it plays an important role in the physiological action of these molecules [39].

The active sites in the imidazole ring are (2, 4) and the electrophilic attack occurs on these two sites, and the diazonium salt is coupled at site (2) to give bright red dyes [40]. Azo imidazole ligand is prepared and substituted at sites (4) and (5) with good yield and high purity [41], as shown in Figure (1.15).

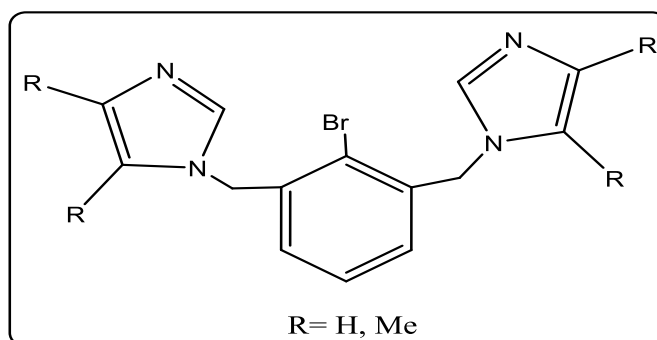


**Figure 1.15:** Substituted imidazole azo ligand [41].

N. N. Kumar Reddy, S. N. Rao, C. Ravi, and S. Adimurthy and method was used to prepare imidazole derivatives by mixing [3+2] cyclization of vinyl azides with amidines and then oxidative cyclization of amidines with vinyl azides in the presence of 1,8-diazabicyclo [5.4.0] undec-7-ene (DBU) in  $\text{CH}_3\text{CN}$  as solvent [37], the reaction mixture shown in Figure (1.16):

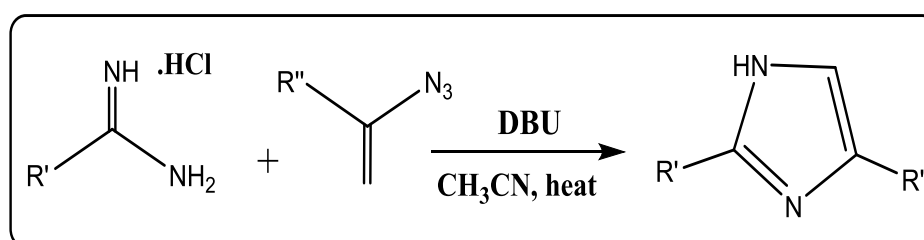


**Figure 1.16:** Preparation of imidazole derivatives [37].

Benzimidazole is a heterocyclic aromatic organic compound. It is an important pharmacophore and a privileged structure in medicinal chemistry. This compound is bicyclic in nature which consists of the fusion of benzene and imidazole. Benzimidazole can act as similar to purines to elicit some optimum biological responses.

## 1.7. Thiazole chemistry

Thiazole is a five-membered heterocyclic ring containing nitrogen and sulfur and belongs to the family of azole heterocycles [42]. It was first discovered by Hantzsch

and J.H. Weber in 1887, then described it as “the pyridine of the thiophene series”[43]. It has two groups: C=N, an electron-accepting group, and an (-S-), electron-donating group. As it delocalizes a lone pair of electrons from the sulfur atom [44]. Hence the name thiazole, where the part (thia) refers to the sulfur atom, while the part (az) refers to the nitrogen atom, and the part (ole) indicates the presence of a five ring. Thiazole has a boiling point of (116-118° c), free thiazole is a pale yellow, flammable liquid with an odor similar to pyridine [43]. Figure (1.17) clarifies the thiazole structure.

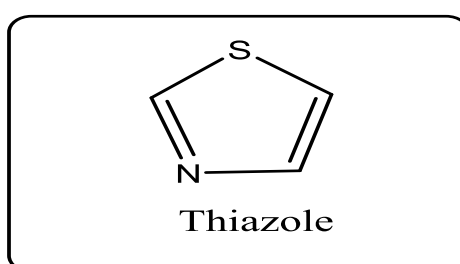


**Figure 1.17:** 1, 3-thiazole structure [43].

### 1.7.1. Synthesis of thiazole

Thiazole ring can be synthesized using the most common and oldest method developed by the German scientist Hantzsch. This method involves  $\alpha$ -halocarbons and many reactants with the N-C-S fraction engaging in a cyclic reaction, like thioamides, and thiourea [45]. The mechanism of preparing thiazoles from  $\alpha$ -halocarbons with thioamides is summarized by attacking a nucleophile by the sulfur atom in the thioamide to the  $\alpha$ -carbon of the  $\alpha$ -halocarbons resulting of an intermediate compound [43], as shown in the following Figure (1.18):

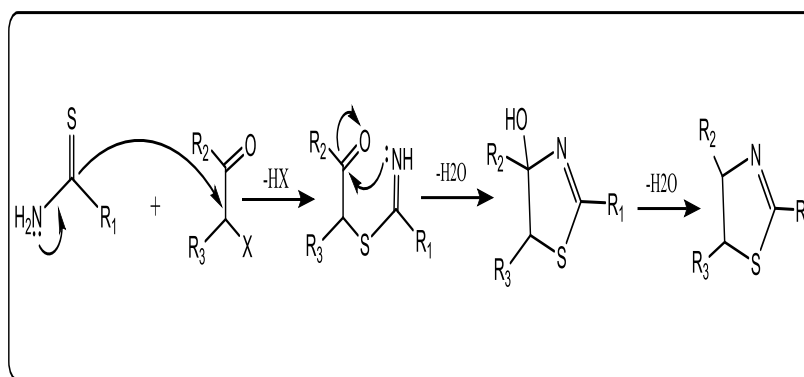


**Figure 1.18:** Hantzsch thiazole synthesis reaction mechanism [43].

### 1.7.2. Application of thiazolyl azo compounds

Thiazoles and their derivatives are characterized by their wide applications in many fields, including medicine. The substituted benzothiazole compound was also used in the formulation of many drugs used to treat many diseases, such as arthritis, asthma, stomach ulcers, and cancer diseases, which attracted the interest of many researchers to study the biological effect of these compounds and their ability to inhibit malignant tumors [46].

In the industry field, thiazoles and their derivatives were used as chromogenic reagents for dyeing textiles, such as polyester, acrylic, nylon threads and were used as indicator. Figure (1.19) shown chemical structure of azo amino thiazole disperse dye [47].

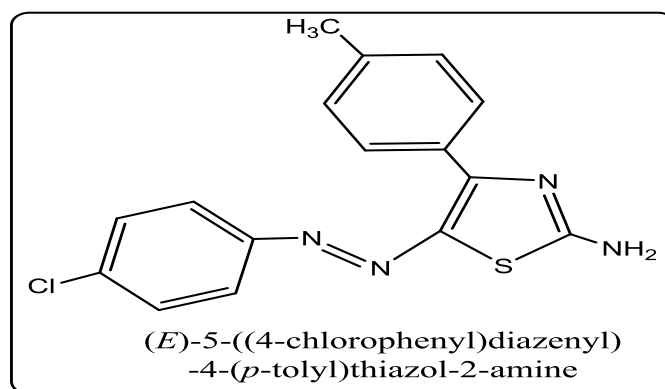


**Figure 1.19:** Chemical structure of azo amino thiazole disperse dye [47].

Thiazolyl azo and their derivatives have important uses in different fields, they used to determine for many metal ions. Thiazole azo dyes have been used for many applications such as, biological activity, analytical reagents, and the clinical field. Because of their interesting biological activity, many studies have been carried on the reactions of heterocyclic thiazole azo dyes and their metalchelates [48].

In 2023 Khalid J. AL- Adilee, and H.A.K. Kyhoiesh were prepared of some transition metallic complexes of new thiazolyl azo ligand of 2-[2' -(6-methoxybenzothiazolyl)azo]-5-dimethylamino benzoic acid (6- MBTADB) with Pt(IV) and Au(III) at (M:L) ratio (1:1). Thiazolylazo ligand complexes are studied on the basis of their analytical, spectroscopic, magnetic susceptibility and conductance data. The stability constants of prepared complexes have been determined by spectrophotometric method. The Au(III) complex structure [49], as shown in Figure (1.20).

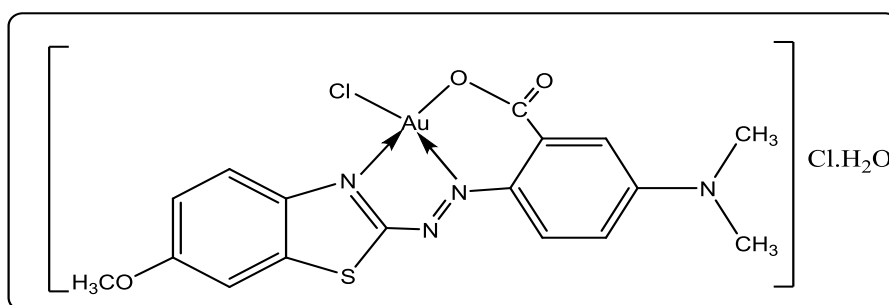


**Figure 1.20:** Au(III) complex with (6- MBTADB) Structure [49].

Khalid J. AL- Adilee, A. K. Abass, and A. M. Taher were prepared a new heterocyclic thiazolyl azo dye ligand, 2- [2- (4, 5- dimethyl thiazolyl) azo] -4-EthoxyPhenol (DMeTAEP), by the diazotization of 4.5-dimethyl thiazolylazonium chloride and coupling with 4-Ethoxy phenol in alkaline alcoholic solution under suitable optimized experimental conditions to yield a new azo dye ligand . The complexes were prepared from Co(III), Ni(II), Cu(II) , Zn(II), Cd(II), and Hg(II) ions

All the compounds were confirmed by XRD, SEM, (TG-DTG) thermal analysis,  $^1\text{H}$ -NMR, UV-vis, mass and FT-IR spectroscopic methods [50], the complex structure is shown in Figure (1.21) .

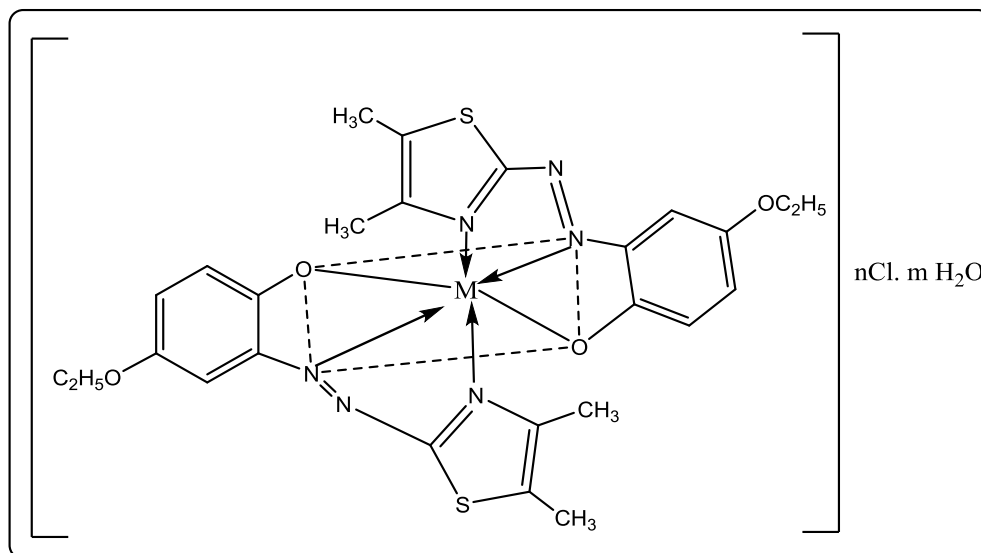


**Figure 1.21:** The chemical structure of metal chelate complexes DMeTAEP where M = Co(III), Ni (II) , Hg (II) , Cu(II) , Zn (II) and Cd (II) [50].

Later, in 2021, Khalid J. AL- Adilee, and Azal S. Waheeb , also synthesised a novel heterocyclic azo dye ligand 2-[2- (4,5-Dimethyl thiazoly)azo]- 4-methoxy phenol (DMeTAMP) which prepared by coupling reaction between diazonium salt produced from diazonited 2-amino- 4,5-dimethyl thiazole with 4 –methoxyphenol . The structures of the azo dye ligand and the metallic complexes were characterized by elemental microanalyses (C.H.N.S),  $^1\text{H}$  and  $^{13}\text{C}$ - NMR, UV-Vis spectroscopy, and FT-IR spectroscopy. The results showed that prepared complexes with [1:2] metal-ligand ratios and the ligand behaved as tridentate chelating [48]. The complex structure is shown in Figure (1.22).

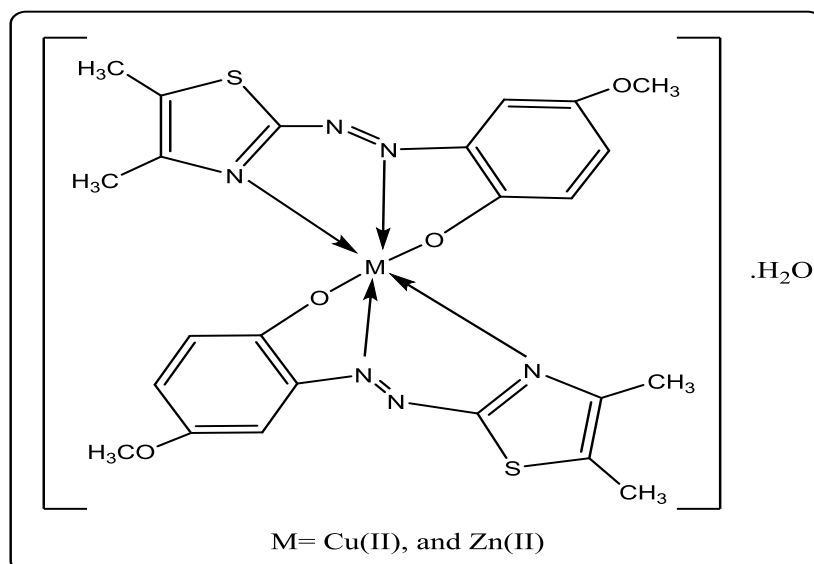


**Figure 1.22:** The chemical structure of metal chelate complexes DMeTAMP where M = Cu(II), Mn(II), and Zn(II) [48]

### 1.8. Biological Activity

Heterocyclic compounds are found in macromolecules like enzymes, vitamins, natural products, and biologically active substances, they are a vital component in medical chemistry [51]. A literature survey shows that thiazole and imidazole derivatives exhibit anti-fungal, anti-inflammatory, anti-bacterial, anti-allergic, herbicidal, and anti-cancer activity [52].

Thiazoles have been known for their broad uses in the medical and pharmacological fields. It has been used as an analgesic, anti-inflammatory, heart stimulant, antifungal, anti-coagulant, and antitumor [53]. 2-Aminothiazole is the starting material for synthesizing many compounds, including sulfuric drugs and fungicides, and can be used as a thyroid inhibitor in treating hyperthyroidism [54].

Thiazole compounds have proven their therapeutic effectiveness as they are considered antimicrobials, so the scientist Bradshaw prepared a number of its thiazole derivatives, including 2-(4-amino phenyl benzo thiazole) [55], the formula is shown in Figure (1.23).

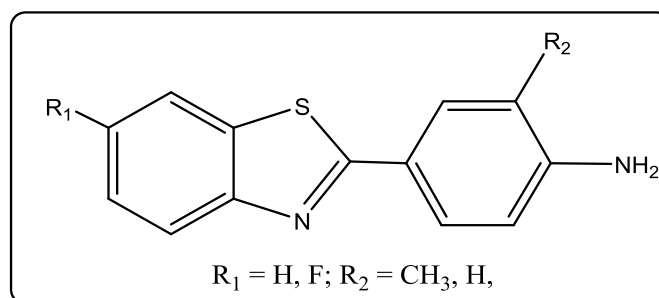


**Figure 1.23:** 2-(4-amino phenyl benzo thiazole) structure [55].

Recent studies have shown that many microorganisms, including bacteria and fungi, cause diseases that are effectively affected by organic and inorganic chemical compounds. In these studies, one type of fungus such as **Penicillium sp.**, In addition, two types of bacteria were utilized with the initial one **Staphylococcus aureus (S. aureus)**, gram-positive bacterium and the other **Escherichia Coli (E. coli)** gram-negative [56].

Bacteria are single-celled primitive microorganisms that exist in several forms, including spherical, bacilli, and spiral, as they are considered one of the pathogens of human diseases. Bacteria enter the food manufatures and pharmaceutical industries. In terms of nutrition, they are autotrophic and non-autotrophic [57].

As for fungi, they are living organisms Eukaryote, carrying spores similar to algae. However, unlike alga, fungi don't posses chlorophyll, and inhabit the same environment as humans. Due to the absence in their cells, fungi rely on autotrophs for sustenance, leading to parasitic life. Fungi reproduce in several ways, such as through binary fission, budding or formation of asexual spores, additionally some fungi reproduce sexually by producing sexual spores [58].

## **1.9. Cancerous tumor**

Cancer in the organs of the human body is a big hazardous health risk whose limitations subjected to hyperthermia therapy should be studied carefully .Cancer is the main cause of death in many countries [59].

Tumours are pathological cellular growth disturbances characterized by uncontrolled and abnormal cell division. Tumours are solid or fluid-filled lumps of abnormal tissue [60]. Solid tumors account for 85% of human cancers, benign tumours do not spread to other parts of the body after removal. However, malignant tumours develop rapidly and invade adjacent tissues, allowing tumour cells to enter the circulatory and lymphatic systems and spread to other body parts [61]. Will be discussed below:

### **1.9.1 Lung cancer**

Lung cancer is caused by abnormal, uncontrolled development of cells in the lungs. This expansion can cause metastasis, invade adjacent tissue, and spread beyond the lungs. Lung epithelial cells cause most primary lung cancers. Lung cancer is the primary killer of males and females compared to other cancers worldwide [62]. Non-small cell (NSCALC) and small-cell (SCALC) lung carcinoma are the two most common forms of lung cancer, characterized by the size and appearance of the malignant cells viewed by a histopathologist under a microscope. Cancer of the small cells of the lung (SCLC) spreads rapidly. It has a significantly greater rate of spread than non-small-cell lung cancer [63]. Mainly, smoking is considered as one of the most critical risk factors for lung cancer, as well as exposure to radon gas or asbestos; patients with lung cancer typically have symptoms, mainly cough. Hemoptysis in

combination with weight loss, loss of appetite, or shortness of breath [64] Figure (1.24) shows Lung cells and tissues infected with a cancerous tumor.

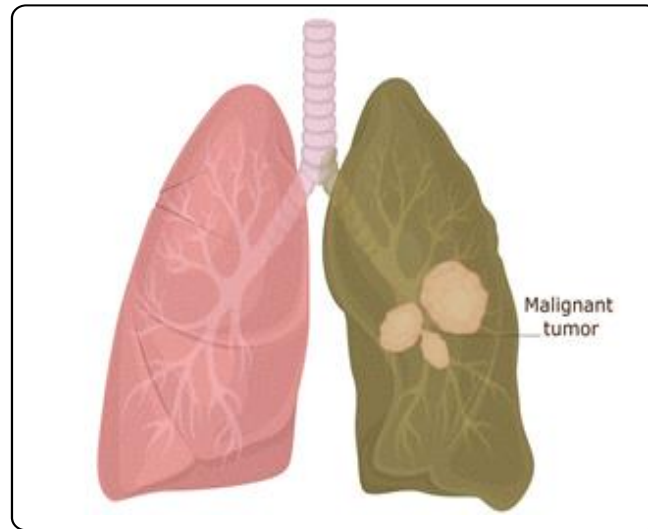


**Figure 1.24:** Lung cells and tissues infected with a cancerous tumor [64].

### 1.9.3. Pancreas cancer

Pancreas cancer is one of the most aggressive and deadly malignant neoplasms. By 2030, it is expected to overtake colorectal, breast, and prostate cancers to become the second most common cause of cancer-related deaths [65]. Just 6.2% of cases of early-onset pancreatic cancer occur before the age of 50, making it a disease mainly affecting the elderly [66]. The median age of diagnosis is 68 years old. Among lifestyle risk factors, diets rich in processed meat, high-fructose drinks, and saturated fat were linked to obesity and diabetes, as well as alcohol and cigarette smoking [67]. Figure (1.25) shows pancreatic cells and tissues infected with a cancerous tumor.

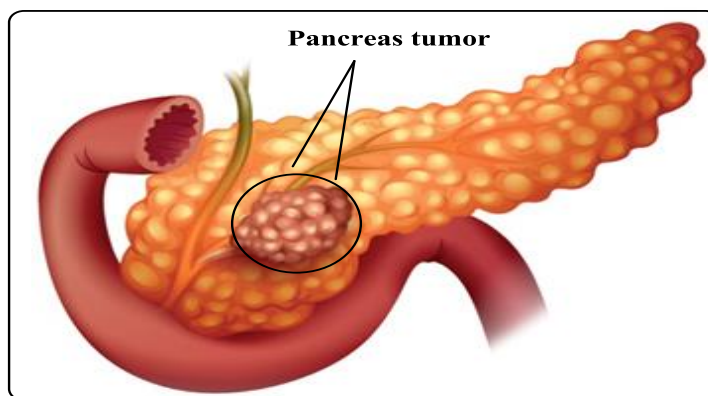


**Figure 1.25:** Pancreatic cells and tissues infected with a cancerous tumor [67].

### 1.10. MTT Assay

The MTT assay is a sensitive and reliable indicator of the cellular metabolic activity. The assay relies on the reduction of MTT, a yellow water-soluble tetrazolium dye, primarily by the mitochondrial dehydrogenases, to blue colored formazan crystals [68]. The percentage of live cells is calculated through a colorimetric test for evaluating the activity of cellular enzymes; as a result, increasing the intensity of the blue color means obtaining a more significant number of living cells. The reason for the color change is the production of mitochondria, the dehydrogenases enzyme, which breaks the tetrazolium ring of the MTT dye [69]. Figure (1.26) shows the mechanism of action of MTT dye.

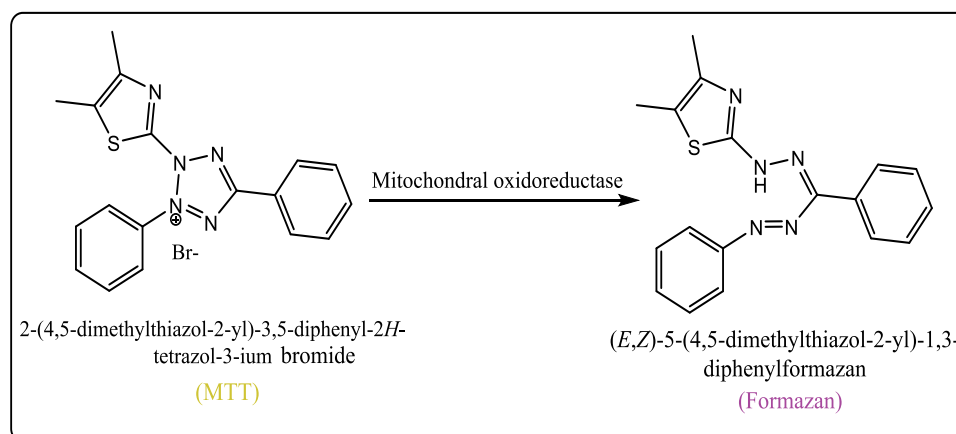


**Figure 1.26:** Mechanism of action of (MTT) dye [69].

### 1.11. The aim of the study

Following is an overview aim of this study:

1. Synthesis of new heterocyclic thiazolyl azo dye ligand with several coordinating complexes of cobalt (III), nickel (II), copper (II), silver (I), and gold (III) ions.
2. Characterizing the prepared compounds through different techniques: C.H.N.S analysis and some spectroscopies like  $^1\text{H-NMR}$ , FT-IR,  $^{13}\text{C-NMR}$ , Mass Spectrometer, UV-Vis and TGA analysis.
3. The investigation of stability of the prepared thiazolyl azo ligand and its corresponding complexes.
4. Studying the crystal structure and structural properties such as crystal size, crystalline phase, and calculating the (d-spacing) between the ligand and its metallic complexes prepared using X-ray diffraction.
5. Studying the surface properties of each ligand and its prepared metallic complexes, surface structure, shape and size of nanoparticles, and the distribution of crystals and clusters using the scanning electron microscope technique in the emitted field.
6. Studying the biological effects of each of the ligands and their metal complexes prepared to evaluate the possibility of using them in the medical field, their influence on inhibiting the growth of different types of bacteria (**Streptococcus**, **Escherichia coli**) and inhibiting the growth of pathogenic fungi (**Penicillium sp**) that cause many common diseases. Studying toxicity tests of certain compounds prepared in this study on human cells assessing the potential for their use as pharmaceuticals for cancer treatment by studying cancerous and healthy cells to compare and determine the feasibility of using these compound in the medical and pharmaceutical aspects.

# *Chapter Two*

*(Materials and methods)*

## 2.0 Materials and methods

### 2.1. Materials

All chemicals were of reagent quality and were utilized without additional purification. Table (2.1) displays the chemicals used in the study.

**Table 2.1:** Chemical materials used in this work and manufacturing companies.

No.	Chemicals	Structure formula	Company	Purity%
1	2-amino-5- methyl thiazole	C <sub>4</sub> H <sub>6</sub> N <sub>2</sub> S	Sigma-Aldrich	98%
2	Ammonium acetate	CH <sub>3</sub> CO <sub>2</sub> NH <sub>4</sub>	Fluka	99%
3	Cobalt(III) chloride hexahydrate	CoCl <sub>2</sub> .6H <sub>2</sub> O	Ridel- deHaën	99%
4	Copper(II) chloride hexahydrate	CuCl <sub>2</sub> .6H <sub>2</sub> O	MERCK	99.9%
5	5,6-dimethylbenzimidazole	C <sub>9</sub> H <sub>10</sub> N <sub>2</sub>	Sigma-Aldrich	98%
6	Dimethyl sulfoxide(DMSO)	C <sub>2</sub> H <sub>6</sub> SO	B.D.H	98%
7	Ethanol	C <sub>2</sub> H <sub>5</sub> OH	J.T.BAKER	99.9%
8	Hydrochloric acid	HCl	B.D.H	37%
9	Hydrogen tetrachloroaurate (III) trihydrate	H [AuCl <sub>4</sub> ]	Glenthams life sciences Ltd	99.9%
10	Nickel(II) chloride hexahydrate	NiCl <sub>2</sub> .6H <sub>2</sub> O	MERCK	99.9%
11	Silver Nitrate	AgNO <sub>3</sub>	B.D.H	99%
12	Sodium hydroxide	NaOH	B.D.H	98%
13	Sodium nitrite	NaNO <sub>2</sub>	B.D.H	98%

## **2.2. Apparatuses**

The following apparatuses have been used for the spectral, physical, analytical, and thermal measurements as well as the magnetic properties to identify the prepared ligand and its metallic complexes. The biological activity of the azo dye ligand and metallic complexes prepared with some antimicrobials were studied. In addition these compounds are used as anti-cancers, as follows:

### **2.2.1. UV-Visible spectrophotometer**

The electronic spectra have been measured for the synthesis compound in ethanolic solution by using a PerkinElmer Ultra Violet-Visible Spectrometer Lambda 35 in the range (200–1100 nm) in the Laboratory of Science College, Department of Chemistry, AL-Muthanna University.

### **2.2.2. FT-IR spectra**

The infrared spectra were recorded from a KBr disc (100 - 1mg) of the solid ligand and metallic complex using a (Shimadzu, FT- IR 8400S Spectrophotometers) at the range (400 -4000)  $\text{cm}^{-1}$  in the Chemistry Laboratory at AL-Muthanna University.

### **2.2.3. $^1\text{H}$ and $^{13}\text{C}$ -NMR Spectroscopy**

The spectra of nuclear magnetic resonance for the prepared ligand and some of the prepared metallic complexes using a 500 MHZ spectrophotometer utilizing DMSO- $\text{d}^6$  as a solvent and quaternary (TMS) silane as a standard reference at Mashhad University of Medical Sciences in Tehran, Iran.

#### **2.2.4. Mass Spectra**

The mass spectra of the synthesized ligand and some of its metallic complexes were determined on a Mass AB Sciex 3200 QTRAP machine at Mashhad Iran University of Medical Science, in Tehran.

#### **2.2.5. Micro Elemental analysis C.H.N.S**

Elemental analysis of ligand and metallic complexes utilizing EA 300 (CHNS) element analyzer. This apparatus has been used for finding the percentage of carbon, hydrogen, nitrogen, and sulfur elements in both ligand and their prepared solid complexes assessed at the University of Isfahan in the Islamic Republic of Iran.

#### **2.2.6. Melting Points**

The SMP, Stuart instrument was applied to determine of the melting point or decomposition temperature for the azo dye ligand and their metal chelates.

#### **2.2.7. Atomic Absorption Apparatus**

Metal content of Co(III), Ni(II), Cu(II), Au(III), and Ag(I) complexes were determined utilizing the flame atomic absorption method by Shimadzu AA-6300 devices, at Ibn-Sina Company, Ministry of Industry Iraq.

#### **2.2.8. Molar Conductivity Apparatus**

A 31A digital Conductivity analyzer in ethanolic solution was used to measure the ligand and solid complexes' molar conductivity in a  $10^{-3}$  M solution at ambient temperature using instruments the Chemistry Department in AL-Muthanna University.

### 2.2.9. Magnetic Susceptibility

Magnetic susceptibility studies of the chelating complexes in powder form were performed using the Balance Magnetic (MSB-MKI) equipment, and by the Faraday method, Pascal's constants and diamagnetic corrections, Magnetic moments of the complexes were calculated using the equation

$\mu_{\text{eff}} = 2.84 [T\chi M^{\text{coord}}]^{1/2}$  [70]. The measurement was carried at College of science/ Al-Nahrain University.

### 2.2.10. XRD Study

X-ray diffraction (XRD) was measured to know the crystalline nature, crystalline size, distances between crystals, properties, and geometrical crystalline shapes for the prepared compounds with an angular range of  $2\theta$  ( $20-80^\circ$ ) using a German-made device (Bestic Aluminium anode) with ( $\text{CuK}\alpha$ ) radiation ( $\lambda=1.5418\text{\AA}$ ) at the University of Kashan, Islamic Republic of Iran.

### 2.2.11. Thermogravimetric Analysis

Thermogravimetric analysis (TGA-TDG) studies of ligand and their complexes were done by using Perkin Elmer, model (TGA 40 0 0), USA Method from 40 to 900 0C under a nitrogen atmosphere with a heating rate of ( $10\text{ }^\circ\text{C min}^{-1}$ ) at the University of Kashan, Islamic Republic of Iran.

### 2.2.12. (FE-SEM) Analysis

The FE-SEM technique was used in the emitted field of a ZEISS EM 3200 to take a much-enlarged image with a magnification of Mag-50.00KX of the samples

using electronic beams that were projected on the surfaces of the material and conduct measurement at Al-Razi laboratories in Tehran, Republic of Iran.

### 2.3. Preparation of Azo dye Ligand (5-MTADMBI)

The azo ligand 2-[2'-(5- methylthiazolyl) azo]-5,6-dimethyl benzoimidazol (5-MTADMBI) was synthesized according to the following procedure [70], [48]. The 2-amino -5- methylthiazol (1.30 g, 0.01 mol) was dissolved in a mixture of hydrochloric acid (5 mL) and distilled water (30 mL) and was rapidly cooled in an ice bath at (0–5) °C. The above mixture was slowly added to a cold solution of sodium nitrite NaNO<sub>2</sub> (0.9 g, 0.01 mol), was dissolved in (35 mL) distilled water with cooling and it was kept at (0–5) °C with constant stirring. After that, it was stirred for another 2 h to complete diazotization. Then , the obtained diazonium salt solution was added to solution 5,6-dimethyl benzoimidazol (1.46 g, 0.01 mol) and dissolved in a mixture (35 mL ethanolic solution, 12 ml 10% NaOH ) in below 5 °C . The formed solid product was separated by filtration, purified by crystallization from ethanol, washed several times with diethyl ether and dried in vacuum over anhydrous calcium chloride to give brawn crystals, yield 85%. The mechanisms of diazotization coupling are shown in Scheme (2.1) below.

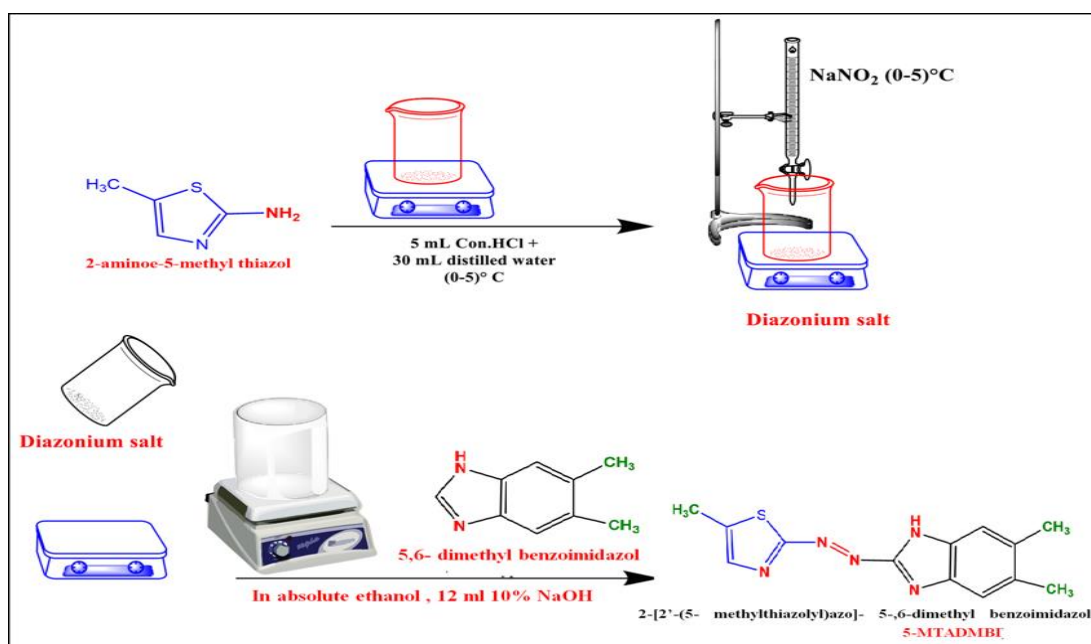


**Figure 2.1:** Synthesis of 2-[2'-(5- methylthiazolyl) azo]-5-,6-dimethyl benzimidazol ligand.

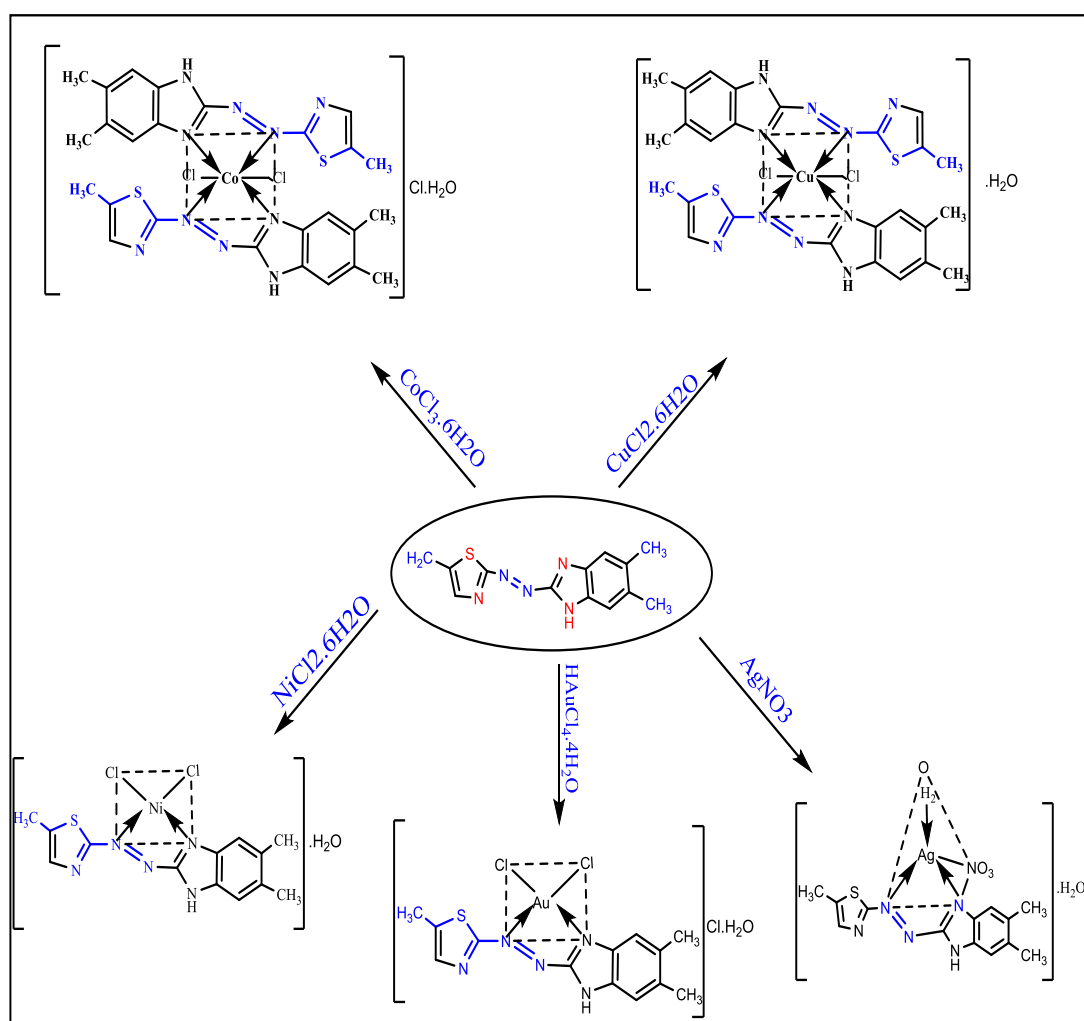
## 2.4. Preparation of Buffer Solutions

Buffer solutions were prepared with a concentration of (0.01 M, 0.771gm) for ammonium acetate  $\text{CH}_3\text{COONH}_4$  in one liter of deionized water. The required pH was obtained through using dilute solution 0.1 M of  $\text{NH}_3$  or  $\text{CH}_3\text{COOH}$  solution into the ammonium acetate solution before completing the volume, these solutions have been prepared to an extent within the pH scope (4 - 9)[71].

## 2.5. General procedure for synthesis metallic complexes

The metal complexes were made from dissolving (0.5426 g, 0.002mol) from the ligand 2-[2'-(5- methylthiazolyl) azo]-5-,6-dimethyl benzimidazol in a hot ethanolic solution (50 mL), then added in drops with stirring continuously to (0.001 mol) amount of 1:2 [M:L] for  $\text{CoCl}_3 \cdot 6\text{H}_2\text{O}$ , and  $\text{CuCl}_2 \cdot 2\text{H}_2\text{O}$  dissolved in from a hot buffer solution(25 mL) (ammonium acetate), while the ligand amount of (0.2713 g, 0.001 mol) added in the same method to a stoichiometric to (0.001 mol) amount of

[1:1] [M:L] for  $\text{NiCl}_2 \cdot 6\text{H}_2\text{O}$ ,  $\text{AgNO}_3$ , and  $\text{HAuCl}_4 \cdot 4\text{H}_2\text{O}$  salt at pH solution for perfect pH, and the mixture of this complex was heated to  $(50 - 70)^\circ\text{C}$  at 2 hour. All complexes left over night (Scheme 2). The solid complexes were filtered off and washed with distilled water and little warm ethanol to remove any unreacted components. Several hours were spent drying the solid complexes in a desiccator over anhydrous  $\text{CaCl}_2$ . [70]. According to (Table 2.2), the produced ligand and their metal complexes exhibit the following physical and analytical properties.



**Scheme 2.1:** Synthesis of metal chelates.

**Table 2.2:** Some physical properties of metal chelates with azo ligand

Compound	Color	m.p °C	$\lambda_{\text{max}}$ (nm)	Yield %	Molecular Formula (M.wt) (g/mol)	Mole ratio [M:L]
(L <sub>1</sub> H) 5-MTADMBI	Brown crystal	128 °C	458	85	C <sub>13</sub> H <sub>13</sub> N <sub>5</sub> S 271.34	---
[Co(L <sub>1</sub> ) <sub>2</sub> ]Cl.H <sub>2</sub> O	Bluish green	231 °C	629	79	C <sub>26</sub> H <sub>28</sub> N <sub>10</sub> OS <sub>2</sub> Cl <sub>3</sub> Co 726.003	1:2
[Ni(L <sub>1</sub> )Cl].H <sub>2</sub> O	Olive green	138 °C	585	72	C <sub>13</sub> H <sub>15</sub> N <sub>5</sub> OSCl <sub>2</sub> Ni 418.962	1:1
[Cu(L <sub>1</sub> ) <sub>2</sub> ].H <sub>2</sub> O	Dark green	227 °C	637	83	C <sub>26</sub> H <sub>28</sub> N <sub>10</sub> OS <sub>2</sub> Cl <sub>2</sub> Cu 695.263	1:2
[Ag(L) <sub>1</sub> (H <sub>2</sub> O)(NO <sub>3</sub> )]. H <sub>2</sub> O	Green	206°C	587	75	C <sub>13</sub> H <sub>17</sub> N <sub>6</sub> SO <sub>5</sub> Ag 477.252	1:1
[Au(L)Cl <sub>2</sub> ]Cl.H <sub>2</sub> O	Bluish violet	184°C	598	70	C <sub>13</sub> H <sub>15</sub> N <sub>5</sub> SOAuCl <sub>3</sub> 592.692	1:1

## 2.6. Preparation of Ligand Solutions

The solutions of the azo dye ligand 2-[2'-(5- methylthiazolyl) azo]-5-,6-dimethyl benzoimidazol have been prepared by dissolving the required weight of the ligand prepared mentioned in paragraph (2.3) of this chapter in an ethanolic solution with different concentrations of the metal ions ranging from ( $1 \times 10^{-2}$  to  $1 \times 10^{-6}$ ) [72].

## 2.7. Determine the Optimum Conditions

In order to find out the optimal conditions for the prepared metallic complexes, several experiments were carried out for solutions of azo dye ligand complexes with the previously mentioned ions, as follows:

### 2.7.1. Identify the Best Concentrations

Several concentrations of the prepared azo ligand and the metallic ions under study were prepared in a range between ( $1 \times 10^{-4}$ - $1 \times 10^{-6}$ ) molar. Preliminary tests were conducted in order to find the best concentrations that obey Lambert-Beer law as well as it was found that the solution concentrations in the range of ( $3 \times 10^{-4}$ - $1 \times 10^{-6}$ ) molar represent the best concentrations as they gave clear solutions and showed acceptable absorption that could be relied upon in measurement [73].

### 2.8. Mole Ratio

The molar ratio method was used upon for the purpose of calculating the metal: ligand ratio [M:L], as the molar absorbance was measured for a group of solutions at the best concentration, and the prepared solutions contained a fixed amount of the metal solution and variable quantities of the azo dye ligand solution prepared by mixing one ml of a solution of the salt of each metal with a specific concentration, with variable volumes of the ligand solution ranging between (0.25 - 3) ml of the same concentration of the relevant ligand solution, with a difference of (0.25) ml between one solution and another. The molar ratio in the solutions of the complexes was obtained by drawing the graphs between the metal: ligand molar ratio on the x-coordinate and corresponding to the molar absorptivity on the y-coordinate [74].

### 2.9. Spectroscopy Measurements of Metallic Complexes

The metallic complexes were characterized utilizing different techniques including elemental microanalyses (C.H.N.S), and measurements UV-Vis spectra were made from the prepared compounds dissolved in ethyl alcohol solution, with concentrations ranging from ( $1 \times 10^{-4}$ - $2.5 \times 10^{-4}$ M) utilizing a path-length quartz cuvette of (1cm) at the maximum wavelength ( $\lambda_{\max}$ ).

The Infrared (FTIR) spectra was recorded for these complexes by using solid tablets (KBr) within the range of wave number (400-4000)  $\text{cm}^{-1}$ . The proton and carbon ( $^1\text{H}$  &  $^{13}\text{C}$  NMR) spectrum was studied in order to know the structures of the prepared azo-dye ligand and some of their metallic complexes using TMS as a standard reference in  $\text{DMSO-d}_6$  as solvent. Mass spectra were taken for the ligand under study and for some prepared metallic complexes. Mixed-ligand complexes of Co(III), Ni(II), Cu(II), Ag(I) and Au(III) were studied using thermal analytical techniques (TGA-DTG), X-ray diffraction (XRD), and emitted field electron microscope (FE-SEM).

### 2.10. Measurements of Conductivity

The molar conductivity ( $\Lambda_m$ ) was measured for the solutions of the metal complexes under study in the ethanol solvent whose concentration ( $1 \times 10^{-3}$  M) for the solutions at the laboratory temperature [75].

### 2.11. Magnetic Susceptibility Measurements

Magnetic susceptibility was measured for some metal complexes prepared depend on temperature in  $25^\circ\text{C}$  utilizing diamagnetic corrections, the Faraday approach, and Pascal's constants by putting the sample in a small thermal glass tube suspended from the pan of the sensitive balance and placed between two electrodes, to obtain the gram susceptibility values ( $X_g$ ) which have been transformed to molar susceptibility ( $X_m$ ) then atomic susceptibility ( $X_A$ ) after finding the value of the correction coefficient (D) from tables of Pascale constants, according to that, we found the values of the effective magnetic moment ( $\mu_{\text{eff}}$ ) according to the following law [76], [77]:

$$\mu_{\text{eff}} = 2.828 \sqrt{X_A T} \text{ B.M}$$

Since (T): represents the absolute temperature degree.

(B.M): Bor.Magnaton which is the unit of measuring the effective magnetic moment.

(X<sub>A</sub>): represents the atomic sensitivity.

### 2.12. Find the Percentage of Chloride in the Metal Complexes

The Mohr method [78] was used to determine if counter-chloride ions were present or absent out side of the coordination sphere. The complex solution was titrated by comparing 0.10 M of standard AgNO<sub>3</sub> to a few drops of 5% (K<sub>2</sub>CrO<sub>4</sub>) as an indication [79]. Ni(II), Cu(II) and Ag(I) complexes were found to be non-electrolytes by the silver nitrate test, which was further supported by the molar conductivity measurement. The Co(III) and Au(III) complexes were shown to have an electrolytic character with a 1:1 ratio according to the silver nitrate and molar conductivity examinations at the same moment.

### 2.13. Biological Activity

The biological activity of the azo dye ligand and its metal complexes were examined against two types of bacteria, **Staphylococcus aureus** (G + ve), **Escherichia coli** (G -ve), as well as the fungus **Penicillium**, by using the diffusion method in agar [80]. Stock solution has been prepared by dissolving all the compounds in DMSO, the ligand and its metal complexes were tested for antimicrobial activity at 0.25 mg/mL in DMSO. On Muller Hinton agar medium and Sabouraud agar, fungus and bacteria cultures were conducted. The diameters of the inhibition zones were measured in millimeters. DMSO inhibitory zone diameters were determined after 24 h and seven days, respectively. The wells have been filled with solutions using a micropipette [81].

Chelation reduces the polarity of the metallic ion by sharing positive charges with the donor atoms in the ligands, and  $\pi$ -electron delocalization may occur during the chelation process. This phenomenon increases the metal chelates lipophilic nature, allowing it to pass more easily through the microorganism's lipid layer, killing it more effectively. The other factors like solubility conductivity and bond length between the metal and ligand also increase the activity [82].

### **2.13.1. Preparation of the Plant's Bacterial Media and Calculation of the Inhibition zone**

The culture medium (Agar) was prepared according to the company's instructions, which are equipped with the type of Muller Hinton Agar, by adding (38 gram) of the prepared culture medium in one liter of boiled distilled water in a conical flask and shake well to completely dissolve the culture medium, after that The prepared medium is placed in an autoclave at a temperature of (121 °C) and under a pressure of 15 pounds / ang<sup>2</sup> for a period of 15 minutes, then these are poured into sterile glass dishes (Petri dish), and left to cool, and a so-called (loop) is used to grow bacteria in Agricultural dishes inside the Hood device, and holes were drilled in these dishes by using a cork-borer sterilized with alcohol, taking into account leaving an appropriate distance between one hole and another in order to avoid overlapping between the inhibition areas. After that, the prepared solutions were added to these holes in an amount of (0.1 mL) using Micropipette, and this occlusion was placed for 24 hours in that incubator at 37 °C. After that, the amount of inhibition of these compounds under study was measured using a millimeter ruler [80].

### **2.13.2. Preparation of the Artificial Center of Fungi and Calculation of the Inhibition zone**

The nutritional medium was prepared according to what was mentioned by the company that supplied it (Sabouraud Agar Medium) by dissolving 62g of it in 1000 mL of distilled water in a glass beaker. The medium was sterilized by an autoclave and poured into dishes, and chemical solutions were added to measure the extent of their inhibition ability against fungi. The plates were left to cool, and the fungi were cultivated on the medium, after which they were placed in the incubator at 28°C for seven days. After that, the diameter of the growing colony was measured with a millimeter ruler [83].

### **2.13.3. Gram Stain Solution**

The stain solutions were prepared and used for studying the morphological properties of the bacteria isolated under microscope.

## **2.14. Cytotoxicity Assays Cell Lines**

### **2.14.1. Cell Lines**

In this study, the lung Carcinoma cell line (A549), and pancreas carcinoma cell line (TP-53), and healthy human cells (HdFn) obtained from the oncology center in Baghdad were used. Cancer cells were maintained and developed, and the necessary tests were conducted on them in the same center that was mentioned above.

### **2.14.2. Measurements of Cell Proliferation**

Lung and pancreatic cancer cell lines were cultured in RPMI-1640 supplemented with 10 % fetal bovine serum, 100 units /mL penicillin, and 100µg /mL streptomycin. The synthesized compounds were tested in vitro against the cell lines A549 and TP-53

in anticancer assays. The MTT [3-(4, 5-dimethylthiazol-2-yl)-2,5-diphenyltetrazolium bromide] colorimetric analysis was employed to identify the vitality of the cells.

Each of the 96 well microliter plates was filled with 200  $\mu$ L of the suspension above, and the plate was left to incubate for twenty-four hours at 37°C in an environment of 5% CO<sub>2</sub> [84]. Aspirating the wasted medium was done after incubation. To each well, 200  $\mu$ L of various test concentrations of a synthesis chemical (12.5, 25, 50, 100, 200, and 400 $\mu$ g /mL from stock solution) were added. The plate was incubated for a full day at 37°C in an environment containing 5% CO<sub>2</sub>.

The examined sample medium was aspirated after the plate was taken out of the incubator. After adding 200 $\mu$ L of media containing 10%MTT reagent to each well, the plate was incubated for three- hours at 37°C in a 5% CO<sub>2</sub> environment to reach a final concentration of 0.5mg/mL. The generated formazan (tetrazoliumchloride), a decreased form of MTT, was then solubilized by adding 100 $\mu$ L of DMSO and carefully shaking the plate in a centrifugal shaker. A micro-plate sensor was used to determine the absorbance at 570 nm and 630 nm, and the % growth inhibition was computed [69]. Using a phase difference inverted microscope to see the cells, the morphological alterations of malignant cells (A549) and (TP-53) were compared with the control and treated samples, and the images were captured on camera.

# *Chapter Three*

*(Results and Discussion)*

### **3.0 Results and Discussion**

Heterocyclic azo dyes have garnered a great deal of attention and have contributed significantly to the advancement of dye chemistry and the dyeing process. All substances that were made and was described utilizing several spectrum analyses, including  $^1\text{H}$  and  $^{13}\text{C}$ NMR, FTIR, and UV-Vis spectrophotometers. Additional biological activities of the created azo compounds, such as anti-pancreas and anti-lung carcinoma, were evaluated. Additionally, the anticancer effects of synthetic substances were investigated versus (A549) cancerous cell lines and pancreas (TP-53) cancer cell lines by MTT assay [51].

#### **3.1. Spectacular spectroscopy of ligand (5-MTADMBI) and their metallic complexes**

The spectral scanning process was carried out for the mixture of ligand-complexes of cobalt (III), nickel (II), Copper (II), silver (I), and gold(III) which were dissolved in absolute ethanol (Et OH) using the UV- Visible at diluted concentrations that ranged between ( $1 \times 10^{-4}$  -  $2.25 \times 10^{-4}\text{M}$ ) to obtain the maximum wavelength ( $\lambda_{\text{max}}$ ) for each of the ligand and their metallic complexes [85]. The metallic complexes displayed new bands, which indicates the occurrence of a coordination process between the ligand and their chelating complexes. The findings are clarified in Table (3.1).

**Table 3.1:** Maximum wavelength, best concentration and molar absorbance of the ligand and their metallic complexes.

Compound	$\lambda_{\max}$ (nm)	Molar absorptivity ( $\epsilon$ ) $\times 10^3$ ( $Lmol^{-1}cm^{-1}$ )	Abs	Optimal Conc. $\times 10^{-4}M$
(5-MTADMBI) $L_1H$	458	1.92	0.24	1.25
[Co(L) $_2$ Cl $_2$ ].Cl.H $_2$ O]	629	1.40	0.21	1.0
[Ni(L) $_1$ Cl $_2$ ].H $_2$ O]	585	1.80	0.27	1.50
[Cu(L) $_2$ Cl $_2$ ].H $_2$ O]	637	2.97	0.52	2.00
[Ag(L) $_1$ (H $_2$ O)(NO $_3$ )].H $_2$ O]	587	3.68	0.46	1.50
[Au(L)Cl $_2$ ].Cl.H $_2$ O]	598	2.75	0.55	2.00

### 3.2. Determine Optimum Conditions

The best conditions for the coordinating of azo- ligand with the metallic ions under study were determined by the following:

#### 3.2.1. Metal Salts Selection

The salts of all the metal ions under study were chosen with a high degree of purity with the negative ion in order to prevent the occurrence of spectral interference. Chlorides were chosen without other negative ions such as nitrates, sulfates and bromides (except for silver chloride, which was not chosen because it is difficult to dissolve in aqueous solutions) [86]. These solutions had to be clear and free from sediment or suspended particles that lead to reflection, absorption or scattering of light during the spectral measurements.

#### 3.2.2. Determination Optimum Concentrations

The importance of selecting the best concentrations of the ligand and its metallic complexes under investigation lies in showing the colors of their complexes clearly and the submission of these concentrations to the Lambert-Beer law [87]. A wide range of concentrations has been studied between ( $1 \times 10^{-6}$  -  $2 \times 10^{-2}M$ ) for the ions of all

the elements concerned, and many of these concentrations were excluded for several reasons, including their inefficiency for spectroscopic measurement and the appearance of absorption peaks outside the measurement limits, because they are either.

The solutions are not clear, as in the case of high concentrations, which are ( $1 \times 10^{-2} - 1 \times 10^{-3}$  M), or they are out of the spectroscopic measurement sites because they gave sediment to metallic complexes upon mixing, and this causes obstruction in the spectroscopic measurement process or non-compliance with these concentrations are according to the law of Lambert-Beer. Although some concentrations are subject to this law, they are inefficient for study because they are almost colorless, as in the case of low concentrations, which are ( $1 \times 10^{-5}$  M).

The indicator of the complex was so weak that it was difficult to be sensed by the device, and the absorption values were weak, so it was excluded, from here it was found that the appropriate concentrations that must be worked out are within the range ( $1 \times 10^{-4} - 2.25 \times 10^{-4}$  M) of each metal ion and its compliance with the Lambert-Beer law appeared as suitable experimental concentrations for each of the ligand solutions and the metallic ions under study [71].

### **3.2.3. Determining Calibration Curves of Metal Complexes**

A group of solutions were prepared, the concentrations of which ranged between ( $1 \times 10^{-4} - 2.25 \times 10^{-4}$  M) for each of the azo-dye ligand and the metallic ions under study after they give them acceptable spectral absorption at the wavelength ( $\lambda_{\max}$ ) specified for each complex [88]. The relationship was drawn between these concentrations represented by the x-axis and the corresponding absorbance represented by the y-axis, as it turned out to be in a compliance with the Lambert-

Beer law and the relationship is linear [89]. As Table (3.2) show the optimum concentrations for these complexes and the absorbance at the greatest wavelength ( $\lambda_{\max}$ ). Figures from (3.1) to (3.2) show the linear relationship of the calibration curves for mixing solutions of the metallic ions with the azo dye ligand at the selected concentrations.

**Table 3.2:** The maximum absorbance at ( $\lambda_{\max}$ ) for the selected concentrations of mixing solutions of the metal ions under study with the azo dye ligand (5-MTADMBI).

Metallic Complex	Molar Conc. $\times 10^{-4}$						
	( $\lambda_{\max}$ ) nm L <sub>i</sub> H = 458	1.00	1.25	1.50	1.75	2.00	2.25
Co(III)-Complex	629	0.147	0.177	0.211	0.243	0.288	0.311
Ni(II)-Complex	585	0.095	0.124	0.139	0.159	0.180	0.212
Cu(II)-Complex	637	0.182	0.222	0.262	0.299	0.336	0.374
Ag(I)-Complex	587	0.0289	0.0393	0.0449	0.055	0.063	0.0679
Au(III)-Complex	598	0.047	0.0584	0.0669	0.079	0.089	0.099

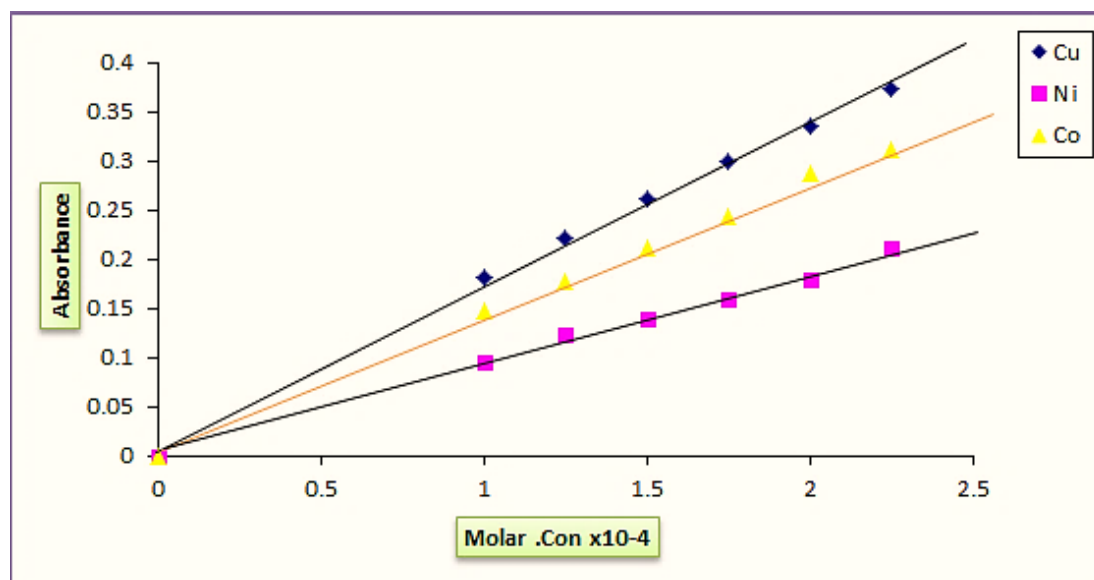


**Figure 3.1:** The linear relationship between the absorbance and the range of concentrations selected at ( $\lambda_{\max}$ ) for each of the metal salts prepared with ligand.

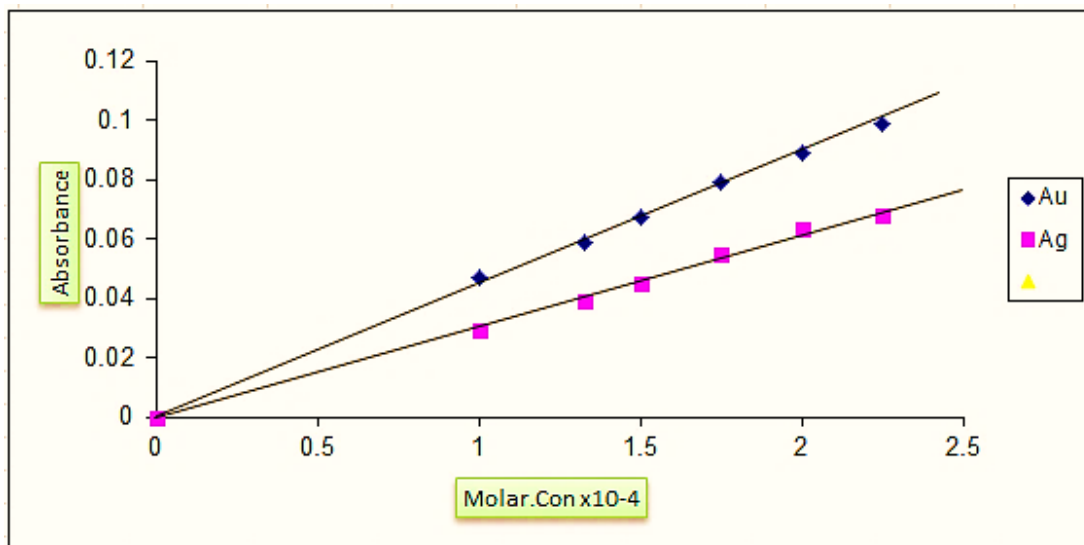


**Figure 3.2:** The linear relationship between the absorbance and the range of concentrations selected at ( $\lambda_{\max}$ ) for each of the metal salts prepared with ligand.

### 3.3. Determination of Possible Compositions of the Chelating Complexes

To find possible structural formulas for complexes, spectral methods are often used, especially if the solutions of the complexes are colored, the ultraviolet-visible spectra are used for this purpose, because the complexes show clear and distinct absorption peaks, and there are many methods used to determine the ratio of [ligand: metal].

Mole ratio method was invented by Yoe and Jones [90], which can be used to find the mole ratios of metal complexes by using absolute ethanol as the solvent, while the continues method depending measured absorbance when the concentration of two compound have been varied. The composition of metal complexes was examined using UV-VIS spectrophotometry at constant metallic ion concentrations and wavelengths ( $\lambda_{\max}$ ), with increasing volumes of ligand' solutions' (0.25 ml every adds up to 3.5ml). The absorbance versus mole ratio of ligand to metal plot gives a straight line that rises until it reaches the mole ratio, at which point the line breaks [91].

The increasing color intensity of metal complex solutions, and the continued stability of color after the point of intersection are excellent indications for the formation of the metal complexes at the typical ratio. The molar ratios [metal: ligand] [1:1] for the synthesis of Ni(II), Ag(I), and Au(III)-complexes and [metal: ligand] [1:2] for the synthesis of Co(III) and Cu(II)-complexes are suggested. The results are in agreement with those reported for metal complexes. Table (3-3) shows the absorption values corresponding to the molar ratio of the solutions of the complexes at the maximum concentration of the metal ion and the ligand, where these concentrations were in compliance with the Lambert-Beer law at the greatest wavelength ( $\lambda_{\max}$ ). Figure (3.3) clarifies the graphic curves obtained for solutions of metallic ions, which are cobalt(III), nickel(II), copper(II), silver(I), and gold(III) respectively with the ligand under study, and the points of intersection of the straight lines represent the ratio of [metal:ligand] involved in the complex composition.

**Table 3.3:** Ultraviolet -visible spectrum values for the mole ratio methodology at ( $\lambda_{\max}$ ), at the optimum concentration of mix metallic ion solutions with azo-dye ligand.

M : L ml:ml	Abs. of complexes				
	Co(III)	Ni(II)	Cu(II)	Ag(I)	Au(III)
1 : 0.25	0.186	0.172	0.055	0.079	0.053
1 : 0.5	0.225	0.284	0.084	0.148	0.111
1 : 0.75	0.289	0.364	0.115	0.207	0.164
1 : 1.00	0.351	0.459	0.153	0.276	0.209
1 : 1.25	0.385	0.483	0.185	0.280	0.212
1 : 1.50	0.430	0.497	0.215	0.287	0.223
1 : 1.75	0.472	0.521	0.246	0.293	0.228
1 : 2.00	0.508	0.525	0.257	0.299	0.244
1 : 2.25	0.537	0.531	0.269	0.309	0.257
1 : 2.50	0.542	0.552	0.280	0.322	0.270
1 : 2.75	0.563	0.562	0.295	0.333	0.281
1 : 3.00	0.574	0.590	0.309	0.339	0.299

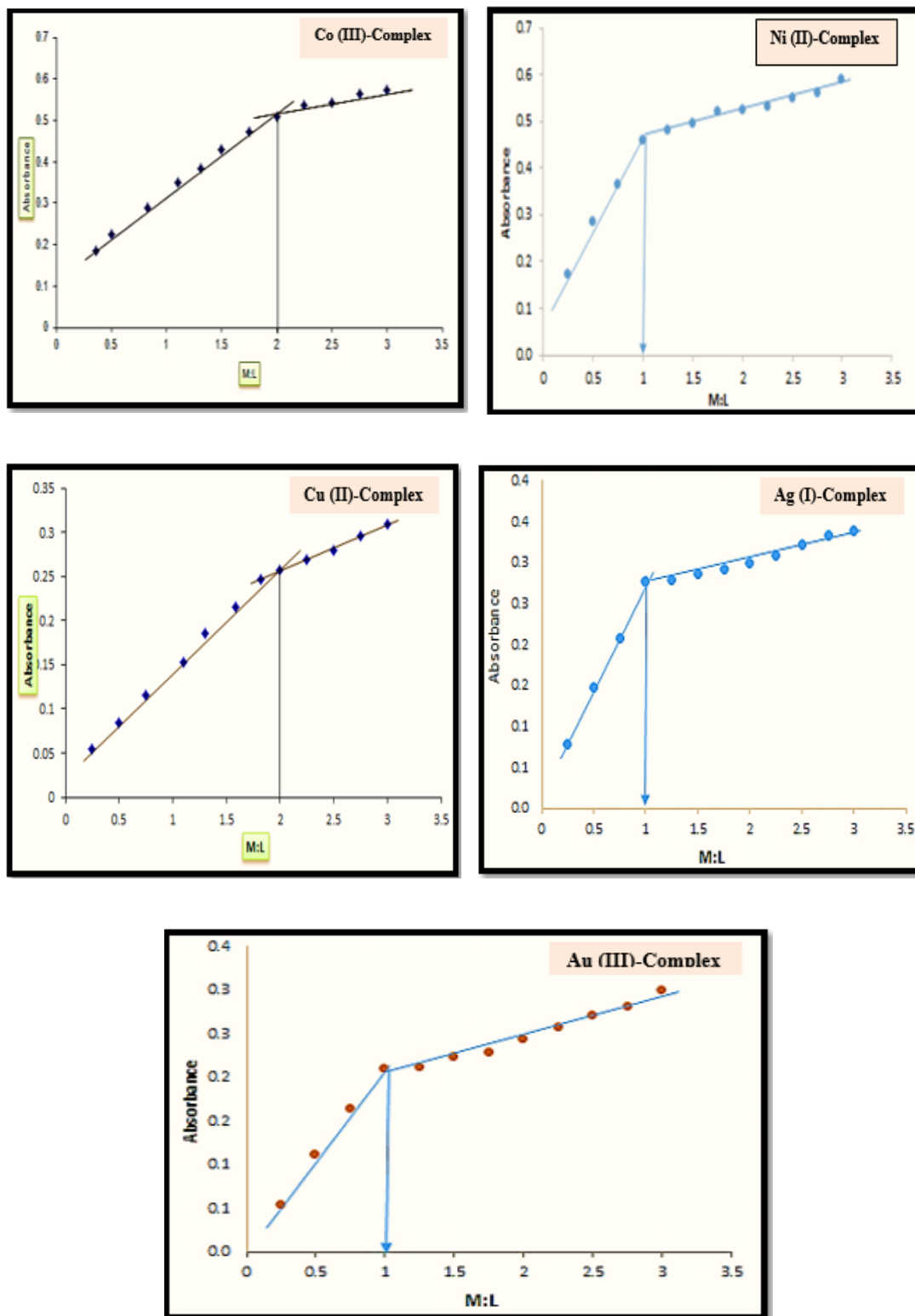
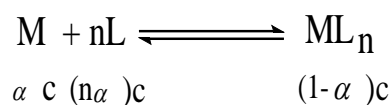


**Figure 3.3:** Molar ratio curves at ( $\lambda_{max}$ ) for cobalt (III), nickel (II), copper (II), silver (I), and gold (III) with ligand.

### 3.4. Stability Studies of Metal Complexes Solutions

The aim of studying the molar ratio of the metallic complexes are to find the ratio of the ligand to the metallic [50], as well as how it can be used in calculating the stability constant by taking the resulting absorption values of the ligand mixing solutions with the metallic ion, for the purpose of calculating the stability constants for all the metallic complexes under study, can be computed according to the equations. [92], [75]:



$$\beta = \frac{[\text{ML}_n]}{[\text{M}] [\text{L}]^n} \quad (3-2)$$

$$\beta = \frac{(1-\alpha)}{\alpha^n c} \quad (3-3)$$

While (n): represents the molar ratio (the number of ligand bonded to the metallic ion), when n= 1.

When n = 2, the value of  $\beta$  becomes:

$$\beta = \frac{(1-\alpha)}{4\alpha^3 c^2} \quad (3-4)$$

$$\alpha = \frac{A_m - A_s}{A_m} \quad (3-5)$$

Where C: concentration at mole/L of the chemical solution

$\alpha$ : degree of dissociation.

As: Absorption in a solution with a similar quantity of metallic ions and ligands.

A<sub>m</sub>: the value of absorption when there is an increase in the ligand component in the solution.

The absorbance values of the metallic complexes of azo-ligand, As, Am and the values of ( $\alpha$ ), ( $\beta$ ), and ( $\text{Log } \beta$ ) have been confirmed in Table (3.4).

**Table 3.4:** Stability Constants for complexes of metal ions under study with azo dye ligand at the best concentration and laboratory temperature.

Compound	Metal Ions	( $\lambda_{\text{max}}$ )nm	Am	As	$\alpha$	$\beta$	Log $\beta$
5-MTADMBI = L <sub>1</sub> H	Co(III)	629	0.574	0.508	0.1149	$6.46 \times 10^9$	9.81
	Ni(II)	585	0.590	0.459	0.2220	$1.05 \times 10^5$	5.02
	Cu(II)	637	0.309	0.257	0.1682	$1.44 \times 10^9$	9.15
	Ag(I)	587	0.339	0.276	0.1858	$1.04 \times 10^5$	5.02
	Au(III)	598	0.299	0.209	0.3010	$4.40 \times 10^4$	4.64

### 3.5. Molar electrical conductivity measurements

The molar conductivity of solutions is widely utilized in the field of coordination chemistry to determine the ionic formulas of the compounds in their solutions; that is, the value of electrical conductivity is directly proportional to the charged fractions in the solution [93]. Table (3.5) shows the values of the molar electrical conductivity for a number of electrolytes with various solvents.

The molar conductivity of the metallic complexes ( $10^{-3}\text{M}$ ) was studied in a pure ethanolic solution (EtOH) and at ambient temperature. The presence/absence of counter chloride ions out of the coordination sphere was confirmed using Mohr Method [18]. The complex solution was titrated versus 0.10 M of standard silver nitrate using a few drops of 5% ( $\text{K}_2\text{CrO}_4$ ) potassium chromate as an indicator. Silver nitrate ( $\text{AgNO}_3$ ) test revealed that Ni(II), Cu(II) and Ag(I) complexes were non-electrolytes, which was also confirmed by the molar conductivity test. At the same time, the silver nitrate ( $\text{AgNO}_3$ ) and molar conductivity tests revealed an electrolytic nature for Co(III) complex, and Au (III) had a ratio of 1:1. The addition of aqueous solution of silver nitrate to the complex of cobalt and gold (III) resulted in white

precipitates, which indicates that chloride ions were present outside the coordination sphere. Table (3.6) provides a summary of the findings.

**Table 3.5:** Molar electrical conductivity values at a concentration ( $1 \times 10^{-3}$ ) for electrolytes in multiple solvents.

Solvent	Non Electrolyte	Electrolyte Kind			
		1:1	1:2	1:3	1:4
Water	0.0	120	240	360	480
(EtOH)	0-20	35-45	70-90	120	160
Nitro Methane	0-20	75-95	150-180	220-260	290-330
Methyl Cyanide	0-30	120-160	220-300	340-420	500
DMF	0-30	65-90	130-170	200-240	300
DMSO	0-20	30-40	70-80	-----	-----

**Table 3.6:** Molar electrical conductivity values at a concentration of  $1 \times 10^{-3}$  M in ethanol solvent at ambient temperature.

Metal Complexes	Molar conductivity $S.cm^2. mol^{-1}$ $L_1H = 5-MTADMBI$	Electrolyte nature
	EtOH	
Co(III)	37.46	Ionic
Ni(II)	10.22	Non
Cu(II)	12.73	Non
Ag(I)	13.67	Non
Au(III)	39.27	Ionic

### **3.6. Magnetic Susceptibility Measurements**

The process of measuring the magnetic sensitivity is one of the techniques for individual electrons, as it is a successful method complementary in its results to the rest of the diagnostic methods to reach a proposal for the steric shapes of the complexes since it offers basic knowledge on the stereochemistry and connecting of metallic complexes. The diamagnetic corrections for the samples were estimated by using Pascal's constant and the magnetic data were corrected for diamagnetic contributions using a sample holder [94].

Magnetic measurements have been widely used in the study of metallic complexes, as most of the transition metals possess single electrons and show paramagnetic properties. Moreover, it provides details on the compound's oxidative state and the electrical structure of the transition metallic atoms. Determining the number of lone electrons for a metal ion shows the state of the complex, whether it is of high or low spin. If the central atom of coordination complexes does not contain single electrons, it will have magnetic properties [70].

At room temperature, the synthesized complexes' magnetic susceptibilities were measured in Table (3.7). The Co (III) complex's magnetic momentum value showed a low spin diamagnetic property, which is an indication that the cobalt (II) ion was oxidized to cobalt (III) while combining. Alterations in the state of oxidation are consistent with a previous finding that the watery solution of Co (II) salt automatically oxidizes to Co (III) in the founding of a potent ligand, for example, an azo-dye ligand, which suggests the formation of a regular octahedral structure ( $t_2g^6eg^0$ ) with  $d^2sp^3$  hybridization [95].

Measuring magnetic moments is very helpful in determining the correct geometry of the Ni (II) complex is square plane with a hybridization of  $dsp^2$ , and in

this instance, a diamagnetic character is shown [96]. The Cu (II) complex's suggests a distorted octahedral geometry ( $t_2g^6e_g^3$ ) magnetic momentum of 1.788 B.M, which is marginally bigger than the spin-only value of 1.73B.M [97]. The magnetic susceptibility of silver (I) and gold (III) complexes shows it has a tetrahedral, square planar shape and a diamagnetic moment ( $\mu_{\text{eff}}=0.0$  B.M (hybridization  $sp^3$ , and  $dsp^2$ ) [98]. Based on the previously described findings, it is possible to suggest the structures of these metallic complexes, as shown in Figure (3.4). Applying the relationship below, one can determine the theoretical magnetic moment of metallic ions:

$$\mu_{s+l} = \sqrt{4S(S+1) + L(L+1)} \text{ .B.M} \quad (3-6)$$

Where S: represent the total number of spins.

L: represents the total number of orbital angular momentums.

The value of the magnetic moment is limited only to the spinning movement in the absence of an orbital contribution to the first transition metal series, i.e. it has a value ( $L = 0$ ), and thus the relationship is limited only to the spin-only formula:

$$\mu_s = \sqrt{4S(S+1)} \text{ .B.M} \quad (3-7)$$

When  $S = n/2$  the relationship is written:

$$\mu_s = \sqrt{n(n+2)} \text{ .B.M} \quad (3-8)$$

Where n: represent the number of lone electrons in a metal atom.

The magnetic sensitivity of all metallic coordination complexes prepared at 25<sup>0</sup>C was calculated, and Pascal's constants were used in order to correct the diamagnetic atoms present in all organic molecules and inorganic radicals, as well as metallic ions.

The values of the magnetic moment were calculated according to the following equations [97], [98]:

$$\mu_{\text{eff}} = 2.828\sqrt{X_A T} \cdot \text{B.M} \quad (3-9)$$

$$X_A = X_M - D \quad (3-10)$$

$$X_M = X_g \times \text{M.wt} \quad (3-11)$$

$$X_g = CL/10^9 \text{m} \times (R - R_0) \quad (3-12)$$

It represents each of:

T : represent the absolute temperature of 298K.

X<sub>A</sub> : represent the atomic sensitivity.

X<sub>m</sub> : represent the molar sensitivity.

X<sub>g</sub>: represent the amorous (gravimetric) sensitivity.

D : represent the diamagnetic correction coefficient.

μ<sub>eff</sub> : represent the efficient magnetic moment.

M.wt : represent the gram molecular weight.

B.M. : represent the unit of magnetic moment (power magneton).

C: 1.53

L: 1cm

R: represent the sensitivity of the tube to the substance.

R<sub>0</sub>: represent the sensitivity of the tube when it is empty.

m: represent weight of the model = weight of the tube with the material - weight of the tube when it is empty.

In the following, we will discuss the method for calculating the effective magnetic moment  $\mu_{\text{eff}}$  of the Copper(II) Complex with the azo dye ligand, and in the same way it is calculated for the rest of the complexes under study:



$$X_g = [\text{CL}/10^9\text{m}] \times (\text{R}-\text{R}^0)$$

$$X_g = [1.53 \times 1\text{cm}/10^9(2.071-2.014)] \times (50-\text{zero})$$

$$X_g = 1.34 \times 10^{-6}$$

$$X_M = X_g \times \text{M.wt} = 1.34 \times 10^{-6} \times 699.16 = 0.93687 \times 10^{-3}$$

$$X_A = X_M - D$$

Calculating the correction factor for the complex (D):

$$H = 32 \times -2.93 \times 10^{-6} = -93.76 \times 10^{-6}$$

$$C = 26 \times -6 \times 10^{-6} = -156 \times 10^{-6}$$

$$C_{\text{ring}} = 20 \times -0.240 \times 10^{-6} = -4.80 \times 10^{-6}$$

$$C_{\text{Shared by two ring}} = 4 \times -3.07 \times 10^{-6} = -12.28 \times 10^{-6}$$

$$N = 10 \times -5.57 \times 10^{-6} = -55.7 \times 10^{-6}$$

$$N_{\text{ring}} = 2 \times -4.61 \times 10^{-6} = -9.22 \times 10^{-6}$$

$$O = 1 \times -4.61 \times 10^{-6} = -4.61 \times 10^{-6}$$

$$S = 2 \times -15 \times 10^{-6} = -30 \times 10^{-6}$$

$$C=C = 6 \times 5.5 \times 10^{-6} = 33 \times 10^{-6}$$

$$N=C = 4 \times 8.15 \times 10^{-6} = 32.6 \times 10^{-6}$$

$$N=N = 2 \times 1.8 \times 10^{-6} = 3.6 \times 10^{-6}$$

$$H_2O = -13 \times 10^{-6}$$

$$Cu^{+2} = -12.8 \times 10^{-6}$$

After summing the values, we get the coefficient of correction for the complex:

$$D = -317.33 \times 10^{-6}$$

$$D = -0.31733 \times 10^{-3}$$

$$X_A = X_M - D = 0.93687 \times 10^{-3} + 0.31733 \times 10^{-3} = 1.2542 \times 10^{-3}$$

$$M_{\text{eff}} = 2.828 \sqrt{X_A T} = 2.828 \sqrt{1.2542 \times 10^{-3} \times 298}$$

$$M_{\text{eff}} = 1.788 \text{ BM}$$

The results of measurements of the magnetic sensitivity of the Copper (II) Complex, under study at ambient temperature, gave clear confirmation of the correctness of the suggested stereotypes for the complexes under study in Table (3.7). The following has been shown:

### 3.6.1. Co (III)-Complex

Measurements of the magnetic sensitivity of the Cobalt (III)-complex under study showed that the complex has a diamagnetic character and takes the electronic arrangement ( $t_{2g}^6 e_g^0$ ), and this indicates that the Cobalt ion (II) is oxidized to the Cobalt ion (III), where the oxidation state changes in the presence of air as well as the aqueous solution because the double oxidation state is active while the inactive triple oxidation state appears in the aqueous solution of double Cobalt salt to triple Cobalt in the presence of a strong ligand, the complex has a low spin state. The proposed shape of the complex is regular octahedral and the hybridization of the central atom is  $d^2sp^3$  and it is considered one of the inner orbital complexes [99], [100].

### **3.6.2. Cu(II)-Complex**

The value of the effective magnetic moment of the Copper(II)-Complex gave paramagnetic properties of the azo- ligand under study. It was found the  $\mu_{\text{eff}}=1.788$  and the reason for that is a single electron present in the 3d shell, and the expected shape of the complex is a deformed octahedron that may be (Z-in or Z-out) and the most probable case is (Z-out) and has the electronic arrangement ( $t_{2g}^6 e_g^3$ ) with  $sp^3d^2$  hybridization and it is an external orbital complex [101] [102].

### **3.6.3. Ni (II), Ag(I), and Au(III)-Complexes**

The measurements of the magnetic sensitivity of the above complexes of the ligand under study gave values of magnetic moments less than one, and thus indicates that the complexes have diamagnetic characteristics. The measurements of the magnetic sensitivity of the above complexes of the ligand under study gave values of magnetic moments less than one, and thus it possesses diamagnetic properties. The proposed geometry is tetrahedral for the Silver complex (I) and has  $sp^3$  hybridization, while the expected geometry for the Nickel complex (II) is Square planner with  $dsp^2$  hybridization, and finally the expected geometry for Gold complex (III) is Square planner with  $dsp^2$  hybridization [103], [98]. The magnetic sensitivity data of metallic complexes is shown in Table (3.7).

## **3.7. Electronic Spectra**

The solutions of complexes of transition elements are characterized by their bright colors because they contain functional groups called (Chromophore), so they show absorptions in the visible region of the spectrum, and other absorptions appear

in the near-infrared and ultraviolet regions, due to the containment of atoms or ions of elements on secondary (d) levels that are partially filled with electrons [104].

### 3.7.1. Electronic Spectra of Free Ligand

The absorption spectrum of the ligand showed three bands. The first and second band at around 458 nm ( $21834\text{cm}^{-1}$ ) and 398 nm ( $25126\text{cm}^{-1}$ ) may be assigned to  $n - \pi^*$  transitions intermolecular transition charge transfer taking place through the azo group and azomethine group, while the third band observed at 326 nm ( $30675\text{cm}^{-1}$ ) is attributed to  $\pi - \pi^*$  transitions of the  $\pi$ -systems of the azo group ( $\text{N} = \text{N}$ ), ( $\text{C} = \text{N}$ ) and allowed the transitions of the benzimidazol ring, respectively [105].

### 3.7.2. Electronic spectra of Co(III)-Complex

The spectrum of Cobalt (III) complex showed three broad bands at 629 nm ( $15898\text{ cm}^{-1}$ ), and 319 nm ( $31348\text{ cm}^{-1}$ ), respectively which can be assigned to the d-d transitions  $\nu_1 = {}^1\text{A}_{1g} \rightarrow {}^1\text{T}_{2g(\text{F})}$ ,  $\nu_2 = {}^1\text{A}_{1g} \rightarrow {}^1\text{T}_{1g(\text{F})}$ , While the band at 266 nm ( $37594\text{ cm}^{-1}$ ) is due to center ligand transition. [99], [100].

### 3.7.3. Electronic spectra of Ni(II)-Complex

The electronic absorption spectrum of Nickel(II) complex in ethanolic solution showed two bands at approximately 585 nm ( $16077.17\text{ cm}^{-1}$ ), and 395 nm ( $25773.20\text{ cm}^{-1}$ ), which can be attributed to the transitions  ${}^1\text{A}_{1g} \rightarrow {}^1\text{A}_{2g}$  and  ${}^1\text{A}_{1g} \rightarrow {}^1\text{B}_{1g}$  transitions respectively. The bands observed at 269 nm ( $33557.05\text{ cm}^{-1}$ ) due to center ligand transitions. These observations suggest a square-planar geometry for the Ni(II) complex [106], [107].

### 3.7.4. Electronic spectra of Cu(II)-Complex

Copper(II) complex exhibited a single broad asymmetric band at around 637nm ( $15923.57 \text{ cm}^{-1}$ ). The broadness of this peak is due to three electronic transitions;  ${}^2B_{1g} \rightarrow {}^2A_{1g}$  ( $dx^2-y^2 \rightarrow dz^2$ ) ( $\nu_1$ ),  ${}^2B_{1g} \rightarrow {}^2B_{2g}$  ( $dx^2-y^2 \rightarrow dyz$ ) ( $\nu_2$ ), and  ${}^2B_{1g} \rightarrow {}^2E_g$  ( $\nu_3$ ) (Charge Transfer), as well as Jahn-teller distortion, which is resulting in a distorted octahedral complex. These results indicate that the Copper(II) ion has a distorted octahedral geometry [101], [102]. As shown in Figure (3.4).

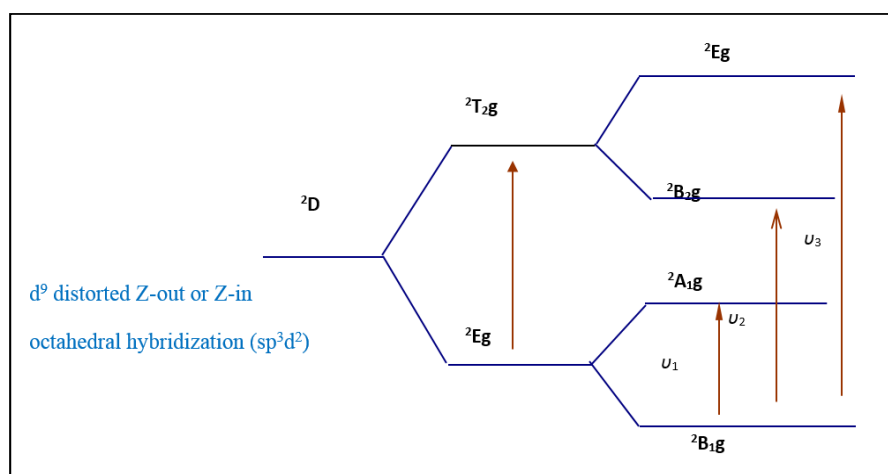


Figure 3.4: Electronic transitions of distorted ( $d^9$ ) octahedral complexes.

### 3.7.5. Electronic spectra of Ag(I)-Complex

The silver Ag(I) complex do not exhibit any (d-d) transition bands due to electron saturation  $d^{10}$ . The bands 587 nm ( $17035.78 \text{ cm}^{-1}$ ), 397 nm ( $25188.92 \text{ cm}^{-1}$ ), and 299 nm ( $33444.82 \text{ cm}^{-1}$ ) could be attributed to the presence of a Charge Transfer  $d\pi(\text{Ag})^{+1} \rightarrow \pi^*(\text{L})(\text{C.T})$  and intra ligand, respectively [103], [98].

### 3.7.6. Electronic spectra of Au (III)-Complex

The electronic spectrum of Au(III) complex exhibited four additional bands 598 nm ( $16722.41 \text{ cm}^{-1}$ ), 410 nm ( $24390.24 \text{ cm}^{-1}$ ), 306 nm ( $32679.74 \text{ cm}^{-1}$ ) and 271 nm ( $36900.37 \text{ cm}^{-1}$ ) attributed to the transitions  ${}^1A_{1g} \rightarrow {}^1A_{2g}$  ( $\nu_1$ ),  ${}^1A_{1g} \rightarrow {}^1B_{1g}$  ( $\nu_2$ ),  ${}^1A_{1g}$

→  ${}^1E_{g(v3)}$  and intraligand, respectively, of square planner geometry (Hybridization  $dsp^2$ ) [108]. We can suggest the possible structure of the metallic complexes, as illustrated in Figure (3.5), because the primary characteristics of all the spectral information of the metallic complexes form an integrated image. Table (3.7) provides the information collected from the synthetic compounds' electronic spectra.

**Table 3.7:** Electronic spectra, magnetic measurements, geometric shapes and hybridization of metallic complexes with ligand at laboratory temperature.

Compounds	$\lambda_{max}$ (nm)	Absorption Bands( $cm^{-1}$ )	Assignment	$\mu_{eff}$ (B.M)	Suggested structure	Hybridization
5- (MTADMBI)  LH	458	21834	$n \rightarrow \pi^*$	.....	.....	.....
	398	25126	$n \rightarrow \pi^*$			
	326	30675	$\pi \rightarrow \pi^*$			
Co(III)- Complex	629	15898	${}^1A_{1g} \rightarrow {}^1T_{2g(F)}(O_{11})$	Dia	Oh. (Regular)	$d^2sp^3$  (Low spin)
	319	31348	Intra ligand			
	266	37594	Intra ligand			
Ni(II) - Complex	585	17094	${}^1A_{1g} \rightarrow {}^1A_{2g1}$	Dia	Square planner	$dsp^2$
	395	2531	${}^1A_{1g} \rightarrow {}^1B_{1g}$			
Cu(II)- Complex	637	15698	${}^2B_{1g} \rightarrow {}^2E_g$	1.78	Octahedral (Distorted) (Z-in or Z-out)	$sp^3$
Ag(I)- Complex	587	17035.78	$d\pi(Ag)^{+1} \rightarrow {}^*(L)(C.T)$	Dia	Tetrahedral	$sp^3$
	397	25188.92	Intra ligand			
	299	33444.82	Intra ligand			
Au(III)- Complex	598	16722.41	${}^1A_{1g} \rightarrow {}^1A_{2g}(v_1)$	Dia	Square Planer	$dsp^2$
	410	24390.24	${}^1A_{1g} \rightarrow {}^1B_{1g}(v_2)$			
	306	32679.74	${}^1A_{1g} \rightarrow {}^1E_g(v_3)$			
	271	36900.37	Intra ligand			

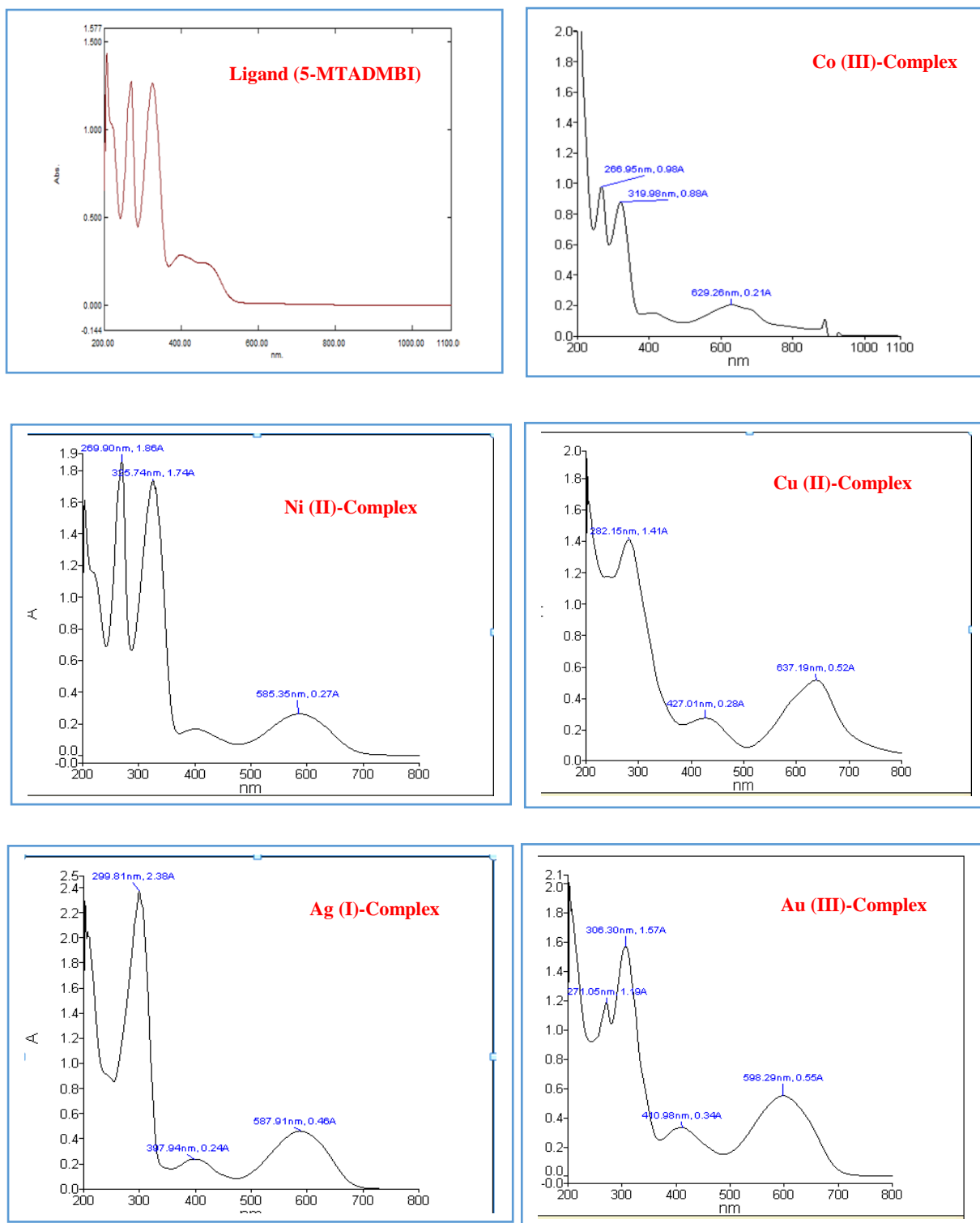


Figure 3.5: UV-Vis spectrum of ligand (5-MTADMBI) and chelate complexes.

### 3.8. C.H.N.S Elemental Analysis

Heterocyclic azo-dye ligand and its solid metallic complexes prepared using the above technique were identified by calculating the ratio of the number of (C, H, N, and S) atoms in the prepared compounds [109]. The proportions of metallic elements in their complexes were also calculated using the flame atomic absorption technique, Table (3.8) includes the results of these analyses. The comparison of the values obtained practically with the values calculated theoretically, it was clearly observed that a great convergence between them was observed, which confirms and shows the accuracy of the molar ratios that were added from [metal: ligand], which supports the accuracy of the expected and proposed formulas for the prepared metal complexes [110].

**Table 3.8:** (C.H.N.S) analysis, and some of the physical properties of (5-MTADMBI) ligand and the synthesized complexes.

Compound	Yield %	Molecular Formula (M. wt) (g/mole)	%Found (Calculated)				Mole ratio [M:L]
			%C	%H	%N	%S	
<b>L<sub>1</sub>H = 5-MTADMBI</b>	85	<b>C<sub>13</sub>H<sub>13</sub>N<sub>5</sub>S</b> 271.34	58.14 (57.54)	5.98 (4.79)	26.11 (25.81)	11.91 (11.82)	---
<b>[Co(L)<sub>2</sub>Cl<sub>2</sub>]Cl.H<sub>2</sub>O</b>	79	<b>C<sub>26</sub>H<sub>32</sub>Cl<sub>3</sub>CoN<sub>10</sub>S<sub>2</sub>O</b> 730	47.25 (46.16)	5.32 (4.47)	21.75 (20.70)	10.18 (9.48)	1:2
<b>[Ni(L)<sub>1</sub>Cl<sub>2</sub>].H<sub>2</sub>O</b>	72	<b>C<sub>13</sub>H<sub>17</sub>Cl<sub>2</sub>N<sub>5</sub>NiSO</b> 420.95	40.12 (38.75)	4.68 (3.75)	18.09 (17.38)	8.21 (7.96)	1:1
<b>[Cu(L)<sub>2</sub>Cl<sub>2</sub>].H<sub>2</sub>O</b>	83	<b>C<sub>26</sub>H<sub>32</sub>Cl<sub>2</sub>CuN<sub>10</sub>S<sub>2</sub>O</b> 699.16	46.11 (45.85)	5.06 (4.44)	21.24 (20.56)	10.37 (9.41)	1:2
<b>[Ag(L)<sub>1</sub>(H<sub>2</sub>O)(NO<sub>3</sub>).H<sub>2</sub>O</b>	70	<b>C<sub>13</sub>H<sub>17</sub>AgN<sub>7</sub>O<sub>2</sub>S</b> 475.24	32.72 (30.99)	3.59 (2.60)	17.61 (16.20)	6.72 (5.47)	1:1
<b>[Au(L)Cl<sub>2</sub>]Cl.H<sub>2</sub>O</b>	73	<b>C<sub>13</sub>H<sub>15</sub>AuCl<sub>3</sub>N<sub>5</sub>S</b> 594.67	26.34 (24.51)	2.55 (2.01)	11.81 (10.55)	5.41 (4.22)	1:1

### 3.9. $^1\text{H}$ NMR Spectra

#### 3.9.1. $^1\text{H}$ NMR spectrum of the ligand ( $\text{L}_1\text{H}$ )

At room temperature, the azo dye ligand underwent detailed  $^1\text{H}$ NMR measurements utilizing a (Bruker 500 MHz) spectrometer utilizing  $\text{DMSO-d}_6$  as a solvent, with a standard reference sample of (TMS) [111]. In  $^1\text{H}$ NMR, the free-ligand spectra in Figure (3.6) displayed a singlet band at ( $\delta = 11.73$  ppm), which can be assigned to the protons of the (-NH-) imidazole molecule. At ( $\delta = 2.19$  and 6.90 ppm), the proton of the methyl and methine groups of the thiazole ring exhibited a singlet signal. Furthermore, the spectrum exhibited signal at ( $\delta = 7.24 - 7.95$  ppm) is labeled to the aromatic protons in the benzimidazole ring. A signal at ( $\delta = 2.39-2.41$  ppm) (s, solvent proton). At ( $\delta = 2.27-2.37$  ppm), the protons of the methyl group in the benzimidazole ring (C-( $\text{CH}_3$ ) appeared as a singlet signal [94].

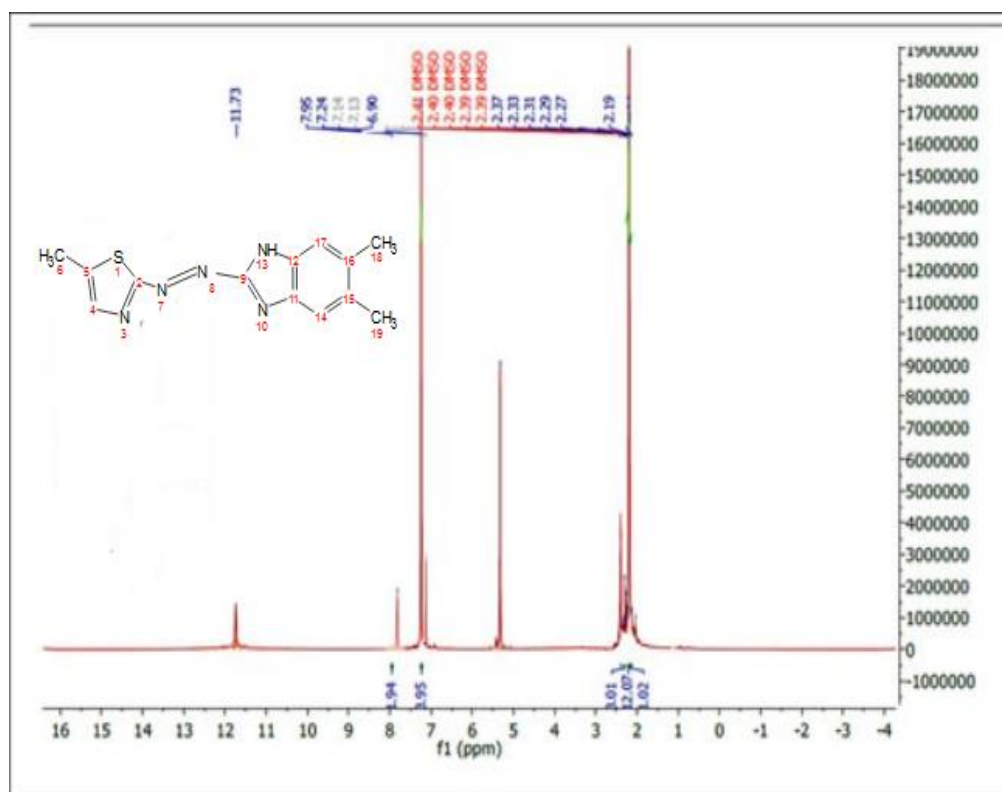


**Figure 3.6:**  $^1\text{H}$ NMR Spectrum of azo dye ligand (5-MTADMBI) in ( $\text{d}_6$ -DMSO) solvent.

### 3.9.2. $^1\text{H}$ NMR spectra of Co(III)-Complex $[\text{Co}(\text{L}_2)\text{Cl}_2]\text{Cl}\cdot\text{H}_2\text{O}$

Nuclear magnetic resonance (NMR) utilizing ( $\text{DMSO-d}_6$ ) as a solvent for the Co(III)-complex and (TMS) as a standard reference, chemical shifts were utilized to determine the molecular structure. The  $^1\text{H}$ NMR spectrum of Co(III)-complex displayed a signal at ( $\delta = 11.73$  ppm) due to the presence of the (NH) group in the imidazole molecule, and the protons of the aromatic ring bonded to the imidazole ring visible at ( $\delta = 6.63 - 7.31$  ppm). The methyl group of the thiazole ring was found to have a signal at ( $\delta = 1.05-2.06$  ppm), whereas the methine group's proton was found at ( $\delta = 5.20$  ppm). The methyl groups of the ( $-\text{C}(\text{CH}_3)$ ) in the benzimidazole ring are what caused the singlet signal visible at ( $\delta = 3.28-3.39$  ppm). A singlet signal at ( $\delta = 2.39$  ppm) (solvent proton) [112], as shown in Figure (3.7).

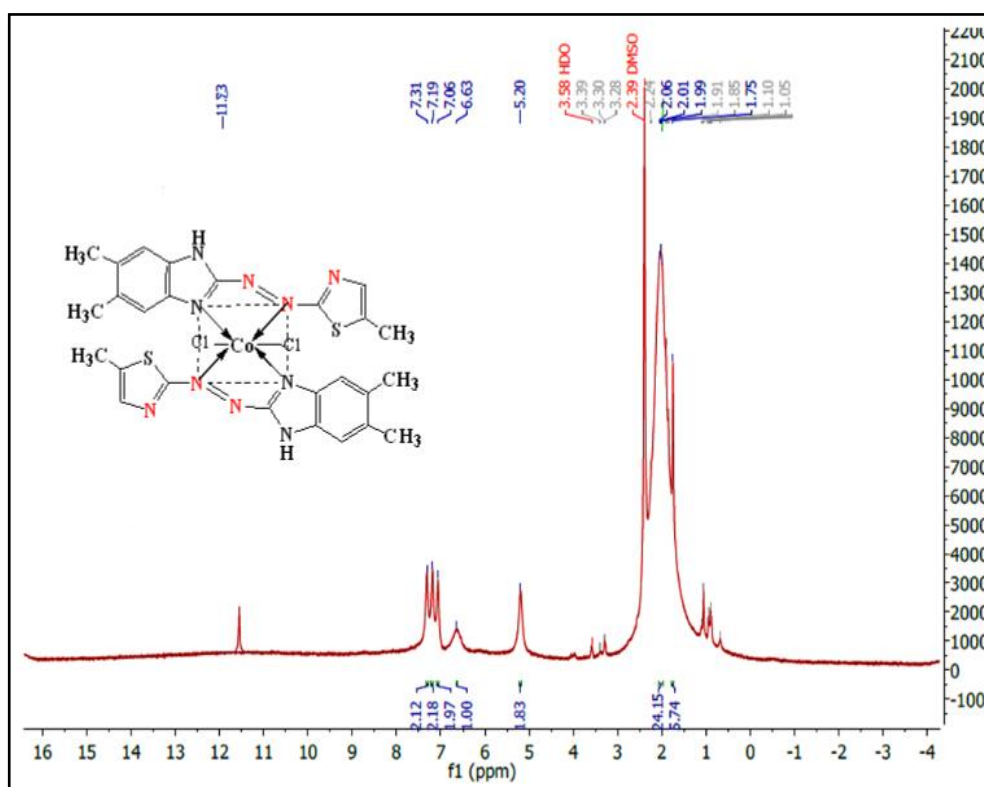


**Figure 3.7:**  $^1\text{H}$ NMR spectrum of Cobalt complex in ( $\text{DMSO-d}_6$ ) solvent.

### 3.10. $^{13}\text{C}$ NMR Spectra

#### 3.10.1. $^{13}\text{C}$ -NMR Spectrum of the Ligand ( $\text{L}_1\text{H}$ )

The  $^{13}\text{C}$ NMR spectra of azo dye ligand has been examined, and signals showed up as a result of the inclusion of various carbon atom types [113]. Many chemical shifts were visible in the  $^{13}\text{C}$ NMR spectra  $^{13}\text{C} = (179.27, 161.76, 156.01, 152.66, 150.57, 143.45, 125.52, 123.54, 55.44, 26.65, 16.06, 14.71, \text{ and } 14.42 \text{ ppm})$  returned to the carbon atoms at the locations ( C2, C9, C11, C16, C13, C14, C12, C15, C4, C5, C6, C18, and C19) respectively [114],  $^{13}\text{C}$ NMR spectra of the ligand (5-MTADMBI) are presented in Figure (3.8) .

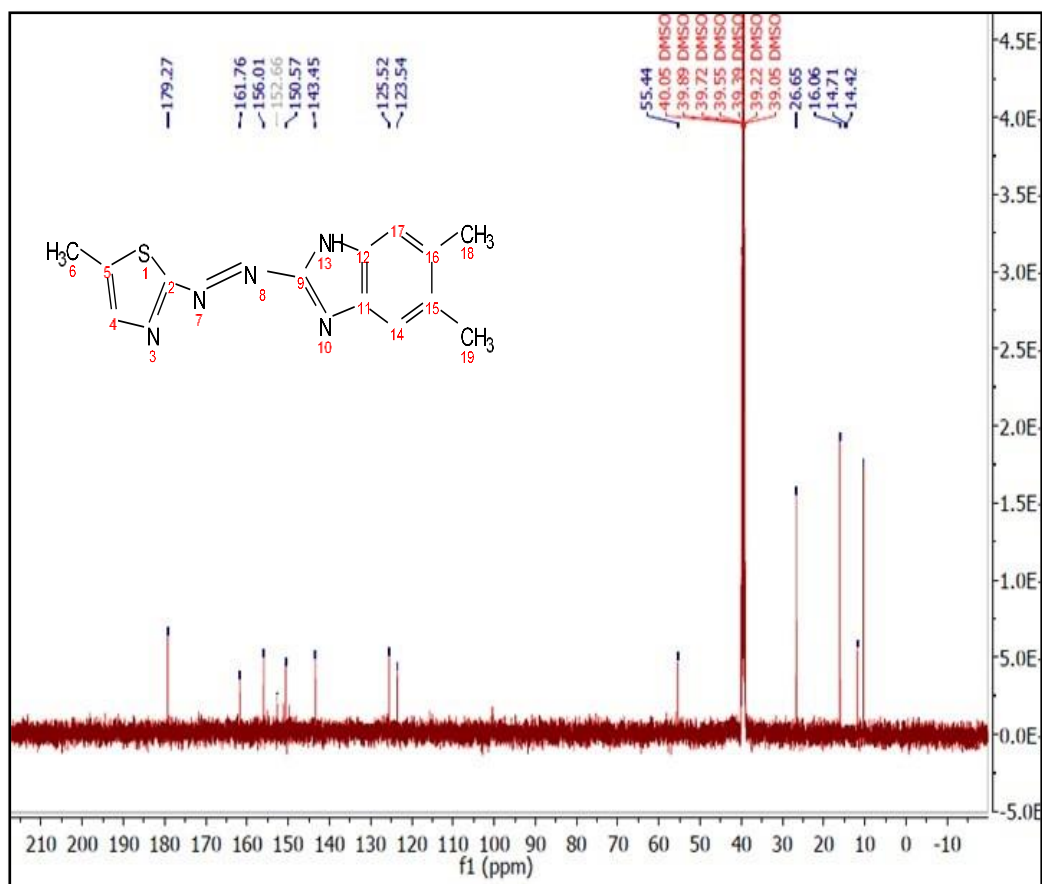


Figure 3.8:  $^{13}\text{C}$ NMR spectrum of ( $\text{L}_1\text{H}$ ) ligand.

### 3.10.2. $^{13}\text{C}$ NMR spectrum of $[\text{Co}(\text{L})_2\text{Cl}_2]\cdot\text{H}_2\text{O}$ Complex

The  $^{13}\text{C}$  NMR of the Co(III)-Complex was investigated in Figure (3.9), and signals appeared due to the presence of different kinds of carbon atoms. The  $^{13}\text{C}$ NMR spectra showed multiple chemical shifts  $^{13}\text{C} = (170.80, 161.79, 156.06, 150.59, 149.93, 140.37, 125.55, 117.79, 40.41, 26.66, 16.07, 14.43, \text{ and } 11.65 \text{ ppm})$  returned to the carbon atoms at the locations (C2, C9, C11, C16, C13, C14, C12, C15, C4, C5, C6, C18, and C19) respectively [115]. The assignment of the  $^{13}\text{C}$ NMR spectra of the ligands (5-MTADMBI) and its Co(III)-complex are displayed in Table(3.9).

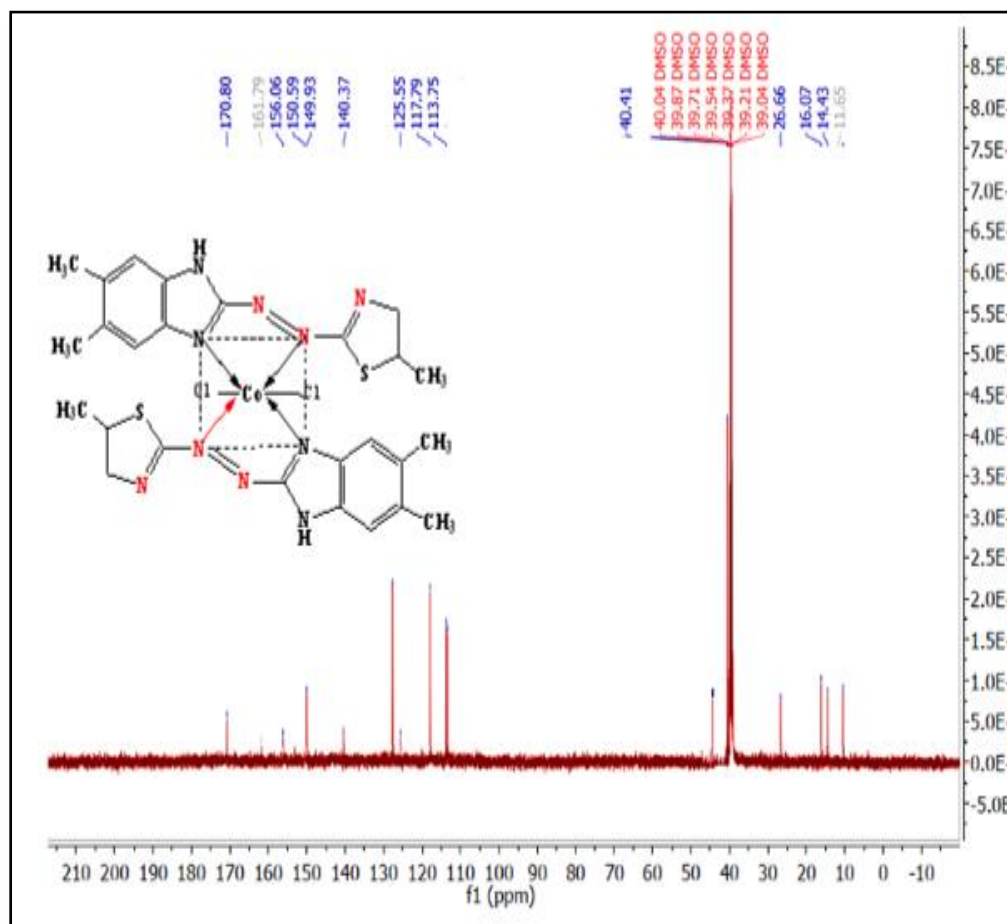


Figure 3.9:  $^{13}\text{C}$ NMR spectrum of Cobalt Complex.

**Table 3.10:** Assignment of the  $^{13}\text{C}$ NMR spectrum of the ligand (5-MTADMBI) and its Co(III)-Complex.

<b>L<sub>1</sub>H = (5-MTADMBI)</b>		<b>Co (III)- Complex</b>	
<b>Position</b>	<b>Chemical shift (ppm)</b>	<b>Position</b>	<b>Chemical shift (ppm)</b>
<b>C<sub>2</sub></b>	<b>179.27</b>	<b>C<sub>2</sub> = C<sub>21</sub></b>	<b>170.80</b>
<b>C<sub>9</sub></b>	<b>161.76</b>	<b>C<sub>9</sub> = C<sub>28</sub></b>	<b>161.79</b>
<b>C<sub>11</sub></b>	<b>156.01</b>	<b>C<sub>11</sub> = C<sub>30</sub></b>	<b>156.06</b>
<b>C<sub>16</sub></b>	<b>152.66</b>	<b>C<sub>16</sub> = C<sub>35</sub></b>	<b>150.59</b>
<b>C<sub>13</sub></b>	<b>150.57</b>	<b>C<sub>13</sub> = C<sub>32</sub></b>	<b>149.93</b>
<b>C<sub>14</sub></b>	<b>143.45</b>	<b>C<sub>14</sub> = C<sub>33</sub></b>	<b>140.37</b>
<b>C<sub>12</sub></b>	<b>125.52</b>	<b>C<sub>12</sub> = C<sub>31</sub></b>	<b>125.55</b>
<b>C<sub>15</sub></b>	<b>123.54</b>	<b>C<sub>15</sub> = C<sub>34</sub></b>	<b>117.79</b>
<b>C<sub>4</sub></b>	<b>55.44</b>	<b>C<sub>4</sub> = C<sub>23</sub></b>	<b>40.41</b>
<b>C<sub>5</sub></b>	<b>26.65</b>	<b>C<sub>5</sub> = C<sub>24</sub></b>	<b>26.66</b>
<b>C<sub>6</sub></b>	<b>16.06</b>	<b>C<sub>6</sub> = C<sub>25</sub></b>	<b>16.07</b>
<b>C<sub>18</sub></b>	<b>14.71</b>	<b>C<sub>18</sub> = C<sub>38</sub></b>	<b>14.43</b>
<b>C<sub>19</sub></b>	<b>14.42</b>	<b>C<sub>19</sub> = C<sub>39</sub></b>	<b>11.65</b>

### 3.11. The Mass Spectra Analysis

#### 3.11.1. The Mass Spectra Analysis of Ligand and Ni (II)-Complex

Mass spectroscopy was used to confirm the ligand and its Ni (II)-Complex's structure. The mass spectra of the ligand's 2-[2'-(5- methylthiazolyl) azo]-5,6-dimethyl benzoimidazol and its Nickel (II)-complex displayed several peaks Figure (3.10) and (3.11). The novel azo dye ligand mass spectrum revealed a base peak at  $m/z = 270.1$ , which was attributed to the ligand's initial molecular weight (271.34),  $[\text{C}_{13}\text{H}_{13}\text{N}_5\text{S}]$ . The molecular formula of the complex (420.95),  $[\text{C}_{13}\text{H}_{17}\text{Cl}_2\text{N}_5\text{NiSO}]$ , matches the molecular-peak of the Ni (II)-Complex that appeared at  $m/z = 421.1$

These data and the corresponding molecular formulas are in good agreement [30], [116].

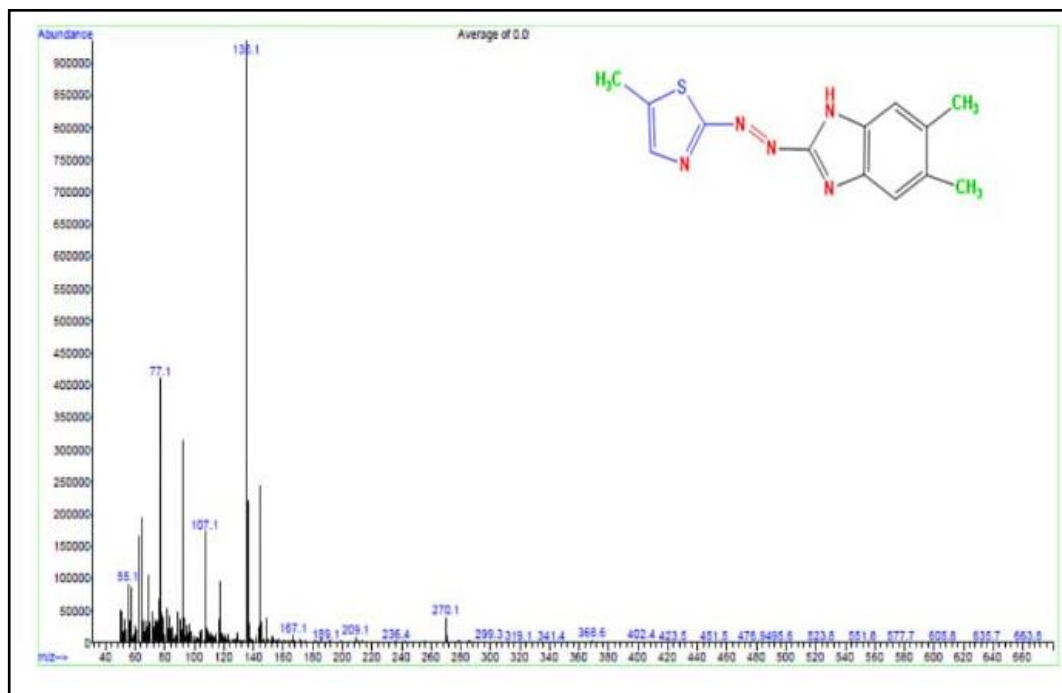


Figure 3.10: The mass fragmentation of (5-MTADMBI) ligand.

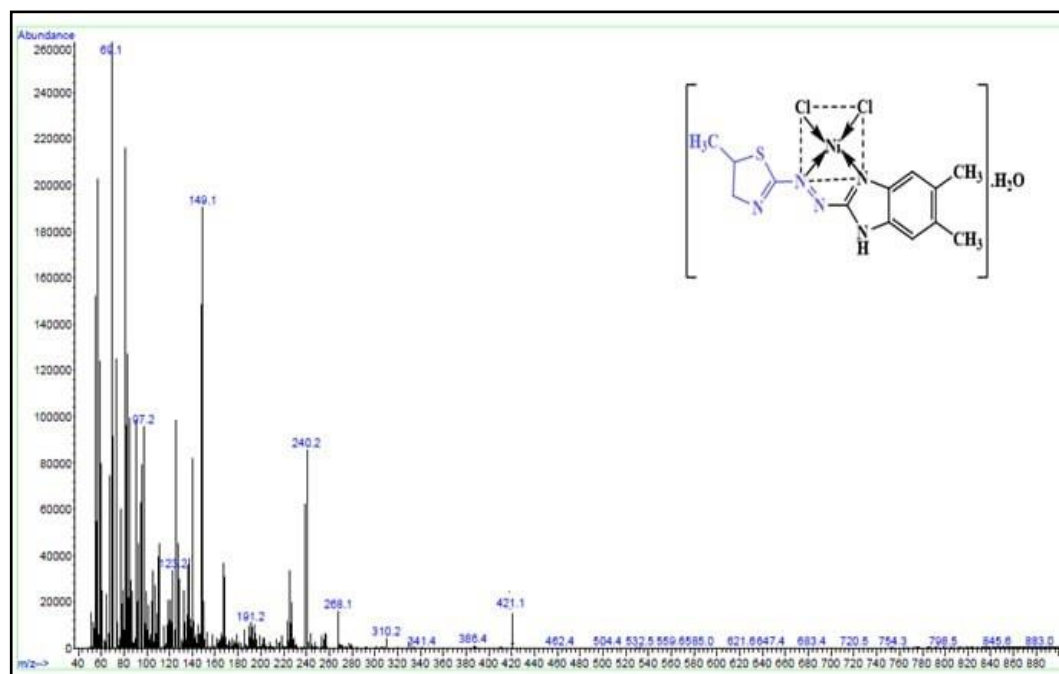


Figure 3.11: The mass fragmentation of Nickel (II)- Complex.

### 3.12. Infrared Spectra

FTIR spectroscopy's purpose is to characterize compounds by determining the presence of functional groups. When the FTIR spectra of the ligand was contrasted to that of its metal complexes, it was seen that some bands shifted and new bands appeared while others stayed the same. This is proof that a complex was formed. FTIR data for the 2-[2'-(5- methylthiazolyl) azo]-5-,6-dimethyl benzoimidazol ligand, as well as their metallic complexes, are detailed in Table (3.11) and shown in Figure (3.12). Using KBr, the vibrations of most moieties were visible in the range of 400-4000  $\text{cm}^{-1}$  [117].

In all the ligand 2-[2'-(5- methylthiazolyl) azo]-5-,6-dimethyl benzoimidazol and their complexes with cobalt (III), nickel(II), copper(II), silver (I), and gold (III), the strong absorption broad bands obtained in the region (3095, 3124, 3203, 3134, 3146, and 3142)  $\text{cm}^{-1}$  are labeled to the (NH) stretching. The presence of (OH) aqua in the spectra for most complexes Co(III), Ni(II), Cu(II), and Au (III) has been suggested by the very broad absorption bands at (3212, 3363, 3335, and 3406)  $\text{cm}^{-1}$  and the absence of this band in the spectra of the free ligand and silver complex [118], [39].

A medium-broad band was seen in the spectra of the (5-MeTADMBI) ligand and complexes at (3030, 2970, 2974, 3080, 2966, and 3031)  $\text{cm}^{-1}$  due to (C-H) aromatic, although the bands at (2962, 2939, 2939, 2978, 2937, and 2922)  $\text{cm}^{-1}$  assigned to (C-H) aliphatic, in that order [119]. There were also additional bands at (1477, 1498, 1502, 1498, 1487, and 1452)  $\text{cm}^{-1}$  in the spectrum of the free ligand and its metallic complexes, which corresponded to the azo stretching modes (N=N), while the band at 1708  $\text{cm}^{-1}$  for 2-[2'-(5- methylthiazolyl) azo]-5-,6-dimethyl benzoimidazol showed to be the molecule C=N for the azomethine group in the benzimidazole ring, proving the

presence of the ligand. This band disappeared in the spectra for the complexes when compared with the ligand spectrum.

The FTIR spectrum of the metallic complex exhibits new bands attributed to  $\nu(\text{M-N}_{\text{azo}})$ , as listed in Table (3.11). The FT-IR spectra for metal complexes suggested that (5-MeTADMBI) can act as an N, N-bidentate ligand, chelating nitrogen from both (N=N) and (C=N) benzimidazole to form pentagonal chelating rings [120].

**Table 3.11:** FTIR spectrum of the (5-MTADMBI) ligand's and its metallic complexes.

Group	LH = 5- MTADMBI	Co(III)- Complex	Ni(II)- Complex	Cu(II)- Complex	Ag(I)- Complex	Au(III)- Complex
$\nu(\text{H}_2\text{O})$	-	*3212 s.br.	*3363 s.br.	*3335 s.br.	-	*3406 s.br.
$\nu(\text{NH})_{\text{Benzimidazole}}$	3095 .w	3124 s.br	3203 s.br.	3134 s.br.	3146 m.br	3142 m.br.
$\nu(\text{CH})_{\text{Aromatic}}$	3030 .m.br.	3124 m.	3082 m.	3080 s.br	3030m.	3031 s.br.
$\nu(\text{CH})_{\text{Aliphatic}}$	2962 .m.br.	2939 m.	2939 m.	2978 s.br.	2937 m.	2922 s.br.
$\nu(\text{C=N})_{\text{Benzimidazole}}$	1708 w.	1653 m.	1653 m.	1653 m.	1683 m.	1653 m.
$\nu(\text{C=N})_{\text{Thiazole}}$	1614 .m	1610 m.br.	1612 m.	1612 m.	1612 m.	1614 m.
$\nu(\text{N=N})$	1477 s.	1498 s.	1502 m.	1498 s.	1487 m.	1452 s.
$\nu(\text{C=C})$	1305 s.	1307 m.	1307 w.	1307 w.	1307 w.	1307 w.
$\nu(\text{C-S})$	1271 s.	1263 s.	1267 m.	1265 m.	1263 m.	1249 m.
$\nu(\text{C-N})$	1159 m.	1203 m.	1203 m.	1207 m.	1134 m.	1122 w.
$\nu(\text{C-C})$	1026 m.	1085 w.	1147 w.	1082 w.	1082 w.	1024 m.
$\nu(\text{M-N})$	-	665 w.	505 m.	537 s.	611 m.	615 w.

S = strong, m = medium, w = weak, br = broad, sh = sharp, \* = ( $\text{H}_2\text{O}$ ) outside of sphere coordination.

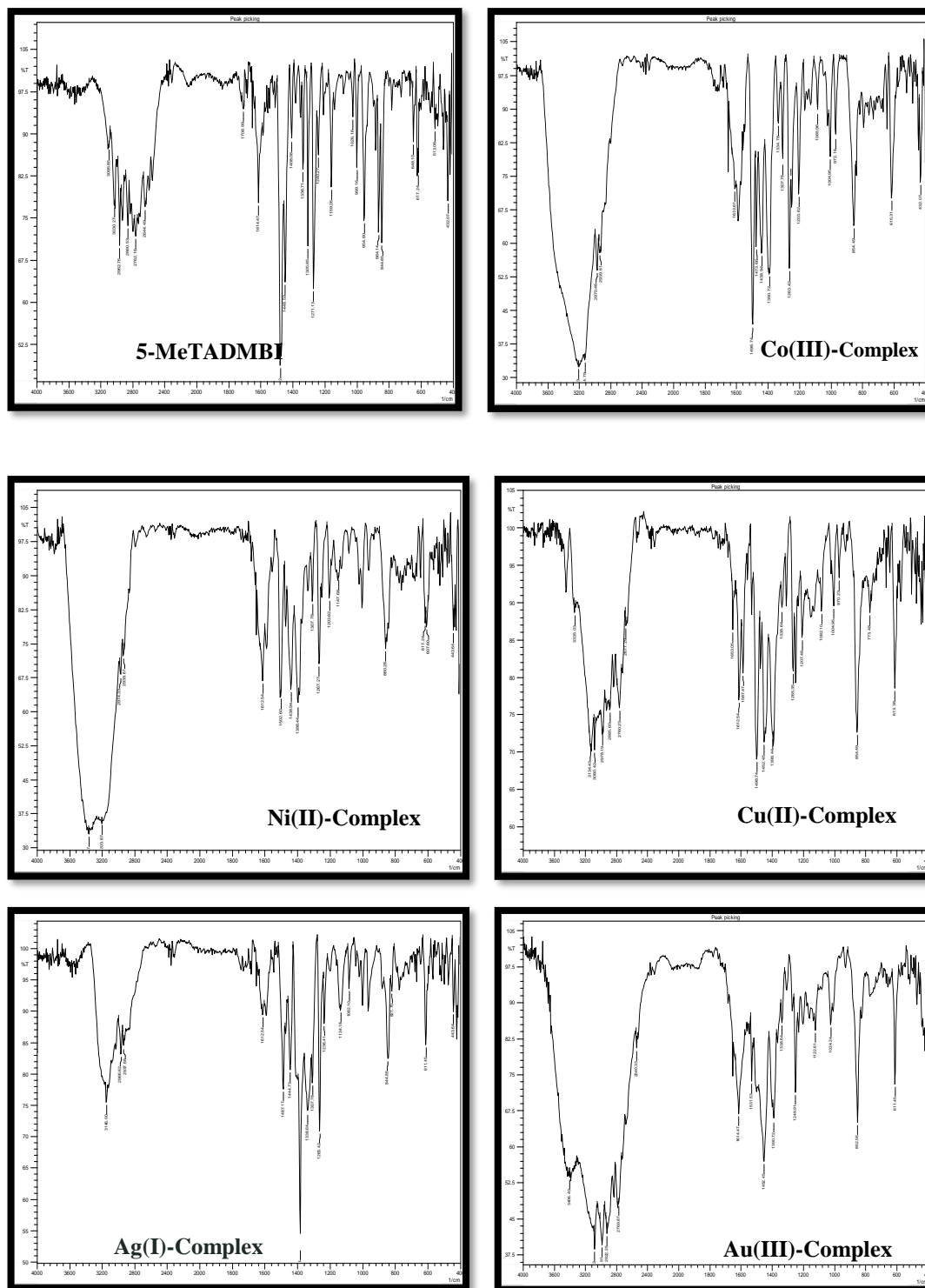


Figure 3.12: FTIR spectra of the (5-MeTADMBI) and its metallic complexes.

### **3.13. Thermal Study**

Thermal stability analysis (TGA sample curve) is used to determine the thermal behavior of the 2-[2'-(5-methylthiazolyl) azo]-5,6-dimethyl benzoimidazol ligand and the corresponding (1-5) complexes between the temperature 40 to 900 °C at a rate of (20 °C/minute) in the nitrogenous environment [121]. As for the remaining materials that are likely to be formed after the completion of the thermogravimetric analysis process into the complexes under study, they are metal atoms, their oxides, and hydrocarbon residues. The thermogram of the ligand shown two degradation ranges, the first appeared approximately 41.17 to 410.98 °C including a mass loss of 76.095%. The second degradation range appeared between 410.98 to 900 °C indicating a mass loss of 23.796%. The thorough degradation of the ligand, the gradient of DTG, there appeared a signal at 296.69 °C. TGA curves show the three-step degradation of the (1-5) complexes in the same range of temperature. Table (3.12), Figure (3.13), summarize thermal degradation information and illustrate a respective diagram of the TGA-DTG.

**Table 3.12:** Thermoanalytical finding (TG-DTG) of ligand (5-MTADMBI) and metal complexes.

	TG range (°C)	DTG max (°C)	% Estimated (Calculated)	Assignment
			Total mass loss	
5-MTADMBI	40.17- 410.98 410.98- 900	296.69	76.095	Evolution of moisture and some other gases
			23.796	Loss Azo group and di methyl amine group
				Loss CO <sub>2</sub> and 2CH <sub>3</sub> and remains of ligand
Co(III)-Complex	39.99- 282.75 282.75- 499.16 499.16- 901.9	167.95 258.28 335.44	13.536	Loss H <sub>2</sub> O molecule and loss of HCl gas
			33.213	Loss Azo group and formation of Co <sub>2</sub> O <sub>3</sub>
			24.511	
Ni(II)-Complex	40.24- 242.29 242.29- 500.66 500.66-901.5	142.92 325.10	16.117	Evolution of moisture
			39.381	Loss Azo group and di methyl amine group and Loss CO <sub>2</sub> and 2CH <sub>3</sub>
			12.969	Loss of residual ligand and formation of NiO
Cu(II)-Complex	40.36- 175.17 175.17- 496.19 496.19- 900	124.48 290.06	5.967	Loss of H <sub>2</sub> O and some other gases
			42.263	Loss CO <sub>2</sub> , Azo group and 2CH <sub>3</sub> and OCH <sub>3</sub> .
			18.213	Loss of residual ligand and formation of CuO .
Ag(I)-Complex	40.00- 298.15 298.15- 450.91 450.91- 900	251.25 393.59	4.405	Loss H <sub>2</sub> O molecule.
			16.138	Loss Azo group , Loss di methyl amine group and Loss CO <sub>2</sub> , 2CH <sub>3</sub> and Loss of the phenyl ring
			16.123	Loss thiazol ring and formation of 1/2Ag <sub>2</sub> O.
Au(III)-Complex	40.00- 169.13 169.13- 363.50 363.50- 900	134.52 275.63 716.28	5.814	Loss of H <sub>2</sub> O and some other gases
			20.959	Loss CO <sub>2</sub> , Azo group and 2CH <sub>3</sub> and OCH <sub>3</sub> .
			55.763	Loss of phenyl ring , thiazol ring and remains of ligand and 1/2Au <sub>2</sub> O <sub>3</sub> .

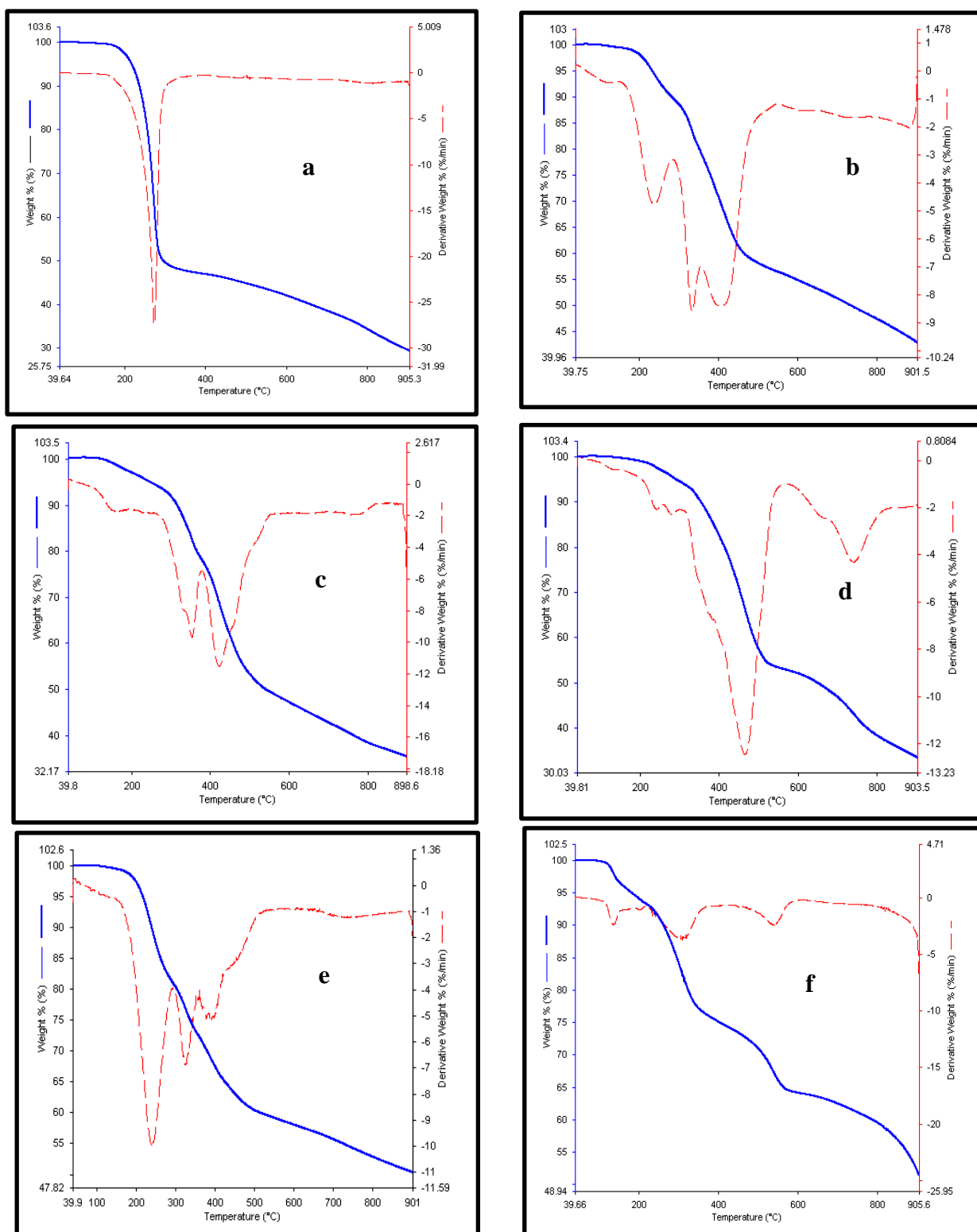


**Figure 3.13:** Thermal gravimetric analysis of (a) (5-MTADMBI), (b) Co (III)- Complex, (c) Ni(II)- Complex, (d) Cu(II)- Complex, (e) Ag(I)- Complex, and (f) Au(III)- Complex.

### 3.14. X-ray crystallography description of the synthesis compounds

The crystallographic information for all the compounds was anticipated by X-ray crystallography. The X-ray diffractograms have been obtained for the 2-[2'-(5-methylthiazolyl) azo]-5-,6-dimethyl benzoimidazol ligand and the respective (1-5) complexes. The measurement of the intensity of Cu K $\alpha$  radiation diffraction was conducted within the range of 0° to 80° at 2 $\Theta$ , using a wavelength of 1.54060 Å and generator parameters of 40 mA/40 kV [122].

The findings exhibited some complexes their semicrystalline character Figure (3.14). Major reflexes were computed using Bragg's equation [103], and the d-spacing values were determined through the application of the formula  $n\lambda = 2d\sin\theta$ , where d represents the lattice spacing, n is a whole number (01, 02, 03, etc.),  $\lambda$  denotes the wavelength of X-rays (CuK $\alpha$  = 1.540598Å), and  $\Theta$  represents the inclination between incident radiation and the diffracted radiation. The Debye-Scherrer equation [123], was utilized to evaluate the mean crystallite size and the size distributions.

The formula for calculating the mean diameter (D) of a crystallite is expressed as  $D = k\lambda\beta\cos\theta$ . In this equation, k is the proportionality constant with a value of 0.891,  $\lambda$  denotes the X-ray wavelength,  $\Theta$  represents the inclination between the incident radiation and the diffracted radiation, and  $\beta$  represents the total width of half of the greatest height (FWHM). The experimental average sizes were for (5-MTADMBI) 41.09 nm, 36.14 nm for Co(III), 62.29 nm for Ni(II), 49.33 nm for Cu(II), 59.03 nm for Ag(I), and 47.06 nm for Au(III) respectively. Based on the size of their crystallites, compounds are proven to have nanostructure characteristics

[124]. Table (3.13) represents the X-RD information of the created ligand and its (1-5) complexes.

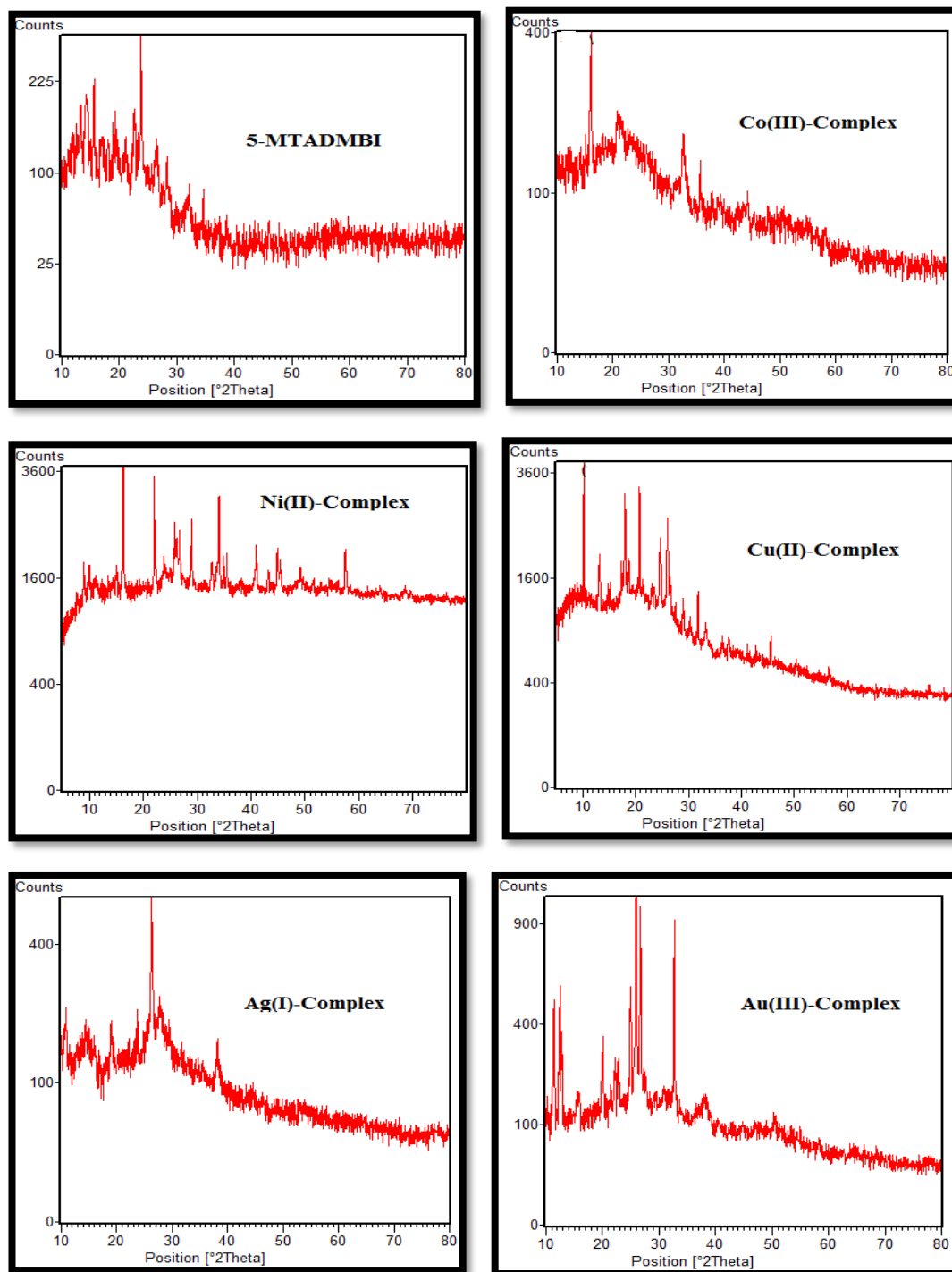


**Figure 3.14:** XRD patterns for ligand (5-MTADMBI) and chelate complexes.

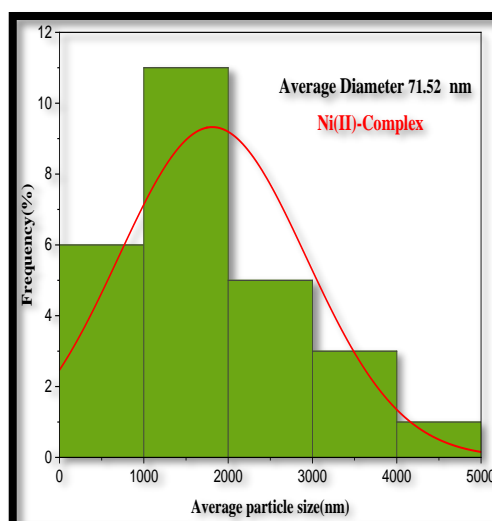
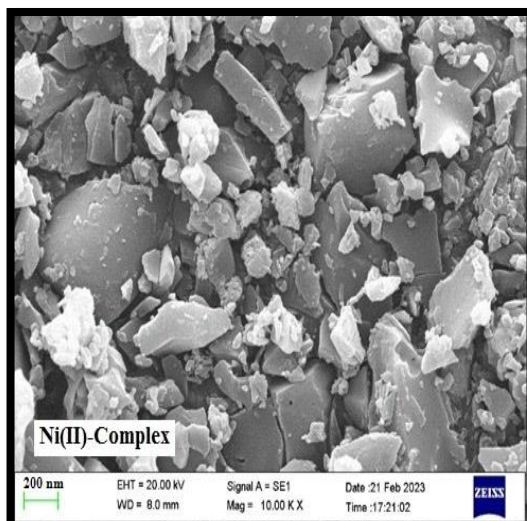
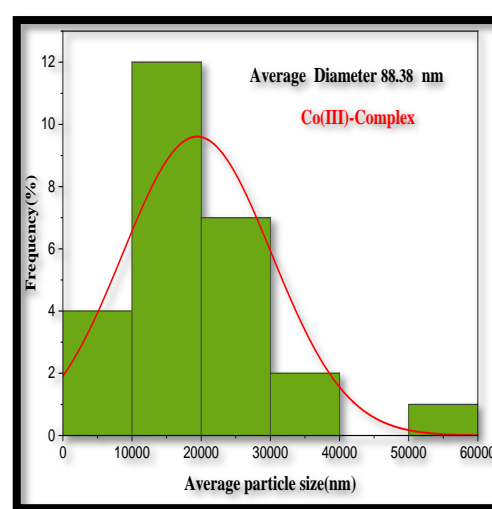
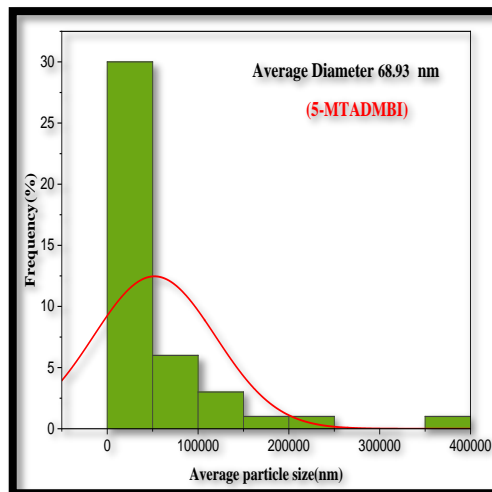
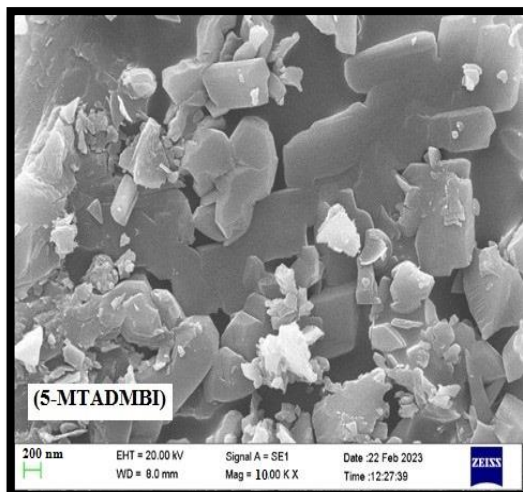
Table 3.13: Crystallographic data for (5-MTADMBI) and chelate complexes.

Compound	No.	$2\theta$ observed	$d$ observed (Å)	(I/I <sub>0</sub> ) %	(FWHM)	Crystallite Size. (nm)	(Lattice Strain)	$\delta_{DX10^{15}}$ (lin m <sup>-2</sup> )
(5-MTADMBI) L <sub>1</sub> H  C <sub>13</sub> H <sub>13</sub> N <sub>5</sub> S	1	11.174	7.91228	100	0.184	45.33	0.0082	0.486
	2	11.62	7.60720	22.13	0.16	52.15	0.0069	0.367
	3	9.86	8.96193	15.57	0.26	32.05	0.0132	0.973
	4	13.47	6.56662	8.49	0.24	34.83	0.0089	0.824
Co (III) complex	1	16.1040	5.50386	100	0.1476	56.8	0.0046	0.309
	2	32.6426	2.74332	51.19	0.3936	21.98	0.0059	0.0020
	3	35.68840	2.51587	32.76	0.1968	44.31	0.0027	0.509
	4	21.0312	4.22423	23.21	0.5904	14.3	0.0139	0.0048
	5	26.4505	3.36978	18.95	0.1968	43.33	0.0037	0.532
Ni (II) complex	1	15.533	5.70018	100	0.38	22.05	0.0122	2.050
	2	11.972	7.38631	82.25	0.095	87.86	0.0040	0.301
	3	11.592	7.62755	44.42	0.11	75.85	0.0047	0.173
	4	17.345	5.10862	15.09	0.20	41.989	0.0057	0.571
	5	15.055	5.88001	14.75	0.10	83.729	0.0033	0.142
Cu (II) complex	1	16.260	5.44695	100	0.175	47.92	0.0053	0.435
	2	22.049	4.02813	86.86	0.11	76.88	0.0025	0.169
	3	8.99	9.82549	20.11	0.22	37.85	0.0122	0.698
	4	9.96	8.87551	16.38	0.25	33.33	0.0125	0.901
	5	49.14	1.85245	15.65	0.18	50.71	0.0017	0.388
Ag (I) complex	1	16.261340	5.44646	100	0.208953	40.13	0.0064	0.620
	2	25.776470	3.45348	90.07	0.121369	70.16	0.0023	0.203
	3	22.382570	3.96887	78.45	0.104557	80.93	0.0023	0.152
	4	31.79	2.81258	71.83	0.12	71.93	0.0018	0.193
	5	9.03	9.78368	65.52	0.26	32.03	0.0144	0.974
Au (III) complex	1	26.303	3.38556	100	0.21	40.59	0.0039	0.606
	2	15.234	5.81127	86.57	0.18	46.53	0.0059	0.461
	3	34.326	2.61036	61.53	0.30	28.97	0.0042	1.19
	4	32.463	2.75580	59.39	0.12	72.05	0.0018	0.192
	5	24.625	3.61227	45.73	0.18	47.2	0.0036	0.448

### **3.15. Field-Emission Scanning Electron Microscope Apparatus (FE-SEM)**

Field-emission scanning electron microscopy (FE-SEM) was carried out experiments, for azo dye Ligand and its chelate complexes along with the distribution, surface, and the generated morphology of particles and aggregations. The FE-SEM image of the ligand and its complexes has been illustrated in Figure (3.15). Particles size around 68.93 nm were haphazardly scattered over the irregularly broken ice rock structures exhibited by the ligand [18]. The Co(III)- Complex FE-SEM image showed the form of the hetero-geneous surface with an average size of 88.38 nm. The average size of the Ni (II)-Complex was 71.52 nm, and it appeared to be a hetero-geneous crystal. The Cu(II)-Complex's FE-SEM image appeared to be glass sheet crystals with an average size of 77.94 nm [125].

In contrast, the Ag(I)- Complex's FE-SEM image appeared to have a uniform crystalline surface with an average particle size of 73.52 nm. At last, the Au(III)-Complex's FE-SEM study showed unevenly sized sheet crystals with an average size of 50.24 nm. The 2-[2'-(5- methylthiazolyl) azo]-5-,6-dimethyl benzoimidazol and its chelates complexes show a wide range of FE-SEM micrographs due to the reason that metallic ions coordinate with ligand donor locations. Additionally, metal complex FE-SEM pictures showed that changing the metallic ions changes the surface structure of metallic complexes. To understand ligands and complexes at the nanoscale, demonstrate that the created compounds' particles are less than 100 nm [98], [121].



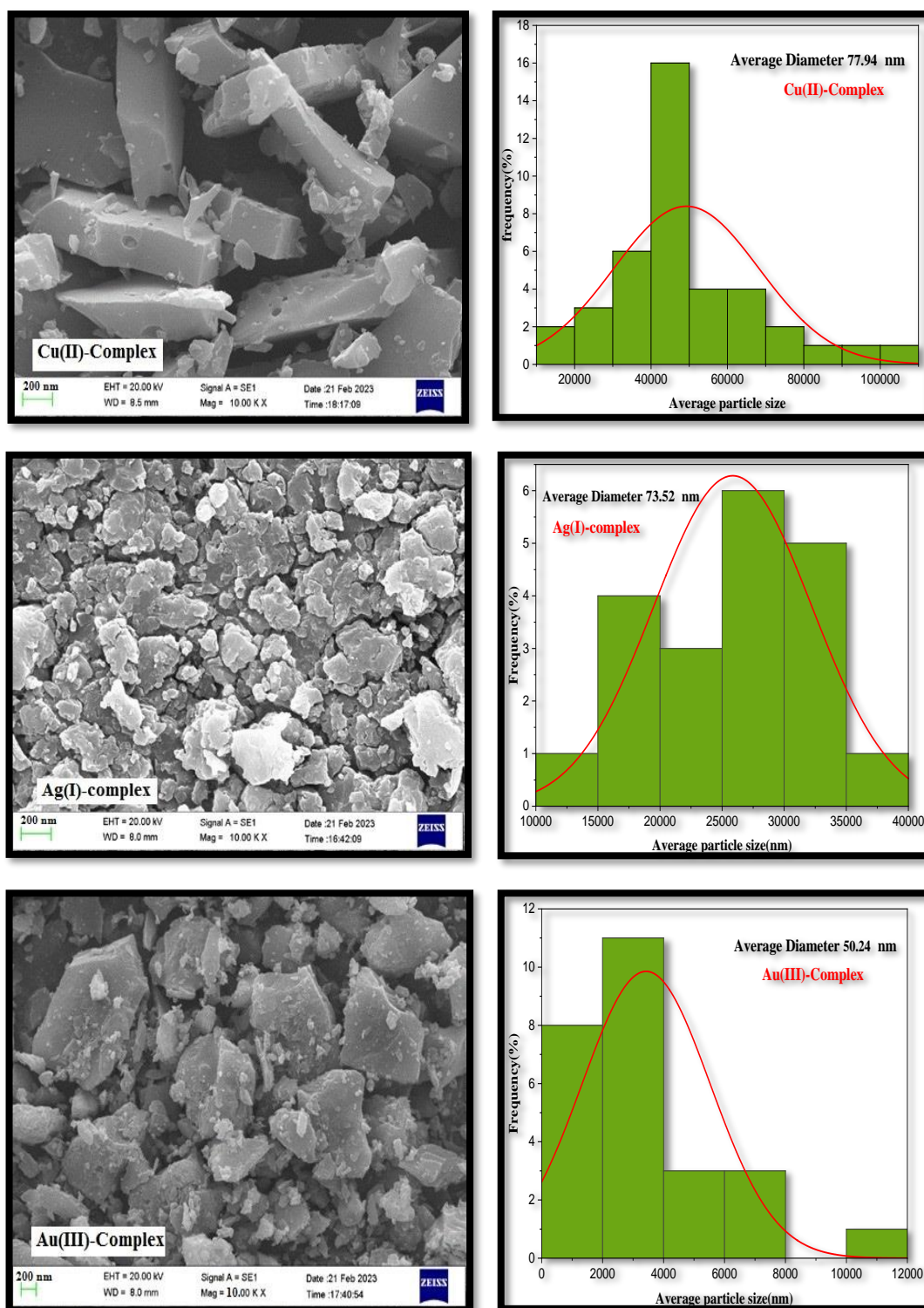
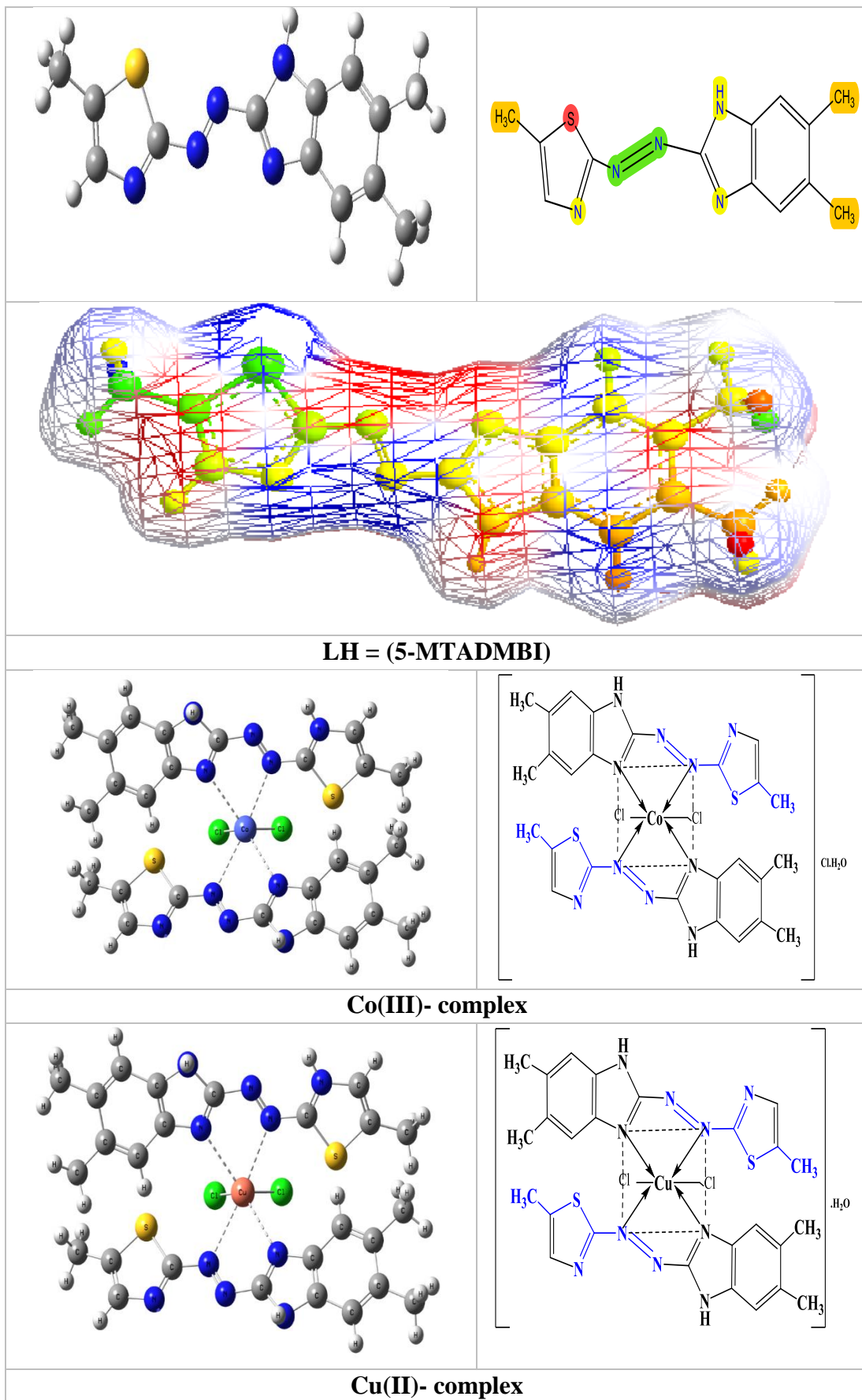
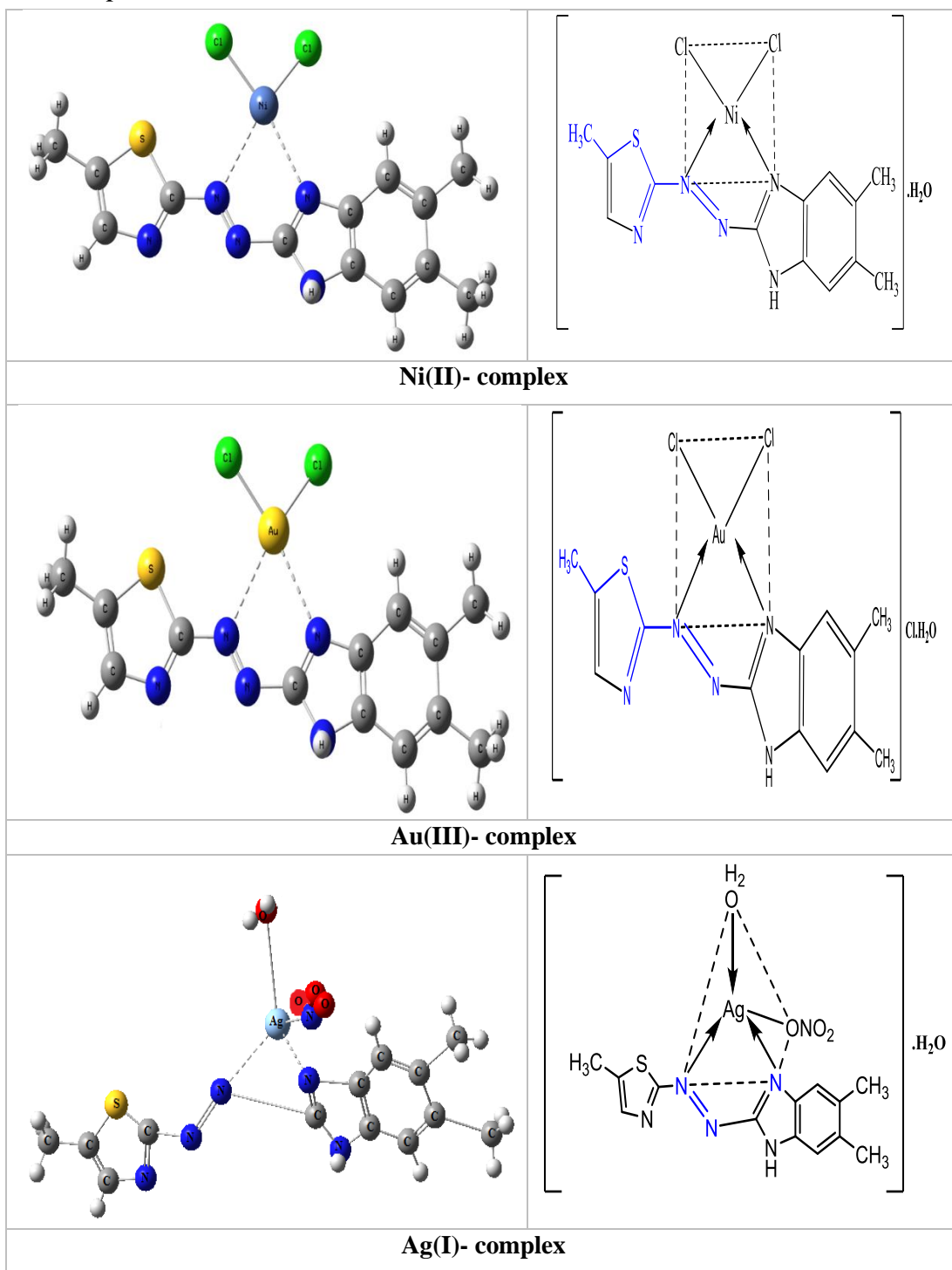


Figure 3.15: FESEM images of the (5-MTADMBI) and its metallic complexes

**3.16. Suggested Structural Formula of Chelate Complexes**

According to the information that was stated in the literature [126], [101] about the coordination sites available in the in the ligand and how they relate to different metal ions by the analytical ,chemical and spectral data that were reached through the results of the evaluation measurements obtained from the molar ratios, magnetic measurements and molar electrical conductivity, as well as the results of the <sup>1</sup>HNMR spectra, the <sup>13</sup>CNMR spectra, the mass spectra, the ultraviolet-visible spectra (UV-Vis), the finding obtained from the infrared spectra (FT-IR), the thermogravimetric decomposition technique (TGA) and DTG) that was conducted, we can conclude that azo ligand behaviour bidentate by the coordination process, and the coordination is via then N- atom of the benzoimidazol ring with the N- atom of the azo bridge group far from the thiazole ring to give two pentagonal chelating rings, which makes the formed metallic compounds more stable [127]. Figure (3.16) shows the proposed structure for the metallic complexes under study.





**Figure 3.16:** Possible geometry for (5-MTADMBI) and their metallic complexes.

### **3.17 Biological Activity**

#### **3.17.1. Antibacterial action in vitro**

The biological activity of the organic ligand and their metallic complex were evaluated versus the (G + ve) and (G -ve) bacteria **Streptococcus** and **Escherichia coli**, furthermore against the fungus **Penicillium sp**, utilizing the diffusion methodology in agar. DMSO was used to dissolve the chemicals in order to prepare the stock solution. Solutions have been added to the wells using a micropipette [128]. The ligand showed great effectiveness versus the studied bacteria and fungi when compared to **Ciprofloxacin** and **Cycloheximide**, two common drugs.

Most tests show that the complexes have stronger biological activity than equivalent azo ligands. After 24 hours and 7 days, respectively, the dimensions of the inhibited zones for fungus and bacteria were assessed. By using the agar well diffusion method, every solution's concentration in DMSO solvent was 0.2 mg/mL. The chelation theory can explain metallic complexes' increased activity, by exchanging positive charges (+) with the donating atoms in the ligand, chelation reduces the polarity of the metallic ion and may lead to  $\pi$ -electron delocalization.

This phenomenon makes the metal chelates more lipophilic, which makes it easier for them to penetrate the lipid layer of the bacterium and more efficiently destroy it [129]. Further factors which impact activity include solubility, conductivity, and the length of the bond between the metallic and the ligand. The results presented in Table (3.14) and Figure (3.17) show that the metallic complexes of Co (III), Ni (II), Cu (II), Ag (I) and Au (III) are strongly active against the chosen bacteria and fungus.

**Table 3.14:** Biological activity data for ligand and their metallic complexes with respect to inhibitory zone.

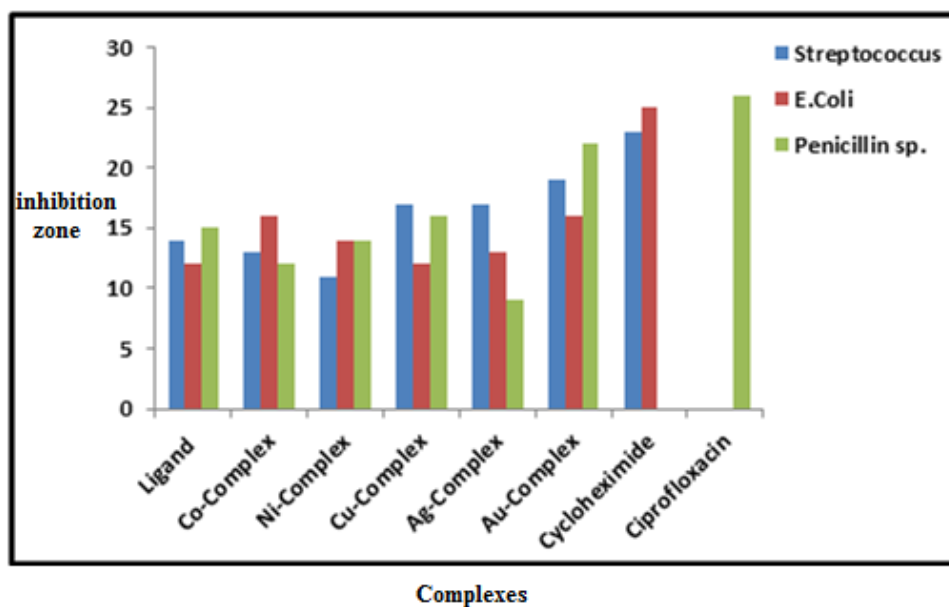
Compound	Bacterial species		Fungi
	G + ve	G -ve	<i>Penicillium sp</i>
	<i>Streptococcus aureus</i>	<i>Escherichia coli</i>	
Ciprofloxacin	+++	+++	...
Cycloheximide	...	...	+++
(5-MTADMBI )	++	+	+
[Co(L <sub>1</sub> ) <sub>2</sub> ]Cl.H <sub>2</sub> O	+	++	+
[Ni(L <sub>1</sub> ) <sub>2</sub> ].H <sub>2</sub> O	...	...	...
[Cu(L <sub>1</sub> ) <sub>2</sub> ].H <sub>2</sub> O	+	+	...
[Ag(L <sub>1</sub> )(H <sub>2</sub> O)].H <sub>2</sub> O	...	+	...
[Au(L <sub>1</sub> )Cl]Cl.H <sub>2</sub> O	...	...	...

Highly active = +++ (inhibition zone > 20 mm)

Moderately active = ++ (inhibition zone 15-20 mm)

Weakly active = + (inhibition zone 10-15 mm)

Inactive = - (inhibition zone <10 mm)

**Figure 3.17:** Organic ligand (5-MTADMBI) and their complexes' in vitro antibacterial activity.



**Figure 3.18:** The inhibition zone for (5-MTADMBI) and their complexes with gram positive Bacteria (*Streptococcus*).

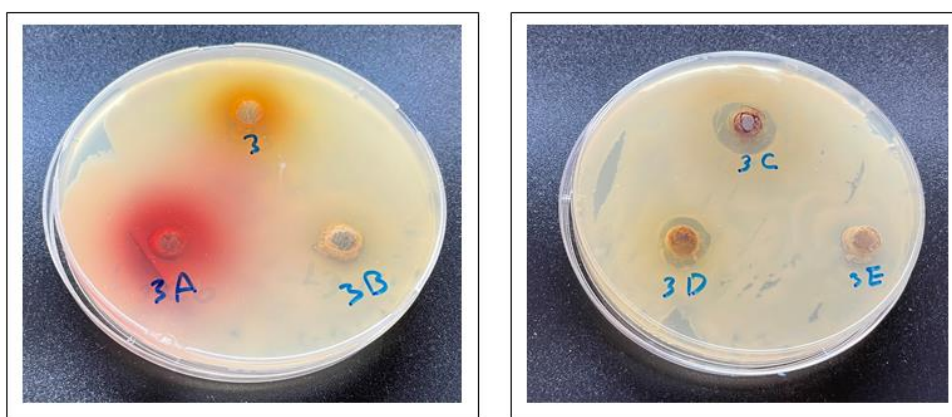


**Figure 3.19:** The inhibition zone for (3) (5-MTADMBI), (a) (Co), (b) (Ni), (c) (Cu), (d) (Ag), (e) (Au) with gram negative Bacteria (*Escherichia coli*).

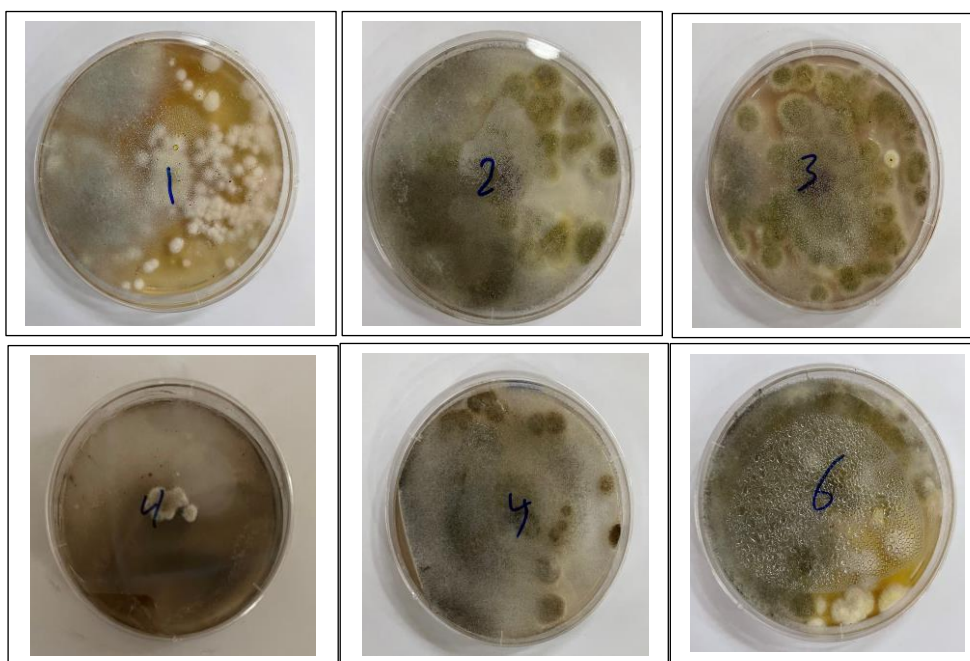


**Figure 3.20:** The inhibition zone for (1) (5-MTADMBI), (2) (Co), (3) (Ni), (4) (Cu), (5) (Ag), (6) (Au) with fungi (*Penicillium sp.*).

### **3.18. Assays for cytotoxicity using (MTT)**

In this study, two types of cell lines were used: lung cancer cell line (A549), pancreas carcinoma cell line (TP-53), and normal cell line (HdFn) for comparison, in order to demonstrate their effectiveness on human body cells and the extent to which they can be used as cancer drugs. In detail, the effect of some of the prepared materials under study on cancer cells and on healthy cells of each type, as the test (MTT) was used for vital examinations of all cells by MTT assay after incubated for 24 hr at 37°C.

#### **3.18.1. Cytotoxic activity of the (5-MTADMBI) ligand and Co(III)-complex on A549 cell viability.**

We have examined the cytotoxicity of the 2-[2'-(5- methylthiazolyl) azo]-5,6-dimethyl benzoimidazol ligand and its corresponding Co(III)-complex versus the lung Malignancy cell line (A549) and the healthy human dermal fibroblast cell (HdFn). The MTT test was employed to assess the cytotoxic study of the compounds after being incubated at 37°C for 24 hr, using varying concentration ranges of 12.5, 25, 50, 100, and 200 µg/mL [130]. The results showed that at 200 µg/ml, the ligand's inhibition cytotoxicity for tumor cells death was 83.52%, and the corresponding complex was slightly higher (90.10%) than the ligand whereas HdFn cells were unaffected at the same concentration.

The results suggest that the tested compounds exhibited the highest degree of inhibition when subjected to 200 µg/ml for a duration of 24 hours, whereas the minimum inhibition was observed when 12.5 µg/ml was used. The IC<sub>50</sub> values for the ligand and the complex were determined to be 68.51 and 64.20 µg/mL, respectively,

against lung cancer cells. The ligand and the complex exhibited cytotoxic potential towards normal cells with an IC<sub>50</sub> value of 76.85 and 83.40 µg/mL respectively.

Figures (3.21) and (3.22) illustrate the percentages of cell viability for the prepared ligand and the complex. The findings indicate the potential of utilizing the synthesized compounds as effective agents in the medical domain. The viability rate data acquired after treating A549 and HdFn cells for 24 hours with varying doses of the selected drugs is shown in Tables (3.15) and (3.16).

**Table 3.15:** The cytotoxicity of (5-MTADMBI) was assessed on the A549 carcinoma cell line and the HdFn cell line following a 24-hour incubation period at 37°C.

Concentration (µg/ml)	LH =5-MTADMBI			
	Cancer line cells		Normal line cells	
	A459		HdFn	
	Cell Viability	% Cell Inhibition	Cell Viability	% Cell Inhibition
	Mean± SD		Mean± SD	
200	16.472±1.13	83.52	88.95±0.81	11.05
100	64.39±4.02	35.61	76.69±2.60	23.31
50	78.395±0.75	21.605	84.33±2.66	15.67
25	94.09±2.20	5.91	86.07±1.91	13.93
12.5	94.869±1.39	5.131	95.216±0.82	4.784
IC <sub>50</sub>	68.51		76.85	

**Table 3.16:** The cytotoxicity of Co(III)-Complex was evaluated versus the HdFn cell line and the A549 cancer cell line following a 24-hour incubation period at 37°C.

Concentration ( $\mu\text{g/ml}$ )	Co-Complex			
	Cancer line cells		Normal line cells	
	A459		HdFn	
	Cell Viability	% Cell Inhibition	Cell Viability	% Cell Inhibition
	Mean $\pm$ SD		Mean $\pm$ SD	
200	9.892 $\pm$ 2.05	90.10	80.20 $\pm$ 1.95	19.8
100	53.43 $\pm$ 7.95	46.57	72.64 $\pm$ 3.1	27.36
50	71.87 $\pm$ 0.46	28.13	85.64 $\pm$ 3.32	14.36
25	84.49 $\pm$ 0.6	15.51	94.17 $\pm$ 0.77	5.83
12.5	96.95 $\pm$ 1.23	3.05	96.18 $\pm$ 0.23	3.82
IC <sub>50</sub>	64.20		83.4	

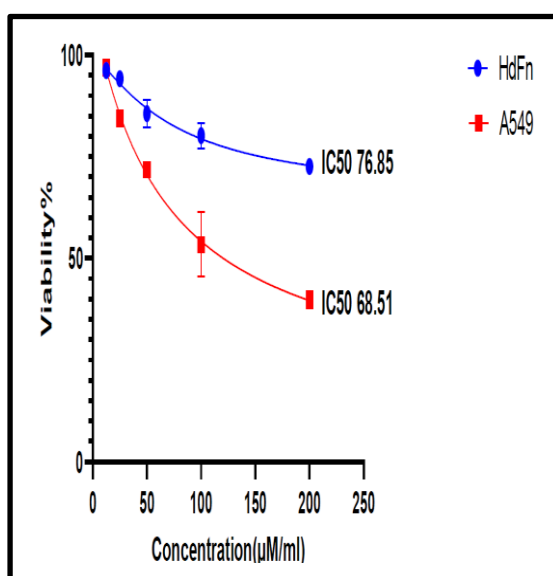


**Figure 3.21:** IC<sub>50</sub> for ligand (5-MTADMBI) in normal (HdFn) and (A549) cell lines

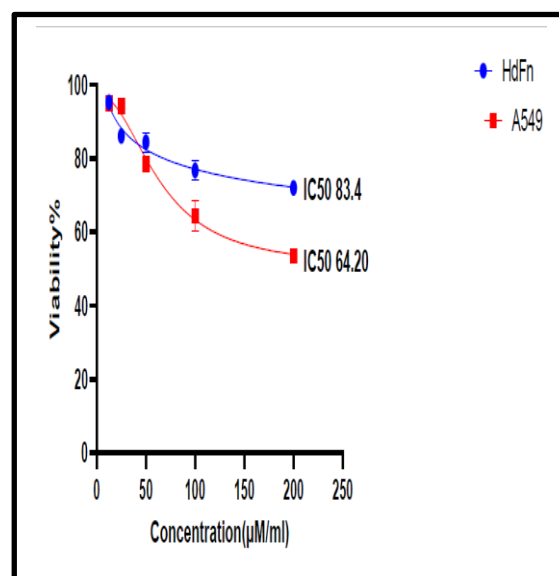


**Figure 3.22:** IC<sub>50</sub> for Co(III)-Complex in normal (HdFn) and (A549) cell lines

### **3.18.2. Cytotoxic activity of the (5-MTADMBI) ligand and Ag (I)-complex on TP-53 cell viability**

Chemotherapy is the main approach for both metastasized and localized cancer [131]. We investigated the cytotoxic activity and mechanism of action of the synthesized 2-[2'-(5- methylthiazolyl) azo]-5-,6-dimethyl benzoimidazol ligand with Ag(I)-Complex against pancreas carcinoma cell line (TP-53) and normal cells human (HdFn) by MTT assay after incubation for 24-hour at 37<sup>0</sup>C and concentrations (12.5, 25, 50, 100, and 200 g/mL).

The ligand 2-[2'-(5- methylthiazolyl) azo]-5-,6-dimethyl benzoimidazol and Ag (I)-Complex inhibited cancer cells dead at a dosage of 100 µg/ml, with a cytotoxic activity of (72.34%) and (58.61%), whereas the percentage inhibition of the normal cells (HdFn) at the same concentration was 28.85 % and 14.36%. Additionally, it can be deduced that dosages of 100 µg/ml inhibited all evaluated substances the most during a 24-hour incubation period, while quantities of 12.5 µg/ml inhibited the lowest. This concentration (IC<sub>50</sub>) destroys about 50% of the cells (IC<sub>50</sub>) of the ligand 2-[2'-(5- methylthiazolyl) azo]-5-,6-dimethyl benzoimidazol ligand demonstrated selective cytotoxicity versus carcinoma cell lines of (TP-53 ) pancreas with IC<sub>50</sub> = 11.92 µg/ml, whereas it was 76.85 µg/ml for healthy human cells (HdFn), the Ag (I)-complex was showed versus carcinoma cell line carcinoma pancreas cell lines (TP-53) with IC<sub>50</sub> = 32.02 µg/ml, while it was 69.93 µg/ml for healthy human cells(HdFn).

The findings indicate the possibility of using the prepared compounds as antitumor drugs in the field of medicine and pharmacy against pancreas cancer. Tables (3.17) and (3.18) demonstrate the IC<sub>50</sub> values and viability rate values observed after treating TP-53 and HdFn cells for 24 hours at various doses of the chosen substances.

Figures (3.23) and (3.24) show the viability rates of TP-53 cells and HdFn cells obtained with the selected compounds.

**Table 3.17:** The cytotoxicity of (5-MTADMBI) was assessed on the TP-53 carcinoma cell line and the HdFn cell line following a 24-hour incubation period at 37°C.

Concentration (µg/ml)	LH =5-MTADMBI			
	Cancer line cells		Normal line cells	
	TP-53		HdFn	
	Cell Viability	% Cell Inhibition	Cell Viability	% Cell Inhibition
	Mean± SD		Mean± SD	
200	27.66±2.27	72.34	62.26±4.62	37.74
100	39.12±3.15	60.88	65.97±1.10	34.03
50	54.012±3.23	45.99	71.142±1.83	28.858
25	64.69±4.71	35.31	86.304±3.74	13.696
12.5	75.038±4.9	24.962	95.37±0.90	4.63
IC <sub>50</sub>	11.92		76.85	

**Table 3.18:** The cytotoxicity of Ag(I) -Complex was assessed versus the HdFn cell line and the TP-53 cancer cell line following a 24-hour incubation period at 37°C.

Concentration (µg/ml)	Ag-Complex			
	Cancer line cells		Normal line cells	
	TP-53		HdFn	
	Cell Viability	% Cell Inhibition	Cell Viability	% Cell Inhibition
	Mean± SD		Mean± SD	
200	41.39±5.75	58.61	72.64±1.9	27.36
100	51.81±0.40	48.19	80.20±3.11	19.80
50	61.96±4.38	38.04	85.64±3.3	14.36
25	73.2±2.71	26.80	94.17±0.77	5.83
12.5	84.14±0.83	15.86	96.18±0.23	3.82
IC <sub>50</sub>	32.02		69.93	

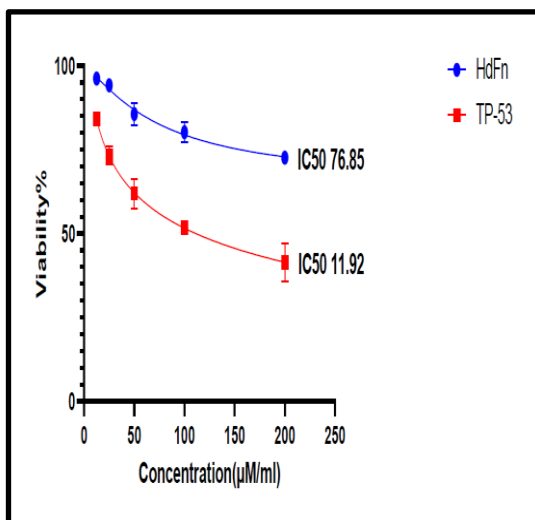


**Figure 3.23:** IC<sub>50</sub> for ligand (5-MTADMBI) in normal (HdFn) and (TP-53) cell lines

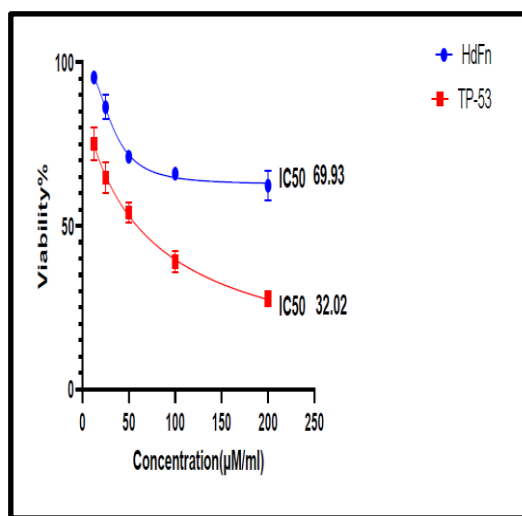


**Figure 3.24:** IC<sub>50</sub> for Ag(I)-Complex in normal (HdFn) and (TP-53) cell lines

# Chapter Four

## *Conclusion & Recommendation*

## 4.0 Conclusion & Recommendation

### 4.1. Conclusions

Based on the results of the spectral and analytical physicochemical studies for the ligand 2-[2'-(5-methylthiazolyl) azo]-5,6-dimethyl benzoimidazol and their complexes, some conclusions have been achieved that lead to establishing the following points:

1. The molar ratio of [metal: ligand] is [1:2] for complexes of cobalt (III) and copper (II), while the molar ratio of [metal: ligand] is [1:1] for complexes of nickel (II), silver (I) and gold (III). These complexes also possessed a non-electrolytic character, a non-ionic character, except the metallic complexes of cobalt (III) and gold (III) ions, which had an electrolytic character.

2. Through the results obtained from the study, it was found that the proposed structural formulas for the prepared metallic complexes, clearly for the ligand, the behavior of the bidentate ligands when coordinated with the metal ions to form two chelating rings through which increase the stability of the formed metal complexes.

3. The thermogravimetric analysis of all the prepared compounds proved that they are not affected by moisture, light, or heat, with high melting points, indicating their high stability and thermal stability.

4. The results of the FESEM analysis showed the homogeneity of the surfaces of some of the prepared compounds under study, as the ligand and some of its prepared metallic complexes showed a granular size of less than 100 nm, meaning that they are within the nanoscale range. These compounds have importance in the industrial and medical fields.

5. The results of the X-ray diffraction analysis showed that ligand thiazolyl azo and its metallic complexes have varying crystalline systems in the crystalline and effects that ligand thiazolyl azo

and complex metals are the granular size of less than 100nm, which is within the nanoscale and at the same time enhances the results for the previous measurements of FESEM.

6. A study of the biological activity of thiazolyl azo ligand and its prepared metal complexes showed their biological effect, with varying degrees, on two types of bacteria (**Streptococcus, Escherichia coli**) and a kind of fungi (**Penicillium sp.**) that cause many common diseases.

7. The toxicological examinations of some compounds conducted on human cells revealed the ligand 2-[2'-(5-methylthiazolyl) azo]-5,6-dimethyl benzoimidazol and the copper(II) complex intensity finding regarding on the growth of lung cancer cell lines (A549), and the silver(I) complex on the growth of pancreatic cancer cell lines (TP-53) and healthy cells (HdFn), these findings shed light on toxic effectiveness on the cells of the human body and the potential treatment of the cancers mentioned above, the thiazolyl azo ligand, and its metallic complexes under study showed a relatively high selectivity in killing cancer cells within the results obtained from the  $IC_{50}$ , where we note the value of the  $IC_{50}$  for normal cells is more elevated, while the value of  $IC_{50}$  for cancer cell lines is less, and this is an essential result in this field of our research, this discovery holds promise for future to be used as a treatment for many types of cancers.

## **4.2. Recommendations**

Based on the above, the following recommendations can be proposed:

1. The possibility of using the thiazolyl azo ligand and its metal complexes is under study as inhibitors of different types of bacteria and fungi that cause many diseases and anti-cancer drugs and benefit from them in the medical and pharmaceutical fields.
2. Through FESEM analysis, it became clear that some of the prepared compounds have a granular size within the nanoscale range, and this characteristic is good and can be used in several fields, including industrial and medical. Therefore, one of the essential things we recommend in the future is to expand the study of these ligands and their metal complexes prepared in the fields mentioned above.
3. The prepared ligand under study can be used to prepare metal complexes with ions of other transitional or representative metallic elements as long as it can coordinate with these ions and be identified by the available analytical and spectroscopic means.
4. Exploiting the color characteristic of solutions of compounds prepared in analytical chemistry for spectroscopic determination or to extract ions of the elements under study and other metal ions due to their ability to form colored metal complexes.
5. The possibility of using thiazolyl azo ligand in dyeing exists because of its high stability towards light, heat, and moisture.
6. The results of toxicity tests on cancerous and healthy cells by the MTT method for the compounds under study showed that the type and concentration of the compound used are two critical factors in determining the percentage of cell inhibition.

# *References*

**References**

- [1] G. Frenking, G. J. Leigh, and N. Winterton, "Modern Coordination Chemistry: The Legacy of Joseph Chatt," *R. Soc. London*, vol. 60, no. 7, p. 111, 2002.
- [2] A. D. Garnovskii and B. I. Kharissov, "Synthetic coordination and organometallic chemistry," *CRC Press*, vol. 26, no. 4, p.446 2003.
- [3] J. R. Gispert, "Coordination chemistry," *Wiley-VCH Weinheim*, vol. 483, no.5, p. 640, 2008.
- [4] G. A. Lawrance, "Introduction to coordination chemistry," *John Wiley & Sons*, vol.28, no.3, p. 290, 2013.
- [5] X.-M. Chen and M.-L. Tong, "Solvothermal in situ metal/ligand reactions: a new bridge between coordination chemistry and organic synthetic chemistry," *Acc. Chem. Res.*, vol. 40, no. 2, pp. 162–170, 2007.
- [6] C. G. Oliva N. Jagerovic, P. Goya, I. Alkorta, J. Elguero, R. Cuberes, and A. Dordal, "N-Substituted-1, 2, 3-triazoles: synthesis, characterization and evaluation as cannabinoid ligands," *Arkivoc*, vol. 2, no.7, pp. 127–147, 2010.
- [7] E. Yates and A. Yates, "Johann Peter Griess FRS (1829–88): Victorian brewer and synthetic dye chemist," *Notes Rec. R. Soc. J. Hist. Sci.*, vol. 70, no. 1, pp. 65–81, 2016.
- [8] P. Saharan, V. Kumar, I. Kaushal, A. Mittal, S. K. Shukla, D. Kumar, A. K. Sharma H. Om "A comprehensive review on the metal-based green valorized nanocomposite for the remediation of emerging colored organic waste," *Environ. Sci. Pollut. Res.*, vol. 30, no. 16, pp. 45677–45700, 2023.
- [9] Y. Ali, S. A. Hamid, and U. Rashid, "Biomedical Applications of Aromatic Azo Compounds," *Mini-Reviews Med. Chem.*, vol. 18, no. 18, pp. 1548–1558, 2018.
- [10] A. A. Mizhir, H. S. Al-Lami, and A. A. Abdulwahid, "Kinetic, Isotherm, and Thermodynamic study of Bismarck brown dye adsorption onto Graphene oxide and Graphene oxide-grafted-poly (n-butyl methacrylate-co-methacrylic Acid)," *Baghdad Sci. J.*, vol. 19, no. 1, pp. 132–140, 2022.

- [11] M. Keiluweit and M. Kleber, "Molecular-level interactions in soils and sediments: The role of aromatic  $\pi$ -systems," *Environ. Sci. Technol.*, vol. 43, no. 10, pp. 3421–3429, 2009.
- [12] A. R. Kennedy, L. K. Conway, J. B. A. Kirkhouse, K. M. McCarney, O. Puissegur, E. Staunton, S. J. Teat, J. E. Warren, "Monosulfonated AZO dyes: A crystallographic study of the molecular structures of the free acid, anionic and dianionic forms," *Crystals*, vol. 10, no. 8, pp. 1–17, 2020.
- [13] F. Wang, J. Huang, and J. Xu, "Continuous-flow synthesis of azo dyes in a microreactor system," *Chem. Eng. Process. - Process Intensif.*, vol. 127, pp. 43–49, 2018.
- [14] R. El-kailany, N. Elsharif, and A. Ahmida, "Chemistry and Applications of Azo Dyes: A Comprehensive Review," *J. Chem. Rev.*, vol. 4, no. 4, pp. 313–330, 2022.
- [15] N. M. Aljamali and H. S. Hassen, "Review on azo-compounds and their applications," *J. Catal. Catal.*, vol. 8, no. 2, pp. 8–16, 2021.
- [16] T. T. Liu, J. Z. Yan, X. W. Cheng, P. Duan, and Y. F. Zeng, "One-pot synthesis of azo compounds in the absence of acidic or alkaline additives," *J. Chem. Res.*, vol. 45, no. 5–6, pp. 486–490, 2021.
- [17] S. S. ad Abdullahi, H. Musa, S. Habibu, A. H. Birniwa, and R. E. A. Mohammad, "Comparative study and dyeing performance of as-synthesized azo heterocyclic monomeric, polymeric, and commercial disperse dyes," *Turkish J. Chem.*, vol. 46, no. 6, pp. 1841–1852, 2022.
- [18] K. J. Al-Adilee, S. H. Jawad, H. A. K. Kyhoiesh, and H. M. Hassan, "Synthesis, characterization, biological applications, and molecular docking studies of some transition metal complexes with azo dye ligand derived from 5-methyl imidazole," *J. Mol. Struct.*, vol. 1295, no. 7, p. 136695, 2024.
- [19] S. Benkhaya, S. M'rabet, and A. El Harfi, "Classifications, properties, recent synthesis and applications of azo dyes," *Heliyon*, vol. 6, no. 1, 2020.

- [20] K. M. A. Abdelmoteleb, M. A. El-Asasery, A. A. F. Wasfy, and S. M. Ahmed, "Synthesis of New Monoazo Disperse Dyes for Dyeing Polyester Fabric Using Two Different Dyeing Methods: Demonstration of Their Antibacterial and Anticancer Activities," *Polym. (Basel)*, vol. 15, no. 14, 2023.
- [21] I. M. Kamal, N. F. Abdeltawab, Y. M. Ragab, M. A. Farag, and M. A. Ramadan, "Biodegradation, Decolorization, and Detoxification of Di-Azo Dye Direct Red 81 by Halotolerant, Alkali-Thermo-Tolerant Bacterial Mixed Cultures," *Microorganisms*, vol. 10, no. 5, pp.1-26, 2022.
- [22] A. Z. Omar, M. A. El-Rahman, E. A. Hamed, S. K. El-Sadany, and M. A. El-atawy, "Synthesis, spectroscopic characterization and dyeing performance of novel bis azo dyes derived from benzidine," *Sci. Rep.*, vol. 13, no. 1, pp. 1–14, 2023.
- [23] J. T. Chacko and K. Subramaniam, "Enzymatic Degradation of Azo Dyes – A Review," *Int. J. Environmental Sci.*, vol. 1, no. 6, pp. 1250–1260, 2011.
- [24] J. Naime, M. S. Al Mamun, M. Aly Saad Aly, M. Maniruzzaman, M. M. R. Badal, and K. M. R. Karim, "Synthesis, characterization and application of a novel polyazo dye as a universal acid-base indicator," *RSC Adv.*, vol. 12, no. 43, pp. 28034–28042, 2022.
- [25] A. Duursma, D. Peña, A. J. Minnaard, and B. L. Feringa, "Improved catalytic asymmetric carbon-carbon bond formation using combinations of chiral and achiral monodentate ligands," *Tetrahedron Asymmetry*, vol. 16, no. 11, pp. 1901–1904, 2005.
- [26] B. Naureen, G. A. Miana, K. Shahid, M. Asghar, S. Tanveer, and A. Sarwar, "Iron (III) and zinc (II) monodentate Schiff base metal complexes: Synthesis, characterisation and biological activities," *J. Mol. Struct.*, vol. 1231, pp. 129946, 2021.
- [27] D. I. Ugwu and J. Conradie, "Anticancer properties of complexes derived from bidentate ligands," *J. Inorg. Biochem.*, vol. 246, no. September, pp. 112268, 2023.

- [28] S. M. Reda and A. A. S. Al-hamdani, “Mn ( II ), Fe ( III ), Co ( II ) and Rh ( III ) complexes with azo ligand : Synthesis , characterization , thermal analysis and bioactivity,” vol. 20, no. 11, pp.1-19, 2023.
- [29] A. A. S. Al-Hamdani and W. Al Zoubi, “New metal complexes of N3 tridentate ligand: Synthesis, spectral studies and biological activity,” *Spectrochim. Acta - Part A Mol. Biomol. Spectrosc.*, vol. 137, pp. 75–89, 2015.
- [30] M. A. I. Al-Gaber, H. M. Abd El-Lateef, M. M. Khalaf, S. Shaaban, M. Shawky, G.G. Mohamed, A. Abdou, M. Gouda, A. M. Abu-Dief , “Design, Synthesis, Spectroscopic Inspection, DFT and Molecular Docking Study of Metal Chelates Incorporating Azo Dye Ligand for Biological Evaluation,” *Mater. (Basel)*., vol. 16, no. 3, pp.1-23, 2023.
- [31] V. G. Vidya and V. Sadasivan, “Synthesis, spectroscopic characterization and biological activities of some metal complexes with new heterocyclic azodye ligand 2-(2-hydroxynaphthalen-1-yl azo)-pyridin-3-ol,” *Curr. Chem. Lett.*, vol. 12, no. 1, pp. 55–64, 2023.
- [32] T. A. Khattab and M. Rehan, “A review on synthesis of nitrogen-containing heterocyclic dyes for textile fibers - Part 1: five and six-membered heterocycles,” *Egypt. J. Chem.*, vol. 61, no. 5, pp. 897–937, 2018.
- [33] K. Mezgebe and E. Mulugeta, “Synthesis and pharmacological activities of azo dye derivatives incorporating heterocyclic scaffolds: a review,” *RSC Adv.*, vol. 12, no. 40, pp. 25932–25946, 2022.
- [34] S. Prakash et al., “Synthesis and characterization of novel bioactive azo compounds fused with benzothiazole and their versatile biological applications,” *J. Mol. Struct.*, vol. 1224, pp. 129016, 2021.
- [35] B. N. Ravi, J. Keshavayya, N. M. Mallikarjuna, and H. M. Santhosh, “Synthesis, characterization, cyclic voltammetric and cytotoxic studies of azo dyes containing thiazole moiety,” *Chem. Data Collect.*, vol. 25, pp. 100334, 2020.

- [36] M. R. Maliyappa, J. Keshavayya, N. M. Mallikarjuna, and I. Pushpavathi, "Novel substituted aniline based heterocyclic dispersed azo dyes coupling with 5-methyl-2-(6-methyl-1, 3-benzothiazol-2-yl)-2, 4-dihydro-3H-pyrazol-3-one: Synthesis, structural, computational and biological studies," *J. Mol. Struct.*, vol. 1205, pp. 127576, 2020.
- [37] G. Patel, D. K. Dewangan, N. Bhakat, and S. Banerjee, "Green approaches for the synthesis of poly-functionalized imidazole derivatives: A comprehensive review," *Curr. Res. Green Sustain. Chem.*, vol. 4, no. 7, pp. 100175, 2021.
- [38] G. G. Sadullayeva, "The use of imidazole in medicine," *Analytical J. edu. dev.*, vol. 02, no.9, pp. 41–47, 2022.
- [39] K. Shahzad, F. Abbas, D. Pandey, S. Ajmal, M. Khadim, and M. U. Tahir, "Synthesis, characterization and biological evaluation of novel tetrasubstituted Imidazole compounds," *Preprints*, vol. 1, no.1, pp. 1-11, 2020.
- [40] A. Bhatnagar, P. K. Sharma, and N. Kumar, "A review on 'imidazoles': Their chemistry and pharmacological potentials," *Int. J. PharmTech Res.*, vol. 3, no. 1, pp. 268–282, 2011.
- [41] S. Rupp, P. D. Dutschke, J. Kinas, A. Hepp, and F. Ekkehardt Hahn, "Synthesis and Metallation of Unsymmetric Tetrakisimidazolium Macrocycles," *Eur. J. Inorg. Chem.*, vol. 2022, no. 20, 2022.
- [42] A. Rusu, I. Moga, and L. Uncu, "The Role of Five-Membered Heterocycles in the Molecular Structure of Antibacterial Drugs Used in Therapy," *Pharmaceutics*, vol.15, no.10, pp.1-51, 2023.
- [43] A. M. Borcea, I. Ionuț, O. Crișan, and O. Oniga, "An overview of the synthesis and antimicrobial, antiprotozoal, and antitumor activity of thiazole and bithiazole derivatives," *Mol.*, vol. 26, no. 3, pp.1-26, 2021.
- [44] C. B. Mishra, S. Kumari, and M. Tiwari, "Thiazole: A promising heterocycle for the development of potent CNS active agents," *Eur. J. Med. Chem.*, vol. 92, pp. 1–34, 2015.

- [45] S. Dey, A. Das, and M. F. Hossain, "Synthetic Strategies for Hydrazinyl Thiazole Derivatives," *ChemistrySelect*, vol. 5, no. 48, pp. 15153–15166, 2020.
- [46] M. A. Meshram, U. O. Bhise, P. N. Makhal, and V. R. Kaki, "Synthetically-tailored and nature-derived dual COX-2/5-LOX inhibitors: Structural aspects and SAR," *Eur. J. Med. Chem.*, vol. 225, pp. 113804, 2021.
- [47] T. A. Elmaaty, S. M. Ramadan, K. El-Nagar, D. Zaghloul, and F. El-Taweel, "One Step Printing and Functionalization of Microwave Pretreated PET Fabric Using New Azo Amino Thiazole Disperse Dye," *Fibers Polym.*, vol. 21, no. 10, pp. 2292–2300, 2020.
- [48] A. S. Waheeb and K. J. Al-Adilee, "Synthesis, characterization and antimicrobial activity studies of new heterocyclic azo dye derived from 2-amino- 4,5- dimethyl thiazole with some metal ions," *Mater. Today Proc.*, vol. 42, no. 2, pp. 2150–2163, 2021.
- [49] H. A. K. Kyhoiesh and K. J. Al-Adilee, "Pt (IV) and Au (III) complexes with tridentate-benzothiazole based ligand: synthesis, characterization, biological applications (antibacterial, antifungal, antioxidant, anticancer and molecular docking) and DFT calculation," *Inorganica Chim. Acta*, vol. 555, pp. 121598, 2023.
- [50] K. J. AL-Adilee, A. K. Abass, and A. M. Taher, "Synthesis of some transition metal complexes with new heterocyclic thiazolyl azo dye and their uses as sensitizers in photo reactions," *J. Mol. Struct.*, vol. 1108, pp. 378–397, 2016.
- [51] E. Kabir and M. Uzzaman, "A review on biological and medicinal impact of heterocyclic compounds," *Results Chem.*, vol. 4, no. 1, pp. 100606, 2022.
- [52] V. Gupta and V. Kant, "A review on biological activity of imidazole and thiazole moieties and their derivatives," *Sci. Int*, vol. 1, no. 7, pp. 253–260, 2013.
- [53] Y. Hu, C.-Y. Li, X.-M. Wang, Y.-H. Yang, and H.-L. Zhu, "1, 3, 4-Thiadiazole: synthesis, reactions, and applications in medicinal, agricultural, and materials chemistry," *Chem. Rev.*, vol. 114, no. 10, pp. 5572–5610, 2014.

## *References*

---

- [54] S. B. Konnur and S. T. Nandibewoor, "Electrochemical behavior of 2-aminothiazole at poly glycine modified pencil graphite electrode," *Anal. Bioanal. Electrochem.*, vol. 12, no. 2, pp. 208–222, 2020.
- [55] L. Yurttas, F. Tay, and S. Demirayak, "Synthesis and antitumor activity evaluation of new 2-(4-aminophenyl)benzothiazole derivatives bearing different heterocyclic rings," *J. Enzyme Inhib. Med. Chem.*, vol. 30, no. 3, pp. 458–465, 2015.
- [56] M. Olle and I. H. Williams, "Effective microorganisms and their influence on vegetable production—a review," *J. Hortic. Sci. Biotechnol.*, vol. 88, no. 4, pp. 380–386, 2013.
- [57] S. R. Singh, N. B. Krishnamurthy, and B. B. Mathew, "A review on recent diseases caused by microbes," *J Appl Env. Microbiol*, vol. 2, no. 4, pp. 106–115, 2014.
- [58] K. Rogers, "Fungi, algae, and protists," *Britannica Educational Publishing*, vol.8, no.3, p. 180, 2010.
- [59] R. W. Y. Habash, "Therapeutic hyperthermia," *Handb. Clin. Neurol.*, vol. 157, pp. 853–868, 2018.
- [60] S. R. Sinha, P. Prakash, R. K. Singh, and D. K. Sinha, "Assessment of tumor markers CA 19-9, CEA, CA 125, and CA 242 for the early diagnosis and prognosis prediction of gallbladder cancer," *World J. Gastrointest. Surg.*, vol. 14, no. 11, pp. 1272, 2022.
- [61] T. A. Martin, L. Ye, A. J. Sanders, J. Lane, and W. G. Jiang, "Cancer invasion and metastasis: molecular and cellular perspective," in *Madame Curie Bioscience Database*, Landes Bioscience, vol.20, no.9, p. 135-168, 2013.
- [62] B. M. M. Qaiser, *Principles and practice of chemotherapy*. Jatpee brothers publishers, vol.5, no.1, p.370, 2012.
- [63] A. Pandi, G. Mamo, D. Getachew, F. Lemessa, V. M. Kalappan, and S. Dhiravidamani, "A brief review on lung cancer," *Int. J. Pharma Res. Heal. Sci*, vol. 4, pp. 907–914, 2016.

## *References*

---

- [64] M. Zhang, Y. Yang, Y. Wang, J. Wang, H. Wu, and Y. Zhu, "Synthesis and evaluation of 2-amine-4-oxyphosanine pyrimidine derivatives as EGFR L858R/T790M/C797S mutant inhibitors," *Chem. Pharm. Bull.*, vol. 71, no. 2, pp. 140–147, 2023.
- [65] K. Szymoński, K. Milian-Ciesielska, E. Lipiec, and D. Adamek, "Current pathology model of pancreatic cancer," *Cancers (Basel)*, vol. 14, no. 9, pp. 2321, 2022.
- [66] R. Andersson, C. Haglund, H. Seppänen, and D. Ansari, "Pancreatic cancer—the past, the present, and the future," *Scand. J. Gastroenterol.*, vol. 57, no. 10, pp. 1169–1177, 2022.
- [67] W. Park, A. Chawla, and E. M. O'Reilly, "Pancreatic cancer: a review," *Jama*, vol. 326, no. 9, pp. 851–862, 2021.
- [68] M. Ghasemi, T. Turnbull, S. Sebastian, and I. Kempson, "The MTT assay: utility, limitations, pitfalls, and interpretation in bulk and single-cell analysis," *Int. J. Mol. Sci.*, vol. 22, no. 23, pp. 12827, 2021.
- [69] S. Kamiloglu, G. Sari, T. Ozdal, and E. Capanoglu, "Guidelines for cell viability assays," *Food Front.*, vol. 1, no. 3, pp. 332–349, 2020.
- [70] A. S. Waheeb, "Spectroscopic, characterization and bioactivity studies of new Ni (II), Cu (II) and Ag (I) complexes with didentate (N, N) donor azo dye ligand," *J. Mol. Struct.*, vol. 1276, pp. 134729, 2023.
- [71] C. Series, "Synthesis and Spectroscopic study of some transition metal complexes with 2- ( 4-Iodo Phenyl Azo ) -4 , 5- Diphenyl Imidazol Synthesis and Spectroscopic study of some transition metal complexes with 2- ( 4-Iodo Phenyl Azo ) -4 , 5- Diphenyl Imidazol," *J. Phys.: Conf. Ser*, IOP Publishing, vol. 1294, no. 11, pp.1-13, 2019.
- [72] H. K. Mahmoud, A. R. Sayed, M. M. Abdel-Aziz, and S. M. Gomha, "Synthesis of new thiazole clubbed imidazo [2, 1-b] thiazole hybrid as antimycobacterial agents," *Med. Chem. (Los. Angeles)*, vol. 18, no. 10, pp. 1100–1108, 2022.

- [73] S. Uzunboy, Ö. Karakaş, S. Demirci-Çekiç, and R. Apak, "Sulfate radical formation by Cr (III) activation of peroxydisulfate–Diphenylcarbazide spectrophotometric determination of sulfate radical and its scavenging activity," *Spectrochim. Acta Part A Mol. Biomol. Spectrosc.*, vol. 260, pp. 119941, 2021.
- [74] H. A. K. Kyhoiesh and K. J. Al-Adilee, "Synthesis, spectral characterization, antimicrobial evaluation studies and cytotoxic activity of some transition metal complexes with tridentate (N, N, O) donor azo dye ligand," *Results Chem.*, vol. 3, pp. 100245, 2021.
- [75] A. S. Waheeb, H. A. K. Kyhoiesh, A. W. Salman, K. J. Al-Adilee, and M. M. Kadhim, "Metal complexes of a new azo ligand 2-[2'-(5-nitrothiazolyl) azo]-4-methoxyphenol (NTAMP): Synthesis, spectral characterization, and theoretical calculation," *Inorg. Chem. Commun.*, vol. 138, pp. 109267, 2022.
- [76] P. Marcon and K. Ostanina, "Overview of methods for magnetic susceptibility measurement," in *PIERS Proceedings*, vol.420, no.3, pp.1-5, 2012.
- [77] G. A. Bain and J. F. Berry, "Diamagnetic corrections and Pascal's constants," *J. Chem. Educ.*, vol. 85, no. 4, pp. 532, 2008.
- [78] N. R. Laoufi, N. R. Laoufi, F. Bouchenak, A. Zouakh, M. Abdelaziz, A. Zerrouk1, D. Saddouki, K. Sobhi, "A new technique for sweat chloride determination using Mohr's silver method: Development and analytical validation," *J. Fundam. Appl. Sci.*, vol. 15, no. 2, pp. 127–137, 2023.
- [79] D. Blagojević, A. Polovina, D. Lazić, and D. Jelić, "Determination of chloride content in bottled mineral water," *Acta Sci. Balc.*, vol. 3, no. 1, pp.1-10, 2022.
- [80] J. Åhman, E. Matuschek, and G. Kahlmeter, "EUCAST evaluation of 21 brands of Mueller–Hinton dehydrated media for disc diffusion testing," *Clin. Microbiol. Infect.*, vol. 26, no. 10, pp. 1412-e1, 2020.
- [81] E. Matuschek, C. Longshaw, M. Takemura, Y. Yamano, and G. Kahlmeter, "Cefiderocol: EUCAST criteria for disc diffusion and broth microdilution for antimicrobial susceptibility testing," *J. Antimicrob. Chemother.*, vol. 77, no. 6, pp. 1662–1669, 2022.

## *References*

---

- [82] D. Nagajothi and J. Maheswari, "Synthesis, Characterization and Antimicrobial Activity Of Schiff Base Ligand Metal Complexes," *GIS Sci. J.*, vol. 8, pp. 1, 2021.
- [83] J. C. Rodrigues, W. L. da Silva, D. R. da Silva, C. R. Maia, C. V. S. Goiabeira, H. D. F. Chagas, G. M. A. D'Elia, G. S. B. Alves, V. Zahner, C. V. Nunez, O. C. C. Fernandes, "Antimicrobial activity of *Aspergillus* sp. from the Amazon Biome: Isolation of kojic acid," *Int. J. Microbiol.*, vol. 2022, pp.1-7, 2022.
- [84] K. Chen et al., "Immune infiltration patterns and identification of new diagnostic biomarkers GDF10, NCKAP5, and RTKN2 in non-small cell lung cancer," *Transl. Oncol.*, vol. 29, no. 10 2022, pp. 101618, 2023.
- [85] M. Mujahid et al., "Structural and Spectroscopic Study of New Copper(II) and Zinc(II) Complexes of Coumarin Oxyacetate Ligands and Determination of Their Antimicrobial Activity," *Mol.*, vol. 28, no.6, pp.1-23, 2023.
- [86] R. M. Banik and S. K. Pandey, "Selection of metal salts for alkaline phosphatase production using response surface methodology," *Food Res. Int.*, vol. 42, no. 4, pp. 470–475, 2009.
- [87] I. Oshina and J. Spigulis, "Beer – Lambert law for optical tissue diagnostics : current state of the art and the main limitations," *J. Biomed. Opt.*, vol. 26, no. 10, pp. 1–17, 2023.
- [88] J. M. M. Al-Zinkee and A. J. Jarad, "Synthesis, spectral studies and microbial evaluation of azo dye ligand complexes with some transition metals," *J. Pharm. Sci. Res.*, vol. 11, no. 1, pp. 98–103, 2019.
- [89] P. C. Austin, F. E. Harrell, and D. van Klaveren, "Graphical calibration curves and the integrated calibration index (ICI) for survival models," *Stat. Med.*, vol. 39, no. 21, pp. 2714–2742, 2020.
- [90] S. D. Naik and N. G. Limbachiya, "2-Hydroxy-5-Chlorobenzophenone Oxime [ HCBO ] as a gravimetric and spectrophotometric reagent for the determination of Mn ( II )," vol. 6, no. 2, pp. 981–985, 2019.

- [91] G. Kaur, S. Kaur, T. K. Pathak, V. Sharma, and K. Tyagi, "Spectrophotometric Investigation of Complexation of Ferrous Ion with 3,5-Dinitrosalicylic Acid," *World J. Chem. Educ.*, vol. 9, no. 3, pp. 77–80, 2021.
- [92] K. J. AL-Adilee and D. Yo Fanfon, "Preparation, Spectral Identification and Analytical Studies of Some Transition Metal Complexes with New Thiazolylazo Ligand and Their Biological Activity Study," *J. Chem. Chem. Eng.*, vol. 6, pp. 1016–1028, 2012.
- [93] N. Mohamed Wannas, A. A. S. Al-Hamdani, and W. Al Zoubi, "Spectroscopic characterization for new complexes with 2,2'-(5,5-dimethylcyclohexane-1,3-diylidene)bis(azan-1-yl-1-ylidene)dibenzoic acid," *J. Phys. Org. Chem.*, vol. 33, no. 11, pp. 0–12, 2020.
- [94] K. Al-Adilee and H. A. K. Kyhoiesh, "Preparation and identification of some metal complexes with new heterocyclic azo dye ligand 2-[2-- (1- Hydroxy -4- Chloro phenyl) azo ]- imidazole and their spectral and thermal studies," *J. Mol. Struct.*, vol. 1137, pp. 160–178, 2017.
- [95] S. Thakurta, R. J. Butcher, G. Pilet, and S. Mitra, "Synthesis of octahedral cobalt(III) complexes with mono- and di-condensed Schiff base ligands: A template-directed approach for the isolation of a rare kind of mixed-ligand complex," *J. Mol. Struct.*, vol. 929, no. 1–3, pp. 112–119, 2009.
- [96] T. Q. Manhee and A. J. Alabdali, "Anticancer Activity against Brain Cancer Using Ni (II), Cu (II), Pd (II) and Au (III) Complexes Derived from Novel Mannich Base," *J. Popul. Ther. Clin. Pharmacol.*, vol. 30, no. 8, pp. 87–100, 2023.
- [97] H. G. Aslan, S. Özcan, and N. Karacan, "Synthesis, characterization and antimicrobial activity of salicylaldehyde benzenesulfonylhydrazone (Hsalbsmh) and its Nickel(II), Palladium(II), Platinum(II), Copper(II), Cobalt(II) complexes," *Inorg. Chem. Commun.*, vol. 14, no. 9, pp. 1550–1553, 2011.

- [98] H. A. K. Kyhoiesh and K. J. Al-Adilee, "Synthesis, spectral characterization and biological activities of Ag (I), Pt (IV) and Au (III) complexes with novel azo dye ligand (N, N, O) derived from 2-amino-6-methoxy benzothiazole," *Chem. Pap.*, vol.1, no.1, pp. 1–34, 2022.
- [99] G. F. Hameed, F. Y. Wadday, M. A. A. Farhan, and S. A. Hussain, "Synthesis, Spectroscopic characterization and bactericidal valuation of some metal (II) complexes with new Tridentate Heterocyclic Azo Ligand Type (NNO) Donor," *Egypt. J. Chem.*, vol. 64, no. 3, pp. 1333–1345, 2021.
- [100] E. I. Teixeira, C. S. Schwalm, G. A. Casagrande, B. Tirloni, and V. D. Schwade, "Binuclear isophthaloylbis(N,N-diphenylthioureate) transition metal complexes: Synthesis, spectroscopic, thermal and structural characterization," *J. Mol. Struct.*, vol. 1210, pp. 1–14, 2020.
- [101] K. J. Al-Adilee and A. Shaimaa, "Synthesis and spectral properties studies of novel hetrocyclic mono azo dye derived from thiazole and pyridine with some transition complexes," *OJC*, vol. 33, no. 4, pp. 1–14, 2017.
- [102] S. A. Shaker, H. A. Mohammed, A. A. Salih, and J. Kajang-puchong, "Preparation , Physico-Chemical and Spectroscopic Investigation of Thiacetazone and Quinalizarin Complexes with Mn ( II ), Fe ( II ), Co ( II ), Ni ( II ), Cu ( II ), Zn ( II ), Cd ( II ) and Pb ( II )," *Aus. J. Basic. & Ap. Sci.*, vol. 4, no. 10, pp. 5178–5183, 2010.
- [103] D. Y. Fnfoon and K. J. Al-Adilee, "Synthesis and spectral characterization of some metal complexes with new heterocyclic azo imidazole dye ligand and study biological activity as anticancer," *J. Mol. Struct.*, vol. 1271, pp. 134089, 2023.
- [104] H. Dinçalp, F. Toker, I. Durucasu, N. Avcibaşı, and S. Icli, "New thiophene-based azo ligands containing azo methine group in the main chain for the determination of copper(II) ions," *Dye. Pigment.*, vol. 75, no. 1, pp. 11–24, 2007.

- [105] N. A. Hussein and A. K. Abbas, "Synthesis, spectroscopic characterization and thermal study of some transition metal complexes derived from caffeine azo ligand with some of their applications," *Eurasian Chem Commun*, vol. 4, no. 1, pp. 67–93, 2022.
- [106] D. Nakane, Y. Wasada-Tsutsui, Y. Funahashi, T. Hatanaka, T. Ozawa, and H. Masuda, "A Novel Square-Planar Ni (II) Complex with an Amino-Carboxamido- Dithiolato-Type Ligand as an Active-Site Model of NiSOD," *Inorg. Chem.*, vol. 53, no. 13, pp. 6512–6523, 2014.
- [107] B. C. Yallur, P. M. Krishna, and M. Challa, "Bivalent Ni (II), Co (II) and Cu (II) complexes of [(E)-[(2-methyl-1, 3-thiazol-5-yl) methylidene] amino] thiourea: synthesis, spectral characterization, DNA and in-vitro anti-bacterial studies," *Heliyon*, vol. 7, no. 4, pp.1-12, 2021.
- [108] N. A. Kryuchkova, I. V Mironov, and V. A. Afanas'eva, "The effect of ligand modification on the structure and electronic spectra of tetraazamacrocyclic complexes Au (III)," *J. Mol. Struct.*, vol. 1224, p. 129162, 2021.
- [109] Z. H. Al-Saffar et al., "Extraction and Characterisation of Maltene from Virgin Asphalt as a Potential Rejuvenating Agent," *Sustainability*, vol. 15, no. 2, p. 909, 2023.
- [110] M. Safaei-Farouji, M. Jafari, A. Semnani, T. Gentzis, B. Liu, K. Liu, M. Shokouhimehr, M. Ostadhassan, "TGA and elemental analysis of type II kerogen from the Bakken supported by HRTEM," *J. Nat. Gas Sci. Eng.*, vol. 103, pp. 104606, 2022.
- [111] M. N. Matada, K. Jathi, M. M. Rangappa, K. Geoffry, S. R. Kumar, R. B. Nagarajappa, F. Noor Zahara "Journal of King Saud University – Science Original article A new sulphur containing heterocycles having azo linkage : Synthesis , structural characterization and biological evaluation," *J. King Saud Univ. - Sci.*, vol. 32, no. 8, pp. 3313–3320, 2020.

- [112] F. Abbas Bayader, S. Abdulla Zeyad, and N. Abid Al-jibouri Mahmoud, "Preparation and Spectroscopic Studies of Some Metal complexes with Azo ligand derived from 2-aminobenzothiazole and 4-Hydroxycoumarin," *Res. J. Chem. Environ.*, vol. 26, pp. 10, 2022.
- [113] K. J. Al-adilee and H. M. Hessoon, "Synthesis, spectral properties and anticancer studies of novel hetrocyclic azo dye ligand derived from 2-amino-5-methyl thiazole with some transition metal complexes," in *Journal of Physics: Conference Series*, IOP Publishing, vol.1, no.11, pp. 12094, 2019.
- [114] G. Mishra, P. K. Dwivedi, N. Verma, S. Srivastava, and A. K. Singh, "Copper Nitrate Catalyzed Synthesis Of Novel Thiazolyl Hydrazones : Anti-Inflammatory Effect Via COX-2 / IL-6 Dual Antagonistic Action," *Journal Pharm. Negat. Results*, vol. 13, no. 10, pp. 3821–3833, 2022.
- [115] M. Bal, "Synthesis and Characterization of Tetradentate Schiff Base Ligand Containing 3, 4- Diamino Benzophenone and Investigation of Complex Formation with Ni ( II ), Cu ( II ) and Co ( II ) Metal Ions," *Cumhuriyet Science Journal*, vol. 44, no. 2, pp. 289–295, 2023.
- [116] G. Y. Nagesh, B.S. Matada , G.B. Vibhutimath , V.D. Biradar , M.R. Karekal , M.D. Udayagiri, M.B. Hire Mathada, "Indole core-based Copper(II), Cobalt(II), Nickel(II) and Zinc(II) complexes: Synthesis, Spectral and Biological Study," *J. Mol. Struct.*, vol., 1248, no.1, pp. 131410, 2021.
- [117] A. G. Prashantha and A. S. Jagadisha, "dyes and its metal complexes Cu," *Results Chem.*, vol. 5, no. 3, pp. 100890, 2023.
- [118] A. Bourouina and M. Rekis, "Comparison in optoelectronic properties of triphenylamine-imidazole or imidazole as donor for dye-sensitized solar cell: theoretical approach," *J. Mol. Model.*, vol. 27, no. 8, pp. 225, 2021.
- [119] M. Ali, M. Hamzah, I. K. Jebur, and A. K. Ahmed, "Synthesis , Characterization and Biological Activity Evaluation of Some New Azo Derivatives from 2-Amino Benzothiazole and Their Derivatives," (*KUJSS*), vol. 13, no. 1, pp.212-227, 2018.

- [120] A. G. Abdulrazzaq and A. A. S. Al-hamdani, "Cr ( III ), Fe ( III ), Co ( II ) and Cu ( II ) Metal ions Complexes with Azo Compound Derived from 2-hydroxy Quinoline Synthesis , Characterization , Thermal Study and Antioxidant Activity," (IHJPAS), vol. 6, no.7, pp. 214–230, 2023.
- [121] A. S. Waheeb and K. J. Al-Adilee, "Synthesis, characterization and antimicrobial activity studies of new heterocyclic azo dye derived from 2-amino-4, 5-dimethyl thiazole with some metal ions," Mater. Today Proc., vol. 42, pp. 2150–2163, 2021.
- [122] A. M. A. Alaghaz, A. G. Al-sehemi, and T. M. El-gogary, "Spectrochimica Acta Part A : Molecular and Biomolecular Spectroscopy Synthesis , characterization and quantum chemical ab initio calculations of new dimeric aminocyclodiphosph ( V ) azane and its Co ( II ), Ni ( II ) and Cu ( II ) complexes," Spectrochim. Acta Part A Mol. Biomol. Spectrosc., vol. 95, pp. 414–422, 2012.
- [123] S. Harisha, J. Keshavayya, S. M. Prasanna, and H. J. Hoskeri, "Synthesis, characterization, pharmacological evaluation and molecular docking studies of benzothiazole azo derivatives," J. Mol. Struct., vol.1218, no.10, pp. 128477, 2020.
- [124] N. Afify, "Materials Science & Engineering B Syntheses of new ( CdO ) ( 1- X ) ( NiO ) X ZnO nanocomposite system : Preparation , structure , and magnetic properties," Mater. Sci. Eng. B, vol. 273, no. 7, pp. 115399, 2021.
- [125] M. Shakir, S. Hanif, M. A. Sherwani, O. Mohammad, and S. I. Al-Resayes, "Pharmacologically significant complexes of Mn(II), Co(II), Ni(II), Cu(II) and Zn(II) of novel Schiff base ligand, (E)-N-(furan-2-yl methylene) quinolin-8-amine: Synthesis, spectral, XRD, SEM, antimicrobial, antioxidant and in vitro cytotoxic studies," J. Mol. Struct., vol. 1092, no. 12, pp. 143–159, 2019.
- [126] E. Rodríguez-Arce and M. Saldías, "Antioxidant properties of flavonoid metal complexes and their potential inclusion in the development of novel strategies for the treatment against neurodegenerative diseases," Biomed. Pharmacother., vol. 143, no. 9, pp. 112236, 2021.

- [127] B. H. Al-Zaidi, M. M. Hasson, and A. H. Ismail, "New complexes of chelating Schiffbase: Synthesis, spectral investigation, antimicrobial, and thermal behavior studies," *J. Appl. Pharm. Sci.*, vol. 9, no. 4, pp. 45–57, 2019.
- [128] K. J. Al-Adilee and S. R. Hasan, "Synthesis, Characterization and Biological Activity of Heterocyclic Azo-Schiff Base Ligand derived from 2-Amino-5-methyl thiazol and some Transition Metal Ions," *IOP Conf. Ser. Earth Environ. Sci.*, vol. 790, no. 1, pp.21, 2021.
- [129] N. Mishra, K. Poonia, S. K. Soni, and D. Kumar, "Synthesis, characterization and antimicrobial activity of Schiff base Ce(III) complexes," *Polyhedron*, vol. 120, no. 1, pp. 60–68, 2016.
- [130] A. Ali, S. Banerjee, S. Kamaal, M. Usman, N. Das, M. Afzal, A. Alarifi, N. Sepay, P. Roy, M. Ahmad, "Ligand substituent effect on the cytotoxicity activity of two new copper(ii) complexes bearing 8-hydroxyquinoline derivatives: Validated by MTT assay and apoptosis in MCF-7 cancer cell line (human breast cancer)," *RSC Adv.*, vol. 11, no. 24, pp. 14362–14373, 2021.
- [131] M. D. Galsky, J. Á. A. Arija, A. Bamias, I. D. Davis, M. D. Santis, E. Kikuchi, X. G. Muro, U. D. Giorgi, M. Mencinger, K. Izumi, S. Panni, M. Gumus, M. Özgüroğlu, A. R. Kalebasty, S. H. Park, B. Alekseev, F. A. Schutz, J. R. Li, D. Ye, N. J. Vogelzang, S. Bernhard, D. Tayama, S. Mariathan, A. Mecke, A. Thåström, E. Grande, "Atezolizumab with or without chemotherapy in metastatic urothelial cancer (IMvigor130): a multicentre, randomised, placebo-controlled phase 3 trial," *Lancet*, vol. 395, no. 10236, pp. 1547–1557, 2020.

## الخلاصة

لقد تضمنت الدراسة تحضير وتشخيص ليكاند جديد من نوع ثيازوليل أزو غير متجانس الحلقة المشتق من 2-أمينو-5-ميثيل ثيازول-2-(2-5-ميثيل ثيازوليل) أزو [5,6-داي مثيل بنزايميدازول]. تم تحضير سلسلة من المعقدات الفلزية الصلبة لليكاند الثيازوليل أزو مع الأيونات  $\text{Co(III)}$  و  $\text{Ni(II)}$  و  $\text{Cu(II)}$  و  $\text{Ag(I)}$  و  $\text{Au(III)}$ . تم تشخيص جميع المعقدات الفلزية المحضرة بواسطة أطياف الأشعة تحت الحمراء FTIR و طيف الرنين النووي المغناطيسي  $^1\text{HNMR}$  و  $^{13}\text{CNMR}$ ، ومطيافية الكتلة mass spectrometry و طيف الأشعة فوق البنفسجية- المرئية UV-Visible و تقنية التحلل الحراري الوزني TGA ومطيافية المجهر الإلكتروني الماسح في المجال المنبعث FESEM و حيود الأشعة السينية XRD بالإضافة إلى التحليل الدقيق للعناصر (C.H.N.S).

لقد أظهرت النتائج أن الصيغ التركيبية المقترحة للمعقدات الفلزية المحضرة، أن ليكاند الثيازوليل أزو 2-[2-(5-ميثيل ثيازوليل) أزو] 5,6-داي مثيل بنزايميدازول يسلك سلوك ليكاند ثنائية السن. إذ تم تحديد النسبة المولية لأيونات الفلزات  $\text{Co(III)}$  و  $\text{Ni(II)}$  و  $\text{Cu(II)}$  و  $\text{Ag(I)}$  و  $\text{Au(III)}$  التي تمت دراستها في معقداتها التناسقية مع ليكاند 2-[2-(5-ميثيل ثيازوليل) أزو] 5,6-داي مثيل بنزايميدازول وكانت 1:2 [ليكاند: فلز]، وبالتالي فإن الشكل المقترح والمتوقع لهذه المعقدات هو ثماني السطوح. في المقابل، فإن النسبة المولية لأيونات فلزات  $\text{Ni(II)}$  و  $\text{Ag(I)}$  و  $\text{Au(III)}$  هي 1:1 [ليكاند: فلز] مع ليكاند 2-[2-(5-ميثيل ثيازوليل) أزو] 5,6-داي مثيل بنزايميدازول وبالتالي فإن الأشكال الهندسية المقترحة لهذه المعقدات هو رباعي السطوح مع أيون  $\text{Ag(I)}$  ومربع مستوي مع أيونات  $\text{Ni(II)}$  و  $\text{Au(III)}$ .

وأخيراً، تم اختبار ليكاند الأزو الجديد ومعقداته الفلزية في المختبر للنشاط المضاد للبكتيريا والفطريات ضد نوعين من البكتيريا (*Escherichia coli*, *Streptococcus aureus*) ونوع واحد من الفطريات (*Penicillium sp*).

تمت دراسة فحوصات سمية بعض المركبات المحضرة على الخلايا البشرية لمرض سرطان (الرئة والبنكرياس)؛ لمعرفة إمكانية استخدام هذا النوع من المركبات كدواء من خلال معاملته مع خلايا سرطانية بشرية مصابة بالسرطان لمعرفة مدى تأثيره، حيث تمت دراسة تأثير ليكاند الثيازوليل أزو ومعقد  $\text{Cu(II)}$  على نمو خطوط خلايا سرطان الرئة (A549)، ومعقد  $\text{Ag(I)}$  على نمو خطوط خلايا سرطان البنكرياس (TP-53) والخلايا الطبيعية (HdFn)، وذلك لمعرفة مدى فعاليتها السمية على الخلايا البشرية ومدى إمكانية استخدامها لعلاج السرطانات المذكورة أعلاه. ومن بين النتائج التي تم الحصول عليها لليكاند ومعقداته الفلزية قيد الدراسة مع خطوط الخلايا السرطانية للرئة (A549)، والبنكرياس (TP-53)، على التوالي، مقارنة مع الخلايا الطبيعية نلاحظ أن قيمة  $\text{IC}_{50}$  أعلى بالنسبة للخلايا الطبيعية، وفي المقابل في حالة خطوط الخلايا السرطانية تكون قيمة  $\text{IC}_{50}$  أقل، وهي نتيجة ممتازة.

## إقرار المشرف

أقر بأن الرسالة الموسومة (تحضير، تشخيص ودراسة الفعالية الحيوية لليكاند صبغة ازو جديدة مع بعض معقداته الفلزية) قد جرت تحت إشرافي في قسم الكيمياء/ كلية العلوم/ جامعة المثنى كجزء من متطلبات درجة الماجستير في علوم الكيمياء.

م.د.مسار علي عواد

جامعة المثنى/ كلية العلوم

التاريخ: / / 2024

أ.م.د. ازل شاكر وهيب

جامعة المثنى/ كلية العلوم

التاريخ: / / 2024

بناءً على التوصيات المقدمة من الأستاذ المشرف، أشرح هذه الأطروحة للمناقشة.

رئيس القسم:

أ.م.د. ازل شاكر وهيب

التاريخ: / / 2024



جمهورية العراق  
وزارة التعليم العالي والبحث العلمي  
جامعة المثنى / كلية العلوم  
قسم الكيمياء

## تحضير، تشخيص ودراسة الفعالية الحيوية لليكاند صبغة ازو جديدة مع بعض معقداته الفلزية

رسالة مقدمة الى

مجلس كلية العلوم/ جامعة المثنى

وهي جزء من متطلبات نيل درجة الماجستير في علوم الكيمياء

من قبل

سهى حسن مجهول

بكالوريوس علوم كيمياء ٢٠١٨

بإشراف

م.د. مسار علي عواد

أ.م.د. أزل شاكر وهيب

٢٠٢٤ م

١٤٤٥ هـ